IMPROVEMENT OF THE ENVIRONMENTAL AND ECONOMIC CHARACTERISTICS OF COOLING TOWERS

PART I of II: HEAT REJECTION FROM HORIZONTAL TUBES TO SHALLOW FLUIDIZED BEDS

by

Bruce R. Andeen
Leon R. Glicksman
Warren M. Rohsenow

Energy Laboratory
in association with
Heat Transfer Laboratory,
Department of Mechanical Engineering
MASSACHUSETTS INSTITUTE OF TECHNOLOGY

Sponsored by:
Empire State Electric Energy Research Corporation
New York

Energy Lab Report No. MIT-EL 74-007
Heat Transfer Lab Report No. 80047-85

June 30, 1974

ABSTRACT

As fluidized beds can result in an order of magnitude increase in the heat transfer coefficinet for a surface, they can potentially be coupled with dry cooling towers for power plant heat rejection. On such a large scale, economic considerations necessitate the use of an inexpensive particle and shallow bed depths. Existing heat transfer mechanism models for fluidized beds are discussed, and a new model presented. Heat transfer coefficients from a horizontal tube in a row of dummy tubes to a shallow fluidized bed were experimentally measured. Coefficients from banks of horizontal tubes are lower than coefficients from vertical walls primarily because of particle stagnation on the tube tops and particle recirculation problems. Experimentally, different tube and distributer geometries were tried in order to reduce stagnations and enhance particle recirculation. Experimental data for these different geometries is compared to exising horizontal tube correlations and the new model. The RMS deviation of data from the model is less than 17%. The best correlation was obtained by modifying the Vreedenberg correlation to include a dependency on the particle fraction of the bed. The RMS deviation of data from the modified Vreedenberg correlation was 13.8%.

Using both experimental data and the modified Vreedenberg correlation, economic optimizations were performed to compare fluidized bed dry cooling towers to a finned tube tower. For a 1000 mw plant, heat exchanger costs are 13% lower for fluidized beds, but the fluidized bed is severely penalized by the cost for the power needed to keep the bed fluidized. The incremental cost of the fluidized bed is 16% higher than that for a finned surface, but rapidly approaches the finned tube incremental cost as the particle size and bed depth are reduced.

ACKNOWLEDGEMENTS

This study was sponsored by the Empire State Electric Energy Research Corporation [ESEERCO]. Their support is gratefully acknowledged.

The ESEERCO technical committee's interest and suggestions were an aid to the study. Members of the committee who deserve a particular note of thanks include Leonard Geller, Paul Torpey, Art Sugden, and Howard Philipp.

Table of Contents

TITLE PAGE..... 1
ABSTRACT..... 3
ACKNOWLEDGEMENTS..... 5
TABLE OF CONTENTS..... 7
LIST OF FIGURES.....11
LIST OF TABLES.....17
NOMENCLATURE.....19

I. INTRODUCTION.....23
II. ANALYTICAL FLUIDIZED BED MODELS.....27
II.1 Models from Literature.....27
II.2 Order of Magnitude of Fluidized Bed Effects.....31
II.2.1 Introduction.....31
II.2.2 Boundary Layer Destruction or Reduction.....37
II.2.2.1 Static Model.....37
II.2.2.2 Dynamic Model.....39
II.2.3 Transient Heating of Particles Passing Through a Gaseous Heated Region.....43
II.2.4 Direct Thermal Interaction between Particle and Wall.....48
II.2.5 General Formulation of h's from These Three Effects.....51
II.2.6 A Second Model for Order of Magnitude Effects.....53
II.2.6.1 Conduction to the Particle.....53
II.2.6.2 Mixing of Gasses at the Wall.....55
II.2.6.3 General Formulation of h's for this Model.....55
II.3 Horizontal Tube Correlations and Experiments.....58
II.3.1 Correlations.....58
II.3.2 Other Horizontal Tube Experiments.....64
III. EXPERIMENTAL PROGRAM.....67
III.1 Introduction.....67
III.2 Test Apparatus.....67
III.3 Calibration of Test Apparatus.....77
III.4 Test Procedure.....79
III.5 Estimation of Error.....80
III.6 Data Reduction.....84

IV. RESULTS OF EXPERIMENTAL AND ECONOMIC STUDIES.....87
IV.1 Introduction.....87
IV.2 Choice of Various Distributer Geometries and Qualitative Results.....87
IV.3 Heat Transfer Coefficients as a Function of Velocity.....93
IV.4 Comparison of Experimental Data with Correlations.....106
IV.4.1 Scope.....106
IV.4.2 Wender-Cooper Correlation of Data.....109
IV.4.3 Ainshtein Correlation of Data.....117
IV.4.4 Vreedenberg Correlation of Data.....125
IV.4.5 Correlation of Data to the Model of Section II.2.6..146
IV.4.6 Comparison of Correlations.....154
IV.5 Comparison of Pressure Drops.....158
IV.6 Economic Comparison of Fluidized Beds to Finned Tubes.....160
IV.7 Fluidized Beds with Water Injection.....172
V. CONCLUSIONS AND RECOMMENDATIONS.....175

REFERENCES.....178
APPENDIX 1: Calculation of spacing between particles (x_n).....181
APPENDIX 2: Calculation of particle collisions per unit area (n)....182
APPENDIX 3: Resistance of metal spacer between heated tube sections.183
APPENDIX 4: Uncertainty of q_{rej} and (T_w-T_b).....185
APPENDIX 5: The effectiveness of a fluidized bed heat exchanger.....187
APPENDIX 6: Comparison of Water Consumption Between A Fluidized Bed with Water Injection or with A Wet Tower Topping Unit.....189
APPENDIX 7: Data.....195

List of Figures

1 Resistance to Heat Transfer Schema.....32

2 Geometry for Transport from a Vertical Wall.....35

3 Linear Relation between Frequency & $V^{1/4}/d_p$.....36

4 Model of Effect #2.....44

5 Fluidized Bed Test Schema.....68

6 Distributer Support Structures.....70

7 Horizontal Heated Tube Assembly Drawing.....72

8 Flattened Tube.....73

9 Wiring Schema.....76

10 Location of Thermocouples in Test Piece.....86

11-14 Geometries Used to Try and Enhance Fluidized Bed Heat Transfer Coefficients.....92

15 Heat Transfer Coefficient vs. Superficial Velocity, Geom 1.....98

16 Heat Transfer Coefficient vs. Superficial Velocity, Geom 2.....99

17 Heat Transfer Coefficient vs. Superficial Velocity, Geom 3.....100

18 Heat Transfer Coefficient vs. Superficial Velocity, Geom 4.....101

19 Heat Transfer Coefficient vs. Superficial Velocity, Geom 5.....102

20 Heat Transfer Coefficient vs. Superficial Velocity, Geom 6.....103

21 Heat Transfer Coefficient vs. Superficial Velocity, Geom 7.....104

22 Optically Measured Void vs. Leva's Relation.....108

23 Data Plotted with Wender-Cooper Parameters, Geometry 1.....110

24 Data Plotted with Wender-Cooper Parameters, Geometry 2.....111

25 Data Plotted with Wender-Cooper Parameters, Geometry 3.....112

26 Data Plotted with Wender-Cooper Parameters, Geometry 4.....113

27 Data Plotted with Wender-Cooper Parameters, Geometry 5.....114

28 Data Plotted with Wender-Cooper Parameters, Geometry 6.....115

29 Data Plotted with Ainshtein Parameters, Geometry 1.....118

30 Data Plotted with Ainshtein Parameters, Geometry 2.....119

31 Data Plotted with Ainshtein Parameters, Geometry 3.....120

32 Data Plotted with Ainshtein Parameters, Geometry 4.....121

33 Data Plotted with Ainshtein Parameters, Geometry 5.....122

34 Data Plotted with Ainshtein Parameters, Geometry 6.....123

35A Data Plotted with Vreedenberg Parameters, Geometry 1.....127

35B Data Plotted with Modified Vreedenberg Parameters, Geometry 1.....128

36A Data Plotted with Vreedenberg Parameters, Geometry 2.....129

36B Data Plotted with Modified Vreedenberg Parameters, Geometry 2.....130

37A Data Plotted with Vreedenberg Parameters, Geometry 3.....131

37B Data Plotted with Modified Vreedenberg Parameters, Geometry 3.....132

38A Data Plotted with Vreedenberg Parameters, Geometry 4.....133

38B Data Plotted with Modified Vreedenberg Parameters, Geometry 4.....134

39A Data Plotted with Vreedenberg Parameters, Geometry 5.....135

39B Data Plotted with Modified Vreedenberg Parameters, Geometry 5.....136

40A Data Plotted with Vreedenberg Parameters, Geometry 6.....137

40B Data Plotted with Modified Vreedenberg Parameters, Geometry 6.....138

41A Data Plotted with Vreedenberg Parameters.....139

41B Data Plotted with Modified Vreedenberg Parameters.....140

42A Vreedenberg's Data Plotted with Vreedenberg Parameters.....141

42B Vreedenberg's Data Plotted with Modified Vreenedberg Parameters...142

43A Petrie's Data Plotted with Vreedenberg Parameters.....143

43B Petrie's Data Plotted with Modified Vreedenberg Parameters.....144

44 Comparison of Data with Model of Section II.2.6, Geometry 1.....147

45 Comparison of Data with Model of Section II.2.6, Geometry 2.....148

46 Comparison of Data with Model of Section II.2.6, Geometry 3.....149

47 Comparison of Data with Model of Section II.2.6, Geometry 4.....150

48 Comparison of Data with Model of Section II.2.6, Geometry 5.....151

49 Comparison of Data with Model of Section II.2.6, Geometry 6.....152

50 Tiered Fluidized Beds for Cooling Tower Use.....161

51 Conceptualization of Fluidized Bed Cooling Towers.....162

52 Incremental Cost vs. Design Temperature for a Fluidized Bed Cooling Tower Using Experimental Data.....168

53 Incremental Cost vs. Design Temperature for a Fluidized Bed Cooling Tower Using Modified Vreedenberg Correlation..169

54 Incremental Cost vs. Design Temperature for a Fluidized Bed Cooling Tower Using Modified Vreedenberg Correlation.....170

List of Tables

1 Modeled Heat Transfer Effects.....57

2 Error Sources.....83

3 Distributer Configurations & Geometries.....105

4 RMS Deviation of Data from Wender-Cooper Correlation.....116

5 RMS Deviation of Data from Ainshtein Correlation.....124

6 RMS Deviation of Data from Vreedenberg Type Correlations.....145

7 RMS Deviation of Data from Model of Section II.2.6.....153

8 Economic Breakdown of Fluidized Bed and Finned Tube Optimizations.....171

Nomenclature

A	area
Ar	Archimedes number
C	specific heat
Cr	correction factor in Wender-Cooper relation
D	initial distance of approach
d	diameter
f	frequency
G	mass flow rate
g	constant: 32.2 lbm-ft/lbf-sec^2
H	height of fluidized bed
h	heat transfer coefficient
k	conductivity
L	solid length
l	thickness
Nu	Nusselt number
n	particles per unit area
n	parameter in equation for velocity distribution in pipe
n_p	number of particles
P_m	power per unit mass
Pr	Prandtl number
Q	heat energy transferred
q	rate of heat transfer
R	Thermal resistance
Re	Reynolds number
T	temperature
t	time
$\bar{t}$	residence time
V	velocity
V	volume
$\tilde{v}'$	mean fluctuational eddy velocity
x_n	spacing between particles (or nozzles)

α	thermal diffusivity
α	vertical distance above distributer
δ	thickness
ε	void
ε	heat exchanger effectiveness
μ	absolute viscosity
ν	kinematic viscosity
ρ	density

Subscripts

a	air
avg	average
b	bubble
b	bed
cl	centerline
e	emulsion
f	frontal
g	gas
h	heated
l	liquid
mf	minimum fluidization
p	particle
s	solid
s	superficial
t	tube
w	wall

I. INTRODUCTION

Present day power plants are at best 40% efficient. This means that for every kilowatt of generated energy, 1.5 kw of heat must be dissipated - or rejected - to a heat sink. Traditionally this heat sink has been our natural water ways; rivers, lakes, and oceans. With the advent of large power plants, which create areas of high energy density, environmentalists have become concerned with the heating of waterways with this rejected heat. The problem is to find an adequate heat sink for power plants; one which is thermodynamically, ecologically, and economically sound.

Both evaporative cooling systems and dry cooling towers are potentially adequate heat exchangers. Dry cooling towers have the ecological advantage in that they are a closed system and don't require make-up water as they have no direct water to air contact. With no water consumption, the dry tower has a greater flexibility of location and will not produce any of the condensate plumes or fog which characterize wet towers. However, primarily because of the high cost of conventionally finned surfaces, dry cooling towers are about twice as expensive as wet towers [30].

Since in air cooled heat exchangers the greatest resistance to heat rejection is on the air side, an increased heat transfer coefficient would be beneficial to the acceptance of dry cooling towers. The purpose of this study was to evaluate the applicability of using fluidized beds as a means of enhancing heat transfer coefficients in air cooled heat exchangers, and in particular, power plant dry cooling towers.

If a steadily increasing updraft of air is allowed to flow through a bed of small solid particles, a point is reached where the drag force on

each particle is equal to the gravitational force. The particles begin to float, and in fact, dart about in apparent random motion. The static particles have been fluidized.

Due to the high mobility of the particles, the fluidized bed tends to maintain a uniform temperature. Hence a primary present use of fluidized beds is in isothermal processes and/or processes requiring large surface areas.

Another characteristic of a fluidized bed is that items immersed in the bed experience a high surface heat transfer coefficient.

An increased heat transfer coefficient would increase the performance of the heat exchanger by increasing the heat rejection capacity for a given air side area, or by reducing the required air side area for a given load. Finned tubes are merely a means of circumventing air's high heat transfer resistance. Fins increase the air side areas without increasing inside areas. A sufficient increase in air side heat transfer coefficient could entirely eliminate the need for finned tubes. The cost savings of being able to use the less expensive bare tubes could be sufficient to make fluidized beds more economically attractive as a dry cooling tower than finned tubes.

Consider a comparison between fluidized beds and finned tubes having an air side to water area ratio of 10:1. Such a finned tube would cost 0.8 - 1.0 $/ft^2$ of air side area [1], and would experience an h of 10 -15 BTU/hr-ft^2-°F. A bare tube would cost 2 - 3 $/ft^2$ of air side area. If bed h's can be achieved between 30 - 45 BTU/hr-ft^2-°F, even though a square foot of air side area would cost three times more, only 1/3 the total surface area would be needed with a fluidized bed, and the capital

cost of fluidized beds and finned tubes would be the same. Higher fluidized bed heat transfer coefficients would yield a cost savings, and make dry cooling towers in general more economically competitive with once through cooling systems than finned systems are now.

Since this study is to evaluate the applicability of using fluidized beds as a means of heat rejection from power plants, it is not only important to have a low initial cost, but also a low operating cost. Subsequently, certain restrictions are placed upon the fluidized bed.

1. The fluidized particle must be inexpensive. An inexpensive particle is required because of the shear quantity of particles needed for a fluidized bed of power plant size. From a cost standpoint, glass and sand appear to be the best. The value of scrap glass, of unsorted color, to the glass manufacturer is .3 - .4 ¢/lb. Grinding, sizing, and transportation operations would bring this figure closer to 1 ¢/lb, which is about the cost of sand delivered to a glass manufacturer. However, waste glass is becoming a sizable disposal problem, and may be available from local dumps for the asking. Some amounts of particles will always be lost from the system by elutriation, or a dusting effect. Therefore for make-up reasons particle cost must be low. From an ecological viewpoint, the elutriated particle should have minimal effects on the environment. Both sand and glass are inert, but pschologically a degree of sand spreading is probably more desirable than spreading 'broken' glass.

2. Air pressure drops through the bed must be kept low. The magnitude of the pressure drops is directly proportional to the power needed to fluidize the bed. Since the pressure drop through the bed is

roughly equivalent the weight per unit area of the bed supported, and since the power consumed in suspending the bed should be kept low, a shallow bed and/or low density particles are desired. Shallow beds, in turn, mandate horizontal tubes.

3. Low cost tubes must be used to keep the initial cost lower than a dry cooling tower with finned tubes. This almost dictates the use of bare tubes.

Besides incurring lower pressure drops, shallow beds have additional advantages. Packets of air, entering and passing through the bed have less time to aglomerate and create large bubbles. This more disperse air phase means more uniform bed conditions, especially at higher void fractions.

Unfortunately, the majority of fluidized bed data and correlations have been obtained from experiments with deep (1-3 feet) beds contained in cylinders (diameter: 4 inches - 3 feet), and have measured heat rejected from the container wall or from an axially aligned vertical tube. A few tests available in the literature have been conducted on heat rejection from horizontal tubes, spheres, and horizontal wires, but none was found that used horizontal tubes and shallow beds.

II. ANALYTICAL FLUIDIZED BED MODELS

II.1 Models From Literature

Models characterizing fluidized bed heat transfer fall into two major classes:

1. Those viewing the resistance to heat transfer as lying within a relatively thin (less than the particle diameter) region at the wall and

2. those viewing the resistance to heat transfer as being within a relatively thick (greater than particle diameter) emulsion layer which is frequently replaced by fresh emulsion from the main core of the fluidized bed.

The class 1 model is typified by the apporach of Leva [2], Mickley and Trilling [3], Levenspiel and Walton [4], and others. They assume that the greatest resistance to heat transfer is the fluid boundary layer surrounding the heat exchanger surface. The particulate phase of the fluidized bed, continually penetrating this boundary layer, reduces the mean film thickness to something less than the particle diameter. The reduction of the fluid film thickness increases the rate of conduction across the film, and consequently increases the heat transfer coefficient. Here the fluid boundary layer is determined by the fluid properties, the velocity of the fluid, and by the intensity of the particle motion which decreases the characteristic boundary layer thickness. Heat transfer coefficients maximize as a result of two counter acting mechanisms. With increasing fluid velocity, the particle motion becomes more intense, but with the increasing bed voidage, there are fewer particles per unit wall surface area.

An example of the class 2 model is the Mickley and Fairbanks [5] 'packet' theory. Mickley and Fairbanks presented a model based upon unsteady state heat conduction by 'packets' of solid particles which are assumed to be periodically displaced from the wall surface by gas bubbles. These packets are viewed to rest on the heat exchange surface, and carry the heat off into the fluidized bed core when displaced from the wall surface. The rate of heat transfer is dependent upon both the rate at which the particles are heated, and the frequency of re-establishing 'packets' at the heat transfer surface. In this model, h initially increases with velocity due to increased packet replacement frequency, but later falls as a result of the continual increase in the number of gas bubbles at the heat transfer surface. This model is based upon the solid particles being the discrete phase, which is acceptable for fluidized beds of voidages of less than .7 - .9 [6]. At higher void fractions, a phase inversion occurs, and the packet mechanism breaks down.

Knuii and Levenspiel further subdivides each of these classes into two subclasses, thereby identifying a total of four heat transfer mechanisms. These mechanisms are[7]:

1. Heat transfer through a thin gas film of the order of d_p or less.

2. Heat transfer in the vicinity of the particle-surface contact points, with frequent replacement of particles at the surface.

3. Unsteady-state absorption of heat by fresh emulsion which is swept up to and then away from the surface. This represents a surface renewal model for the emulsion.

4. Steady state conduction through the emulsion layer which is seldom swept away. This represents a film model for the emulsion.

Note that the sum of the first two mechanisms form the thin film model, while the second two comprise the extremes of the emulsion theory - depending upon the frequency of the emulsion replacement.

Any one of these mechanisms may be the controlling factor in heat rejection, and the controlling mechanism may change with the fluidizing conditions as well as with the location and geometry of the heat exchanger surface. For example, with horizontal tubes in a fluidized bed, particles tend to accrue in the stagnant downstream side of the tubes, creating a 'cap' of slow moving or stagnant sand over the tube top. Hence, on the tube tops, mechanism 4 would probably predominate, while mechanism 1 or 3 would predominate on the tube sides where particle action is much greater.

Knuii and Levenspiel point out that as particle contact time decreases the resistance to heat transfer by thermal conduction through the gas film (mechanism 1) is greater than the resistance of the emulsion layer (mechanism 3), and consequently, mechanism 1 becomes the dominant mechanism. In propounding this view, Knuii and Levenspiel make use of a model developed by Wicke and Fetting [8]. Wicke and Fetting model the combination of mechanisms 1 and 3 by proposing that heat q from a surface of solid height L_h is first conducted through a gas layer of thickness l_g, and is then taken up by solids flowing parallel to the surface in an emulsion region of thickness l_e. Some of the heat goes into sensible heat of the solids, and the rest is transferred into the core by particle interchange. Ignoring the heat transferred by particle interchange, and this premise is highly questionable with regards to Mickley's packet theory, yields a relation for the heat transfer coefficient from a wall to the bed emulsion layer [7]:

$$\frac{2h_w L_h}{k_l} = 1 - \exp\left(- \frac{2 L_h}{l_g} \frac{k_g}{k_l} \right) \tag{1}$$

where k_l is the equivalent conduction of the emulsion layer at minimum fluidization, or

$$k_l = \rho_s (1 - \varepsilon_{mf}) C_s V_s l_e \tag{2}$$

Now if the quantity $(-\frac{2 L_h}{l_g} \frac{k_g}{k_l})$ is small,

$$\frac{2 h_w L_h}{k_l} = \frac{2 L_h k_g}{l_g k_l} \tag{3}$$

or

$$h_w = \frac{k_g}{l_g} \tag{4}$$

and therefore $$Nu_w = \frac{h_w d_p}{k_g} = \frac{d_p}{l_g} \tag{5}$$

This is valid within a 20% error if the quantity $- \frac{2 L_h}{l_g} \frac{k_g}{k_l}$ is smaller than 0.4, or if

$$L_h < .2 \frac{k_l l_g}{k_g} = .2 \frac{\rho_s (1 - \varepsilon_{mf}) C_s V_s l_e l_g}{k_g} \tag{6}$$

Knuii and Levenspiel propose that conduction through a gas layer controls when $h_w \propto 1/l_g$, which is the case in the above analysis when the exponential is small. Therefore conduction controls when

$$\bar{t} = \frac{L_h}{V_s} < .2 \frac{\rho_s (1 - \varepsilon_{mf}) C_s l_e}{Nu_w (k_g/d_p)} \tag{7}$$

where $\bar{t}$ is the residence time of the emulsion adjacent to the heat transfer surface. Equation 7 will be discussed further in section II.2, 4.

II.2 Order of Magnitude of Fluidized Bed Effects

II.2.1 Introduction

In order to understand the potentials and effects of the different proposed mechanisms, a rough order of magnitude comparison of effects follows.

Consider the effects leading to heat transfer augmentation by the presence of particles. These effects include:

1. Destruction or reduction of the boundary layer caused by the presence of particles. This enhances the rate of conduction from the wall to the emulsion layer.

2. Transient heating of the particles as they pass through some heated region of thickness δ, or the heating of the particles in the emulsion layer.

3. Actual thermal interaction between the particle and the wall by direct contact.

Looking at the net flow of heat, heat leaves the surface and is absorbed by the particles by 2 paths or methods: transfer through the boundary layer (effect 1) and then to the particles in an emulsion layer of thickness δ (effect 2); or directly through particle contact (effect 3). A schematic diagram of the resistance to heat transfer is shown in Figure 1. Consequently, basing the h of each effect on the tube area so that the areas drop out of the relation, the over-all wall heat transfer coefficient is

$$h_{total} = \frac{h_1 h_2}{h_1 + h_2} + h_3 \qquad (8)$$

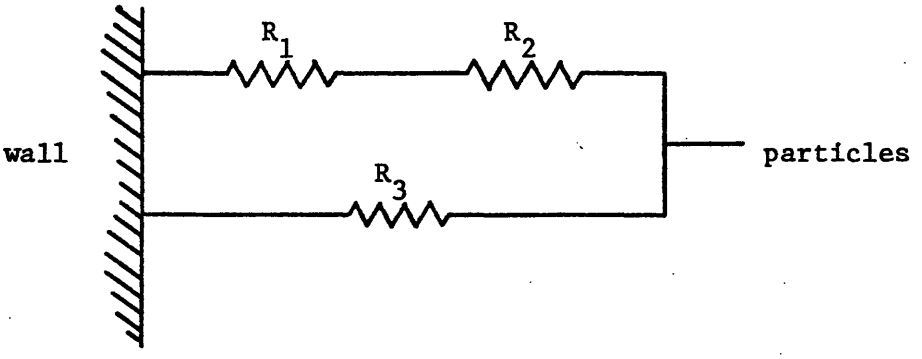

R_1 = Resistance through boundary layer (conduction).

R_2 = Resistance between gas and particles (emulsion).

R_3 = Resistance from wall to particle by direct contact.

where resistance (R) = $\frac{T_1-T_2}{q}$, or for a surface to a liquid,

$$R = \frac{1}{A\ h}$$

RESISTANCE TO HEAT TRANSFER
schema for model of Section II.2.1

Figure 1

The first term can be controlled by either effect 1 or 2, but may be obscured by the second term (effect 3), depending upon h_3's relative magnitude.

Consider transport from a vertical wall (see Fig. 2). With the main velocity component parallel to the wall (x direction), assume that normal particle velocities (y direction) are proportional to the root mean square of the y directional fluctuational velocity ($\tilde{v}'$). In fact, for this simplistic order of magnitude approach, assume that particles have small enough inertial forces such that the velocities are equal to $\tilde{v}'$. This assumption is supported by the studies of several investigators. A summary of some of their investigations can be found in reference 9. According to Davies [10], for isotropic turbulence,

$$\tilde{v}' = (\nu P_m)^{1/4} \tag{9}$$

where P_m is the power/unit mass, and is proportional to the air velocity in the x direction. Consequently,

$$\tilde{v}' = V_p = (\nu g V_x)^{1/4} \tag{10}$$

Further assume that the frequency of these particles is identical to the eddy frequency ($\tilde{v}'/1$) where the characteristic length is the particle diameter, (d_p). Thus

$$f = \frac{\tilde{v}'}{d_p} = \frac{(\nu g V_x)^{1/4}}{d_p} \tag{11}$$

This frequency dependency is borne out by Mickley, Trilling, and Hawthorn's [11] data, in which they measured the frequency of surface renewal of glass particles as a function of particle size and fluid velocity. Fig. 3 illustrates the linearity between f and $V^{1/4}/d_p$ as

measured in Mickley's data. Here it is assumed that this V is the superficial velocity of the flowing air.

These three effects are discussed in the following sections and summarized in Table 1.

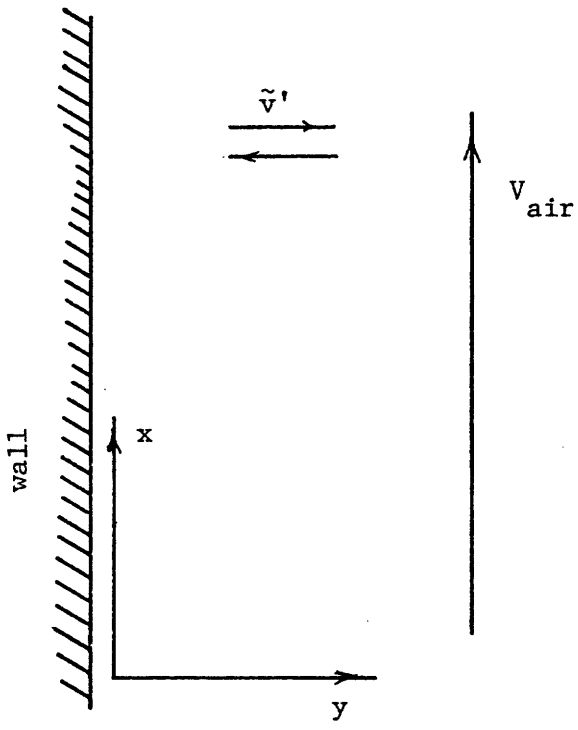

GEOMETRY FOR TRANSPORT FROM A VERTICAL WALL

Figure 2

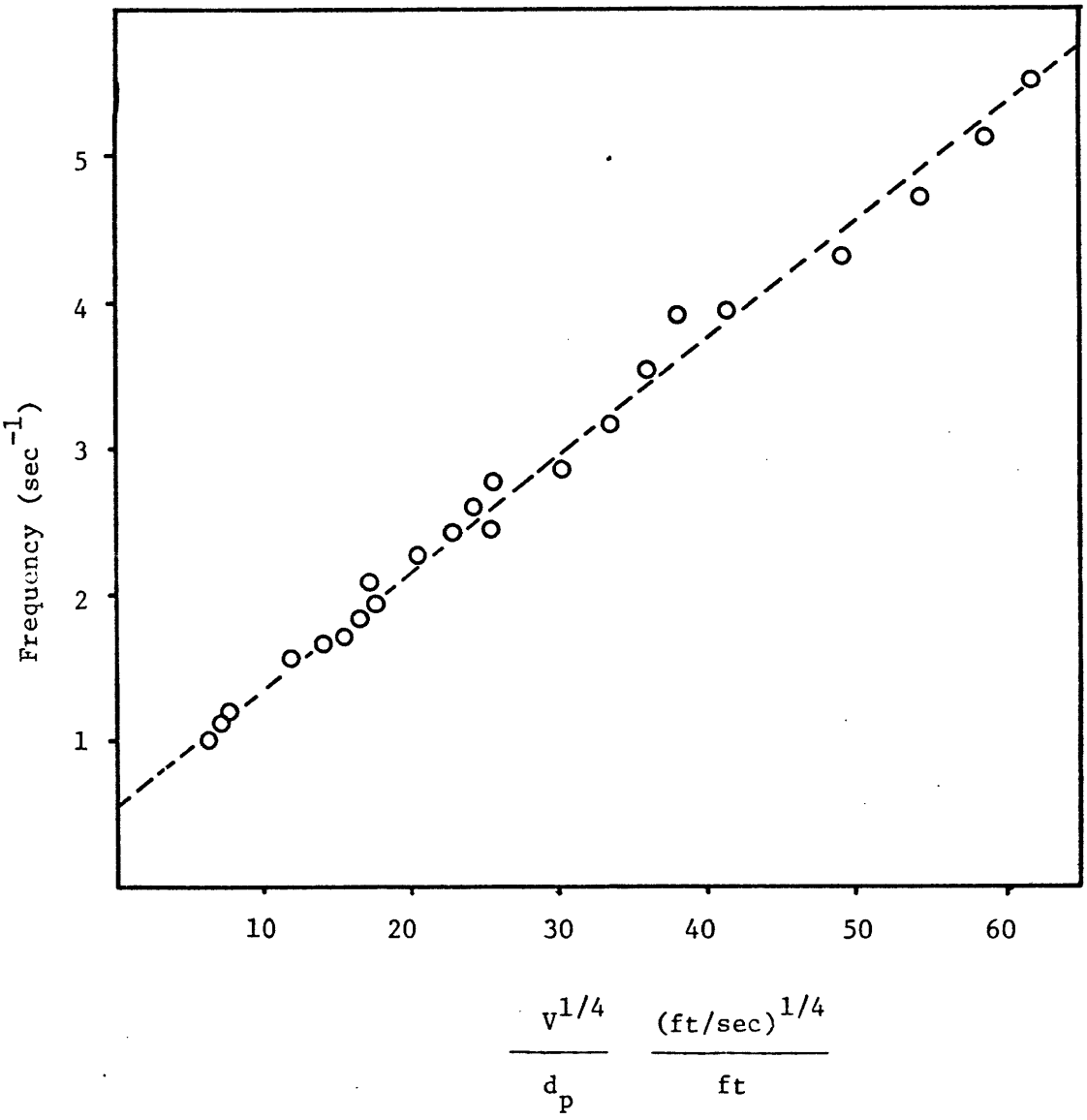

LINEAR RELATION BETWEEN FREQUENCY & $\frac{V^{1/4}}{d_p}$

from data of reference 11

Figure 3

II.2.2 Boundary Layer Destruction or Reduction

II.2.2.1 Static Model

First consider a simplistic example. Zabrodsky [12] notes that the mean air space thickness between a surface and spherical particles completely covering the surface is $d_p/6$. This mean thickness should increase as fewer particles touch the surface; in other words as the particle fraction $(1 - \varepsilon)$ decreases. Hence, an approximation of this thickness (δ) is:

$$\delta = \frac{d_p}{6\ (1 - \varepsilon)} \tag{12}$$

Since this heat transfer consists of conduction across a gas layer of this average thickness, the effective h averaged over the tube surface is

$$h_{1\ \text{static}} = \frac{k_g}{\delta} = \frac{6\ (1 - \varepsilon)\ k_g}{d_p} \tag{13}$$

Using parameters typical of the experimental data of Chapter IV, or

$\varepsilon = 0.6$, $d_p = 0.014"$, and air at 100°F ($k_g = 0.016$ BTU/hr ft °F)

$$h_{1\ \text{static}} = 33\ \text{BTU/hr ft}^2\ °\text{F} \tag{14}$$

This is the right order of magnitude of the measured h for a horizontal tube. However, inherent in this model is the fact that the boundary layer thickness is independent of time. The rate of particle impingement is not included in this model. The boundary layer thickness is assumed to be the minimum thickness rather than the time averaged thickness, which is essentially assuming infinite particle velocities. The model is a static one, and does not consider any dynamic effects of the particle

entering or leaving the boundary layer. One would expect some displacement of the boundary layer as the particle enters, and some mixing of the hot boundary layer fluid and cold core fluid as the particle departs. This static model hardly seems to model the dynamic situation within the bed.

II.2.2.2 Dynamic Model

The displacement of the boundary layer by the entrance of the particle is similar to the displacement of the boundary layer caused by the impingement of a gas stream upon a flat plate.

Gardon and Cobonpue [13] investigated flat plate cooling by the impingement of jets of air and recommend the relation

$$Nu_{avg} = 0.0286\ Re_a^{.625} \tag{15}$$

where

$$Nu_{avg} = h_{avg}\ x_n/k_g$$

$$Re_a = V_a\ x_n\ \rho_g$$

x_n is the spacing between nozzles and V_a is the arrival velocity of air, assuming the plate is not present.

Extending this analysis to the fluidized condition, assume that x_n is the average spacing between particles, and V_a is the velocity of the particle ($\tilde{v}'$) normal to the wall. Assuming a uniform voidage throughout the bed and a hex pack formation of particles, x_n can be shown to be (Appendix 1).

$$x_n = d_p \left(\frac{\pi\sqrt{3}}{8\ (1-\varepsilon)}\right)^{1/3} \tag{16}$$

Substituting equations 10 and 16 into 15 yields an effective h of the entering particles of:

$$h_{1\ enter} = 0.0286\ \frac{k_g}{x_n}\ \left(\frac{V_p\ x_n\ \rho_g}{\mu}\right)^{.625} \tag{17}$$

$$= 0.03 \frac{k_g(1-\varepsilon)^{1/8}}{d_p^{.375}} \left[\frac{(\nu\, g\, V_g)^{1/4}\, \rho_g)}{\mu}\right]^{.625} \qquad (18)$$

Assuming air properties at 100°F, a particle fraction $(1 - \varepsilon)$ of 0.4, A particle diameter of 0.014", and a V_g of 2 ft/sec (approximately the velocity needed to attain a particle fraction of 0.4),

$$h_{1\ enter} = 0.63\ \text{BTU/hr ft}^2\ °\text{F} \qquad (19)$$

Therefore this effect is negligible.

Part of the boundary layer will adhere to the particle as it leaves the surface. This effect strips the surface of the boundary layer, thereby enhancing the local h. Mikic and Rohsenow [14] employ a similar model in describing the boundary layer stripping caused by the departure of a bubble from a surface in boiling. In nucleate boiling the augmentation in heat transfer is due primarily to the disturbance of the boundary layer by the bubble departure, not the phase and enthalpy change going from liquid to vapor. Hence this model is applicable to the fluidized bed case, assuming the particles strip off the gas boundary layer in much the same manner as gas bubbles do the liquid layer. Mikic and Rohsenow assume that the area of influence is equal to $\pi\, d_b^2$. With this they deduce that the average h over the area of influence would be:

$$h_{1\ exit} = \frac{q}{A\Delta T} = \frac{2\, k_1}{\sqrt{\pi \alpha_1}} \sqrt{f} \qquad (20)$$

and assuming the areas of influence do not signify overlap, the average effective h over the whole boiling surface is:

$$h_{1\ exit} = 2\sqrt{\pi\ k_1\ \rho_1\ C_1\ f}\qquad d_b^{\,2}\ \ n \tag{21}$$

where n is the number of active sites per unit area of the heated surface, and the subscripts b and 1 in both relations refer to the bubble and fluid respectively.

If it can be assumed that the area of influence remains the same, these relations may be extended to the fluidized particle leaving the surface by changing liquid and bubble properties to gas and particle properties. In the fluidized case, the active sites per unit area (n) is interpreted to be the number of collisions per unit area, and can be shown to be (appendix 2)

$$n = \frac{8}{\sqrt{3}\ d_p^{\,2}}\quad \left[\frac{1-\varepsilon}{\pi\sqrt{3}}\right]^{2/3} \tag{22}$$

assuming the void near the wall is the same as in the bed core.

However, relation 21 is valid only when the areas of influence do not strongly overlap, or when $x_n \geq 2d_p$. Using equation 16 for x_n, this is true when

$$1-\varepsilon \leq \frac{\pi\sqrt{3}}{64} = 0.085 \tag{23}$$

or at very small particle fractions. Consequently, in fluidized beds with particle fractions larger than this the surface is one large area of influence, and has an effective h as in relation 20. It may be questioned as to whether the area of influence is as large as assumed. Assuming a smaller area of influence may reduce the fraction of total wall surface area which is included in an area of influence. For example, if it is assumed that the area of influence is half that of before, or

$\pi\ d_p^2/2$, the areas of influence will not strongly overlap when $x_n \geq \sqrt{2}\ d_p$. Again using equation 16, this is when

$$1 - \varepsilon \leq .24 \tag{24}$$

Therefore assuming this smaller area of influence, the entire wall will behave as an area of influence so long as the void (ε) remains below .76. The use of equation 20 will yield the h for this model so long as the entire wall behaves as an area of influence.

Using equation 11 for f, equation 20 reduces to

$$h_{1\ exit} = 2\left[\frac{k_g\ \rho_g\ C_g\ (g\nu\ V_g)^{1/4}}{\pi\ d_p}\right]^{1/2} \tag{25}$$

For the same condition as in equation 19, i.e., $d_p = .014"$, $V_g =$ 2 ft/sec, and air properties at 100°F,

$$h_{1\ exit} = 18.7\ \text{BTU/hr ft}^2\ °\text{F} \tag{26}$$

The estimation of the dynamic effect of particles entering and leaving the boundary layer on the effective wall h is the sum of equations 18 and 25. For the specific values considered, the effective h attributable to these effects is 19.3 BUT/hr ft^2 °F. The 'dynamic' effective h is 60% of the static model (equation 14).

Both the simplistic (static) and 'dynamic' models underestimate the measured h for a horizontal tube. This underestimation is further increased by recognizing that h for a vertical wall should be greater than that for a horizontal tube, as the entire surface of the tube is not active and the average tube h includes the effect of the low h regions.

II.2.3 Transient Heating of Particles Passing Through a Gaseous Heated Region

Here is considered the order of magnitude effect on the heat transfer caused by particles being transiently heated while passing through a heated gaseous region of thickness δ, rebounding off the heat transfer surface, and traveling back through the region (see figure 4). Several assumptions are made:

1. $V_p = \tilde{v}' = (g\nu V_a)^{1/4}$ (as in section II.2.1)
2. elastic collision at the wall
3. T_g within the layer δ varies linearly from T_w to T_b
4. $Nu_p = 2$, i.e. $h_p = k_g/d_p$

hence, on a particle basis,

$$dq_p = h_p A_p d(T_g - T_p) \tag{27}$$

where

$$T_g = - \frac{T_w - T_p}{\delta} x + T_w \tag{28}$$

assuming $d(T_w) = 0$, and that $d(T_p)$ is small, this yields:

$$d(q_p) = \frac{h_p A_p}{\delta} (T_w - T_p) dx \tag{29}$$

or

$$q_p = 2 \int_o^\delta \frac{h_p A_p}{\delta} (T_w - T_p) dx \tag{30}$$

Now if δ is about the same size as d_p, A_p will be much less than the total particle surface area. Assume $A_p = \pi d_p^2/4$, or 1/4 of the total surface area. This, with the assumed value for h_p yields:

$$q_p = k_g \frac{\pi d_p}{\delta} (T_w - T_p) \left. x \right|_o^\delta = \pi k_g d_p (T_w - T_p) \tag{31}$$

To check the assumption that dT_p is small, an energy balance gives

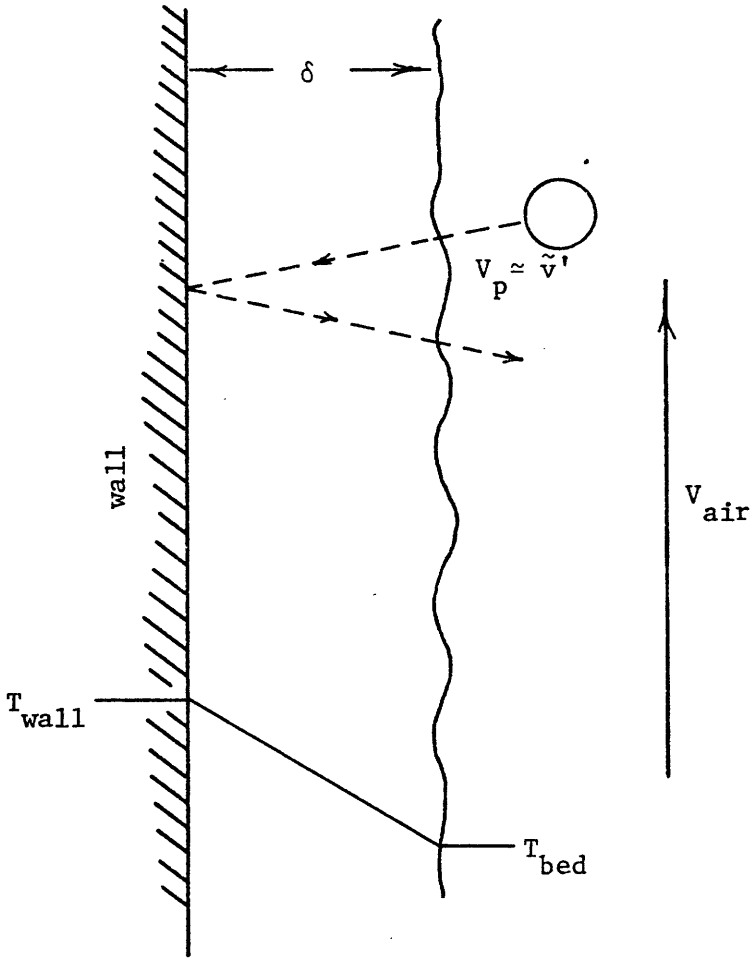

MODEL OF EFFECT #2

Figure 4

$$q_p = \pi k_g d_p (T_w - T_p) = C_p \rho_p \frac{\pi d_p^3}{6} \frac{\Delta T_p}{t} \tag{32}$$

where $t = \frac{2\delta}{\tilde{v}'} = \frac{2\delta}{(g\nu V_g)^{1/4}}$ (33)

therefore $\Delta T_p = \frac{12 k_g (T_w - T_p) \delta}{C_p \rho_p d_p^2 (\nu g V_g)^{1/4}}$ (34)

For properties of sand and air at 100°F, an air velocity of 2 ft/sec, and assuming that $\delta = d_p$,

$$\Delta T_p = .0043 (T_w - T_p) \tag{35}$$

which is indeed small. The effective heat transfer coefficient for the heated surface due to this effect is:

$$h_2 = \frac{q}{A_w \Delta T} = \frac{q_p n_p}{A_w (T_w - T_p)} \tag{36}$$

where n_p is the number of particles involved in the interaction.

$$n_p = A_w \delta(1 - \varepsilon) \frac{6}{\pi d_p^3} \tag{37}$$

therefore substituting equations 32 & 37 into 36 yields:

$$h_2 = \frac{6 (1 - \varepsilon) k_g \delta}{d_p^2} \tag{38}$$

Assuming properties as in prior sections,

$$h_2 = 32.9 \text{ BTU/hr ft}^2 \text{ °F} \tag{39}$$

Note that h_2 increases linearly as the considered δ increases. If, in fact, δ is much larger than d_p, the A_p in equation 27 is no longer

as small as $\pi d_p^2/4$ and ΔT_p may become significant. With the assumption that for the particle, $Nu_p = 2$, for air and sand properties, the Biot modulus = $h_p\ d_p/k_p = 2\ k_g/k_p \simeq 1/15$. Hence it may be assumed that the sand particle is essentially isothermal.

Applying transient analysis to a lumped sand particle yields:

$$\frac{T_g - (T_p + \Delta T_p)}{T_g - T_p} = \exp\left(-\frac{A_p\ h_p}{V_p\ \rho_p\ C_p}\ t\right) \qquad (40)$$

where $t = 2\delta/\tilde{v}'$, $h = 2\ k_g/d_p$ and for a sphere, $V_p/A_p = d_p/6$. Combining these, and assuming a mean T_g of $(T_w + T_p)/2$ yields:

$$\Delta T_p = 0.5\ (T_w - T_p)\ \left[1 - \exp\left(-\frac{24\ k_g\ \delta}{d_p^2\ \rho_p\ C_p\ (g\nu\ V_y)^{1/4}}\right)\right] \qquad (41)$$

for which ΔT_p is still small until δ gets large. Employing equations 36, 32, 37, and 41, the corresponding effective wall h is:

$$h_2 = .25\ C_p\ \rho_p\ (1 - \varepsilon)\ (g\nu\ V_g)^{1/4}\left[1-\exp\left[-\frac{24\ k_g\ \delta}{d_p^2 \rho_p\ C_p\ (g\nu\ V_y)^{1/4}}\right]\right] \qquad (42)$$

for a $\delta = 5\ d_p$ and properties as used before, this yields

$$h_2 = 161\ \text{BTU/hr ft}^2\ ^\circ\text{F} \qquad (43)$$

This h_2 is very dependent upon the assumed δ or the emulsion thickness. Emulsion layers smaller than d_p physically don't make sense, as they imply a 'package' of particles less than a particle thick. As the emulsion model envisions a packet of particles behaving for a short period of time as a separate entity from the bed core, one would expect the emulsion to be at least several particles thick or have a minimum thickness somewhere in the range of the mean free particle path. By considering equation 8, the analysis of section II.2.3, and ignoring

h_3, h_2 dominates only when the emulsion thickness is small so as to have no physical meaning; and is of virtually no consequence to the h_{net} when the thickness is of a practicle size. This being the case, the model is irrelevant to the heat transfer mechanism.

II.2.4 Direct Thermal Interaction Between Particle and Wall

In this mode, the particle is transiently heated by direct contact with the wall. The time of contact is approximated, assuming an elastic collision, by the time necessary for the compression wave to travel the length of the particle and return. Consequently,

$$t = \frac{2\, d_p}{V_{sound}} \tag{44}$$

where V_{sound} of fused silica is about 10500 ft/sec. For lack of a quantitative figure for the contact resistance between the particle and wall, assume zero contact resistance, and conduction through a contact area or diameter $d_p/10$ and across the mean distance of the particle, $d_p/2$. Consequently,

$$q_p = \frac{\pi}{200}\, K_p\, d_p\, (T_w - T_p) \tag{45}$$

These assumptions are very generous, and the results should be viewed as an upper limit which is impossible to achieve. By an energy balance,

$$q_p = \rho_p\, C_p\, \frac{\pi d_p^{\,3}}{6}\, \frac{\Delta T_p}{t} \tag{46}$$

and assuming ΔT_p is small so as not to affect $(T_w - T_p)$ in equation 45, these two equations may be related to yield ΔT_p.

$$\Delta T_p = \frac{6}{200}\, \frac{K_p\, (T_w - T_p)\, t}{\rho_p\, C_p\, d_p^{\,2}} \tag{47}$$

Using t from equation 44 and particle values employed in prior sections yields

$$\Delta T_p = 2.13 \times 10^{-8}\, (T_w - T_p) \tag{48}$$

Hence the assumption of ΔT_p being small is realized. The net q from the wall is

$$q_{net} = q_p \; n \; A_w \tag{49}$$

where n is the number of paticles per unit area, as in section II.2.2.2, and hence the effective wall h can be determined from

$$q_p \; n \; A_w = h_3 \; A_w \; (T_w - T_p) \tag{50}$$

Using equations 22 & 45,

$$h_3 = .0234 \frac{k_p}{d_p} (1 - \varepsilon)^{2/3} \tag{51}$$

and by using comparitive values as before:

$$h_3 = 5.43 \text{ BTU/hr ft}^2 \text{ °F} \tag{52}$$

As noted before, this effective h is an impossible upper limit because of the assumption of no contact resistance between the wall and particle. The inclusion of contact resistance will greatly diminish the value of h_3.

Consider now equation 7 of section II.1. Using the particle and fluid values consistant with those used throughout sections II.2.2 - II.2.4 and assuming that $l_e \simeq 2d_p$, equation 7 states that conduction through the film layer ($h_{1 \text{ static}}$ or $h_{1 \text{ dynamic}}$) dominates when

$$\bar{t} < 1.18 \text{ seconds}$$

where $\bar{t}$ is the residence time of the emulsion layer. Using equation 11, and assuming that $\bar{t} = 2/f$,

$$\bar{t} = \frac{2 \; d_p}{(g\nu \; V_x)^{1/4}} \tag{53}$$

and again for values consistent with sections II.2.2 - II.2.4, this yields

$$\bar{t} = 7.16 \times 10^{-3} \text{ sec.}$$

for the residence time of a sand particle with $d_p = .014"$, and $V_x = 2$ ft/sec. Hence the values in the order of magnitude analysis satisy the condition

for conduction dominance of equation 7, and from equation 8 and the order of magnitude of h's, h_1 clearly dominates. Equation 7 also states that the emulsion layer dominates only with large residence times -- times which are unrealistally large for fluidized beds. This is further evidence of the inconsequential nature of the emulsion model and its resistance.

II.2.5 General Formulation of h's from These Three Effects

From the analysis of sections II.2.2 - II.2.4, the general formulations of h_{1-3} are:

$$h_{1\ static} = 6\,\frac{k_g\,(1-\varepsilon)}{d_p} \propto \frac{(1-\varepsilon)}{d_p} \tag{54}$$

$$h_{1\ dynamic} \simeq \left(\frac{2\,k_g\,\rho_g\,C_p\,(g\,\nu\,V_g)^{1/4}}{\pi\,d_p}\right)^{1/2} \propto \frac{V_g^{1/8}}{d_p^{1/2}} \tag{55}$$

$$h_2 = 6\,\frac{(1-\varepsilon)\,k_g\,\delta}{d_p^{\,2}} \propto \frac{(1-\varepsilon)}{d_p} \tag{56}$$

$$h_3 = .0234\,\frac{k_g}{d_p}\,(1-\varepsilon)^{2/3} \propto \frac{(1-\varepsilon)^{2/3}}{d_p} \tag{57}$$

All show an increase in h with a decrease in particle size, and with the exception of $h_{1\ dynamic}$, a decrease in h with an increase in superficial air velocity (particle fraction decreases with increased velocity). However $h_{1\ dynamic}$'s dependency on V_g is not a strong one. Hence, without the inclusion of $h_{1\ dynamic}$ in the over-all h, or unless the contact resistance of h_3 is a function of V_g, it is difficult with this analysis to account for the initial rise in h with velocity which is characteristic of fluidized beds. The breakdown in this analysis at lower velocities may be in the assumption that particle velocities are equal to the eddy velocity of isotropic turbulence. At low superficial air velocities, and consequentially low voids, the particle fraction and interference between particles may be too high to allow particles to achieve eddy velocities.

This analysis also only considers particles interacting normal to the surface, and does not consider particles being swept up the surface by the vertical flow of air. However, it does establish the order of magnitude of h for the different modes of heat transfer.

The similarity in formulation of the different effects (equations 54 - 57) makes it difficult or impossible to experimentally separate the contribution of each. Surely specific effects predominate at different conditions of fluidization, particle densities, geometries, Reynolds numbers, etc. Because of the similarity in formulation, over a narrow range of variables, data can probably be well correlated by either Leva's thin film model or Mickley's packet model.

It must be noted that implicit in the formulation of the order of magnitude analysis is the assumption of heat transfer from a vertical wall. Horizontal tubes essentially have horizontal walls as well as vertical walls, and now the dominant mechanism for heat transfer can vary about the circumference of the tube.

II.2.6 A Second Model for Order of Magnitude Effects

The basic mechanism of section II.2.1 can also be modified to allow a different order of magnitude analysis. Here two effects are postulated:

1. Conduction of heat from the wall to discrete particles through a gas layer that is equal to the distance between the particle and the wall. This layer deminishes and then grows in thickness as the particle approaches, strikes, and recedes from the wall.

2. The discrete particle, in approaching the wall, displaces the hot gas at the wall. When the particle leaves the wall, unheated gas assumes the particle's position. This effect essentially creates a mixing of air at the wall surface, and is identical to the dynamic case of section II.2.2.2.

These effects are discussed the the following sections, and are summarized in Table 1.

II.2.6.1 Conduction to the Particle

The rate of heat transfer from the wall to a discrete particle is:

$$q = \frac{dQ_p}{dt} = \frac{k_g A}{L} (T_w - T_p) \ . \qquad (58)$$

Assuming that the length L is the average instantaneous distance from the wall to the near side of the particle, $L = x + d_p/6$, where x is the smallest instantaneous distance between the particle and the wall; and that A is the plane area of the particle,

$$\frac{dQ_p}{dt} = \frac{\pi\, k_g\, d_p^{\,2}}{4\,(x + \frac{d_p}{6})}\,(T_w - T_p)\ . \qquad (59)$$

Now, $(T_w - T_p) = (T_w - T_b - dT_p)$, where T_b is the bed temperature. For a particle approaching the wall from an initial distance D, $x = D - V_p t$, where V_p is assumed to be equal to $\tilde{v}'$ (equation 10). Therefore, assuming that dT_p is small,

$$Q_{p\ \text{approach}} = -\frac{\pi}{4}\,\frac{k_g\, d_p^{\,2}\,(T_w - T_b)}{V_p}\int_D^0 \frac{1}{x + \frac{d_p}{6}}\,dx \qquad (60)$$

$$Q_{p\ \text{approach}} = \frac{\pi}{4}\,\frac{k_g\, d_p^{\,2}\,(T_w - T_b)}{V_p}\,\ln\left(\frac{6D}{d_p} + 1\right) \qquad (61)$$

For the assumption that ΔT_p is small, $Q_{p\ \text{approach}} = Q_{p\ \text{recede}}$, therefore:

$$Q_{p\ \text{net}} = \frac{\pi}{2}\,\frac{k_g\, d_p^{\,2}\,(T_w - T_b)}{V_p}\,\ln\left(\frac{6D}{d_p} + 1\right) \qquad (62)$$

For heat rejection from the wall as a whole,

$$\frac{q_w}{A_w} = h_4\,(T_w - T_b) = \frac{n\,Q_p}{t} \qquad (63)$$

where n, the number of particle per unit area, is given by equation 22. Assuming that $t = 2/f$, (where f is the frequency of particles striking the wall, given by equation 11), yields

$$h_4 = \frac{n\,Q_p\,f}{2\,(T_w - T_b)} \qquad (64)$$

Substituting equations 22, 62, and 11 into 64 gives

$$h_4 = 1.17\ (1-\varepsilon)^{2/3}\ \frac{k_g}{d_p}\ \ln\left(\frac{6D}{d_p} + 1\right) \qquad (65)$$

It can be seen that h_4 increases as the value for D increases, but as the particle recedes farther and farther away from the wall, the path of conductance is broken by other particles. A reasonable value of D would be the mean interparticle spacing, x_n (equation 16). Using x_n for D yields:

$$h_4 = 1.17\ (1-\varepsilon)^{2/3}\ \frac{k_g}{d_p}\ \ln\left(\frac{5.27}{1-\varepsilon} + 1\right) \qquad (66)$$

For the same particle and gas properties as used in prior sections,

$$h_4 = 23\ \text{BTU/hr-ft}^2\text{-}^\circ\text{F} \qquad (67)$$

The actual value used for D is not critical. Doubling the value of D, so that $D = 2\ x_n$, only increases the value of h_4 by 24%.

II.2.6.2 Mixing of Gasses at the Wall

This effect is analogous to $h_{1\ \text{dynamic}}$ of section II.2.2.2, and is given by the sum of equations 18 and 25.

II.2.6.3 General Formulations of h's for this Model

From equations 55 and 66,

$$h_{1\ \text{dynamic}} \propto \frac{V_g^{1/8}}{d_p^{1/2}} \qquad (68)$$

$$h_4 \propto \frac{(1-\varepsilon)^{2/3}}{d_p}\ \ln\left(\frac{1}{1-\varepsilon}\right) \qquad (69)$$

The same relations as for the prior model are observed: h increases with decreased particle size; and for h_4, with increased particle fraction. Both of these effects act in parallel. Consequently, for this model,

$$h_{net} = h_4 + h_{1\ dynamic} \tag{70}$$

Since both h_4 and $h_{1\ dynamic}$ are both of the same relative magnitude, the value of D in h_4 has an even smaller effect on h_{net}. Doubling D will only increase h_{net} by about 12%.

Transient particle heating by direct wall contact (h_3, section II.2.4) could be also added to this but is left off because of the uncertainty of the contact resistance being small enough for h_3 to have any effect. The sum of the h_4 and $h_{1\ dynamic}$, ignoring h_3, for particle and gas properties consistent with this section, is:

$$h_{net} = 42\ BTU/hr\text{-}ft^2\text{-}°F \tag{71}$$

This is in good agreement with the value measured for horizontal tubes.

Table 1

Modeled Heat Transfer Effects

Effect	Model	Basic Assumptions	General form
$h_{1\ static}$	conduction through gas layer as means of heat transfer from wall to emulsion layer	minimum gas layer thickness equals $d_p/6$, and increases with void.	$\propto \frac{(1-\varepsilon)}{d_p}$
$h_{1\ dynamic}$	mixing of hot air in wall vicinity by particle entering & leaving region near wall	entering particle displaces boundary layer like an impinging gas stream. departing particles have an area of influence large enough to overlap	$\propto \frac{V^{1/8}}{d_p^{1/2}}$
h_2	particle transiently heated as passing through emulsion layer	elastic collision at wall, particle Nu = 2, temperature in layer varies linearly from T_w to T_b, ΔT_p is small, $V_p=\tilde{v}'$	$\propto \frac{(1-\varepsilon)}{d_p}$
h_3	particle heated by direct contact with wall	elastic collision, no contact resistance, contact area = $d_p/10$, ΔT_p is small	$\propto \frac{(1-\varepsilon)^{2/3}}{d_p}$
h_4	conduction to particle through gas layer whose thickness diminishes as particle approaches wall and grows as particle receeds	$V_p=\tilde{v}'$, ΔT_p is small	$\propto \frac{(1-\varepsilon)^{2/3}}{d_p} \ln\left(\frac{1}{1-\varepsilon}\right)$

Model 1: $h_{net} = \frac{h_1 \cdot h_2}{h_1+h_2} + h_3$

Model 2: $h_{net} = h_{1\ dynamic} + h_4$

II.3 Horizontal Tube Correlations and Experiments

II.3.1 Correlations

Vreedenberg [15] did probably the initial horizontal tube work, and worked with a bed 0.565 meters in diameter, 1.2 meters deep (in the non-fluidized state, and a single horizontal tube 0.85 meters above the distributer. Three tube diameters were used (0.664" - 2.0") and particle densities were varied from about 100 to 325 lbm/ft^3. Vreedenberg developed two correlations and uses the magnitude of a Reynolds type group ($G\ d_p\ \rho_p/\rho_g\ \mu$) to distinguish which correlation should be utilized. Such a Reynolds group is employed because of Vreedenberg's assumption that particle paths differ in gas currents in accordance with the predominance of viscous or inertial forces. Vreedenberg assumes that 'fine and light' particles will almost exactly follow the paths of the gas, while due to inertia, larger particles will follow paths less dependent upon the gas flow. If this be true, then one would also assume that the 'fine and light' particles would also achieve the eddy velocities as well, as in the analysis of section II.2.1. The transition region for Vreedenberg's data was determined to be between 2050 and 2550 for his Reynolds group number. Vreedenberg's correlation which applies to air fluidized particles of density equal to that of sand and greater than 7 mills in diameter is:

$$\frac{h\ d_t/k_g}{(C_g\ \mu/k_g)^{.3}} = 420 \left(\frac{G\ d_t\ \rho_p}{\rho_g\ \mu} \cdot \frac{\mu^2}{d_p^3\ \rho_p^2\ g} \right)^{0.3} \qquad (72)$$

This is the Vreedenberg correlation we are most interested in, as it applies to the particle densities and sizes which would be used in power plant heat rejection. In this correlation, Vreedenberg explains the factor ($\mu^2/d_p^3\ \rho_p^2\ g$) as being the ratio between a particle Froude groupe ($G^2/d_p\ \rho_g^2\ g$) and the square of the particle Reynolds group ($G\ d_p\ \rho_p/\rho_g\ \mu$). However, a quick juggling of Vreedenberg's dimensionless numbers shows that rather than having a Reynolds type group and a combination of particle Froude and Reynolds numbers, he has:

$$\frac{G\ d_t\ \rho_p}{\rho_g\ \mu} \cdot \frac{\mu^2}{d_p^3\ \rho_p^2\ g} = \frac{G\ d_t}{\mu} \cdot \frac{\mu^2}{d_p^3 \rho_g\ \rho_p\ g}$$

which is, assuming $\rho_p >> \rho_g$, the tube Reynolds number divided by the particle Archimedes number, where the Archidedes number is

$$Ar = \frac{d_p^3 \rho_g\ (\rho_p - \rho_g)\ g}{\mu^2} \qquad (73)$$

The Archimedes number is the ratio between the buoyancy forces. Unfortunately, the buoyancy forces as described in equation 73 are so small in comparison to the viscous forces that the inclusion of the Archimedes number becomes questionable. For example, in Vreedenberg's experiments, his tube Reynolds numbers were in the range of

$$0.455 < Re_t < 3200$$

while his Archimedes numbers were in the range of

$$2.72 \times 10^{-4} < Ar < 8.7 \times 10^{-4}$$

The buoyancy force experienced by a discrete particle can be significant, for it is buoyed up by the mean density of the bed, ρ_b, where

$$\rho_b = \varepsilon \rho_g + (1-\varepsilon) \rho_p .$$

The use of $(\rho_p-\rho_b)$ instead of $(\rho_p-\rho_g)$ in the Archimedes number would more accurately describe the buoyancy forces. Likewise, using Vreedenberg's explaination of Froude/Reynolds[2], the use of the Froude number is questionable. Vreedenberg acknowledges that this ratio is introduced into the correlation only because, with it, a good description of the experimental data can be obtained. It seems that Vreedenberg, in varying both his tube and particle diameters by a factor of three, found that h was proportional to $V^{\cdot 3}\ d_t^{-\cdot 7}\ d_p^{-\cdot 9}$, and merely used dimensionless parameters which provide these variables to the desired degree. His total scatter is not more than 29% as predicted by the correlation.

It is interesting to note that his correlation includes no effect of reduced particle fraction $(1-\varepsilon)$ which occurs with increased velocity. As indicated in the description of fluidized bed heat transfer mechanisms, both major models and all but one effect in the order of magnitude analysis account for a falling off of h with increased velocity after h has attained a maximum value. Recall that increased velocity increases the particle motion, but by expanding the bed, decreases the number of particles present, or the particle fraction. Vreedenberg's correlation, by not including such an effect, implies that by continually increasing velocities, one will continually increase

the h. Vreedenberg's recorded mass velocities of air and Leva's [16] relation between mass velocity and void fraction indicate that for the larger Reynolds group particles, Vreedenberg tested void fractions of less than 0.55. Consequently, the falling of h with larger voids was neither observed nor encorporated in his correlation.

Ainshtein [17] also ran experiments on a single horizontal tube. His tests were conducted in a 275 mm diameter bed with an initial (non-fluidized) bed height of 350 mm. Two tube diameters (22 and 30 mm) and three different diameters of sand particles (.0064", .0088", .0112") were used. His correlation is:

$$\frac{h\, d_p}{6(1-\varepsilon)\, k_g} = 0.96 \left(\frac{G\, d_p}{\mu\, \varepsilon} \right)^{0.34} Pr^{.33} \left(\frac{\alpha}{d_{bed}} \right)^{.16} \qquad (74)$$

where α is the distance between the tube and the distributer. Here the characteristic dimension used in the Nusselt number is the average fluid thickness between the heated tube wall and all the particles immediately surrounding the tube. For static spherical particles, this thickness is 1/6 of the particle diameter, and is assumed to increase in direct proportion with the decrease in particle fraction as the particles are fluidized (see $h_{1\ static}$, section II.2.2.2). The Reynolds group is based upon the particle diameter and the actual local fluid velocity. Actual fluid velocity is determined by dividing the superficial velocity by the void fraction. Ainshtein also found a slight dependence of h on the tube distance above the distributer -- increasing slightly with distance; but no

dependency on tube diameter.

Wender and Cooper [18] have provided a generalized relation:

$$\frac{h\, d_p}{k_g} = 0.01844\ Cr\ (1-\varepsilon)\left(\frac{C_g\ \rho_g}{k_g}\right)^{.43}\left(\frac{G\, d_p}{\mu}\right)^{.23}\left(\frac{C_p}{C_g}\right)^{.8}\left(\frac{\rho_p}{\rho_g}\right)^{.66} \qquad (75)$$

Although this relation is empirically arrived at from data of several investigations on vertical tubes in cylindrical beds, Bright and Smith [19] consider it useful in predicting h's. Note that the factor $(C_g\ \rho_g/k_g)$ is dimensional, and that Cr is a correction factor which varies with the location of the tube with respect to the bed axis. Here, as in the Ainshtein relation, h decreases with increased void (decreased particle fraction).

By inspection of the three correlations (equations 72, 74, & 75), one can determine the predicted dependency of h on various parameters: for the Vreedenber correlation:

$$h \propto \frac{V^{.3}}{d_t^{.7}\, d_p^{.9}}$$

for the Ainshtein correlation:

$$h \propto (1-\varepsilon)\left(\frac{V}{\varepsilon}\right)^{.34}\frac{1}{d_p^{.66}}$$

and for the Wender-Cooper correlation:

$$h \propto (1-\varepsilon)\frac{V^{.23}}{d_p^{.77}}$$

In general, the dependency of h is very similar to the order of

magnitude analysis summarized in sections II.2.5 and II.2.6.3; increasing with a decreasing particle size and fraction.

Similarities and differences between these correlations are worth noting:

Velocity: all three are dependent on velocity to about the same degree.

Particle diameter: Dependency varies, as the powers range from -.66 to -.9. It is of interest to note that Vreedenberg experimentally varied his particle diameter by a factor of 3, while Ainshtein varied particle diameter by a factor of 1.75. The generalized relation (Wender-Cooper) is compiled from data from many investigators, in which the particle diameter varies by a factor of 22.

Tube diameter: It is not surprising that the Wender-Cooper correlation is not dependent on tube diameter, as it is derived from vertical wall, and not horizontal tube, data. Of the two horizontal tube correlations, only Vreedenberg's relates h as a function of d_t. However, again Vreedenberg experimentally varied d_t by a factor of 3, while Ainshtein varied d_t by only a factor of 1.36.

Void and particle fraction: Only Vreedenberg's is not a function of particle fraction; both others are directly proportional to $(1-\varepsilon)$. As noted before, Vreedenberg apparently ran experiments in a fairly small range of voids, and hence found h to be independent of particle fraction. Note that the use of $1/\varepsilon$ in the Ainshtein correlation is only used to relate superficial velocity to a realistic inter-particle velocity.

Experimental data will be compared to these correlations in Chapt IV.

II.3.2 Other Horizontal Tube Experiments

Heat transfer coefficients also vary circumferentially about horizontal tubes. References 20 and 21 indicate that measured heat transfer coefficients are highest on the side of the tubes and lowest on the tops of the tubes. Upstream zone h's are small because a region of low particle concentration forms under the tube, and downstream zone h's are small because of a region of stagnant or slow moving particles. Gel'perin et al [22] showed that the relative magnitude of these h's change with fluidizing velocity. The lateral zones of the tube, where particle action is most vigorous remains about the same, while local h's in both downstream and upstream regions increase with velocity. Downstream values increased most rapidly.

Petrie et al [23], working on tube bundles in deep beds, proposed a correlation of their own, but found the data correlated well with Vreedenberg's single tube correlation. Petrie also found no adverse effect on measured h's caused by the proximity of the other tubes in the tube bundle. However, the minimum tube spacing for Petrie's case was approximately 43 particle diameters, which is probably more than the mean free path of the particles.

Lese and Kermode [24], measuring heat transfer from a horizontal tube in the presence of unheated tubes measured up to a 56% deterioration in h when neighboring tubes were brought into close proximity of each side of the heated tube. The maximum deterioration occured with a surface to surface tube spacing of 1/8", or a spacing to particle ratio of about 11:1. Tube diameters were 1.125". In close tube proximities, Lese and Keremode observed stagnant particles on top

of the tubes, and a stable gas pocket located between horizontally aligned tubes. This void was probably due to high local gas velocities and became more unstable with increased tube spacing; disappearing at separations of greater than one tube radius. Using Mickley and Fairbank's particle renewal theory, both stagnations above tubes and high voids resulting from close proximity of tubes cause a deterioration of h over what would be expected for a vertical wall in a fluidized bed. At best conditions, Lese and Kermode measured an overall heat transfer coefficient of 35 BTU/hr-ft^2-°F.

Bowman [25] visually observed fluidized bed flow with 1 or 2 rows of glass tubes. Viewing the particle action from the inside of a tube by means of a borescope, Bowman noticed three major flow conditions around the tube: a particle stagnation region on the tube tops, leading into a region of particles moving slowly down the tube, and finally, along the sides of the tubes, a region of very active particles.

From these works it is still uncertain as to what magnitude of h would result from shallow beds and whether any of the single tube correlations are applicable to a tube row in a shallow bed. However, they do imply that to attain the maximum possible heat transfer coefficient, the tubes must be kept a minimum distance apart and the entire tubular surface area must be kept active.

One fact should be noted. All correlations relate the heat transfer coefficient to other parameters by means of the Nusselt number. Consequently, in air fluidization, h's may be raised by

50% merely by increasing the conductivity of air by raising the bed temperature from 100°F to 500°F. Heat transfer coefficients should really be mentioned only in conjunction with bed temperatures or as a Nusselt number. This is of utmost importance when considering heat rejection from power plants. If one could achieve an h of 60-70 BTU/hr-ft^2-°F at a bed temperature of 100°F, a fluidized bed dry cooling tower would be strongly competitive with finned tube systems. However, if such an h required a bed temperature of 400°F, rejecting heat at this temperature would wreak havoc with the power plant's Rankine efficiency, and such a fluidized bed would be unacceptable as a heat rejection system.

III. EXPERIMENTAL PROGRAM

III.1 Introduction

An experimental rig was constructed in order to measure heat transfer coefficients from a horizontal tube to a shallow bed of fluidized sand. The sections of this chapter describe the apparatus, its design, its calibration, the means of measuring the variables, the test procedure, and the means of data reduction. Also included is an estimation of the error in measuring h.

III.2 Test Apparatus

Heat transfer measurements were made in a two foot square bed. A schema of the apparatus is shown in fig. 5. Air was delivered to the test section by coupling an electric motor with a Sturduvant Planovane Exhauster (Design 3, size 35). The electric motor was a Sprague Electric Works Dynomometer rated at 50 hp. and equipped with variable speed controls. Because of a limited ceiling height the exhauster discharged horizontally and the air stream was turned vertically by means of an elbow with turning vanes. This vertical flow was expanded to the test section size by means of a two 2-dimensional vaned diffusers designed in accordance with Renean's criteria [26] for no appreciable stall along the walls. The upper diffuser was twisted 90° with respect to the lower, essentially creating a 3-dimensional diffuser out of two 2-dimensional ones. Between the elbow and the lower diffuser and between the two diffusers were small straight sections with screens to establish relatively uniform flow conditions after each section. During assembly, a hot wire probe was traversed over each such straight section before attachment of the next uppermost section. This allowed adjustment of the screens at each section to correct major nonuniformities as far upstream as possible. Immediately

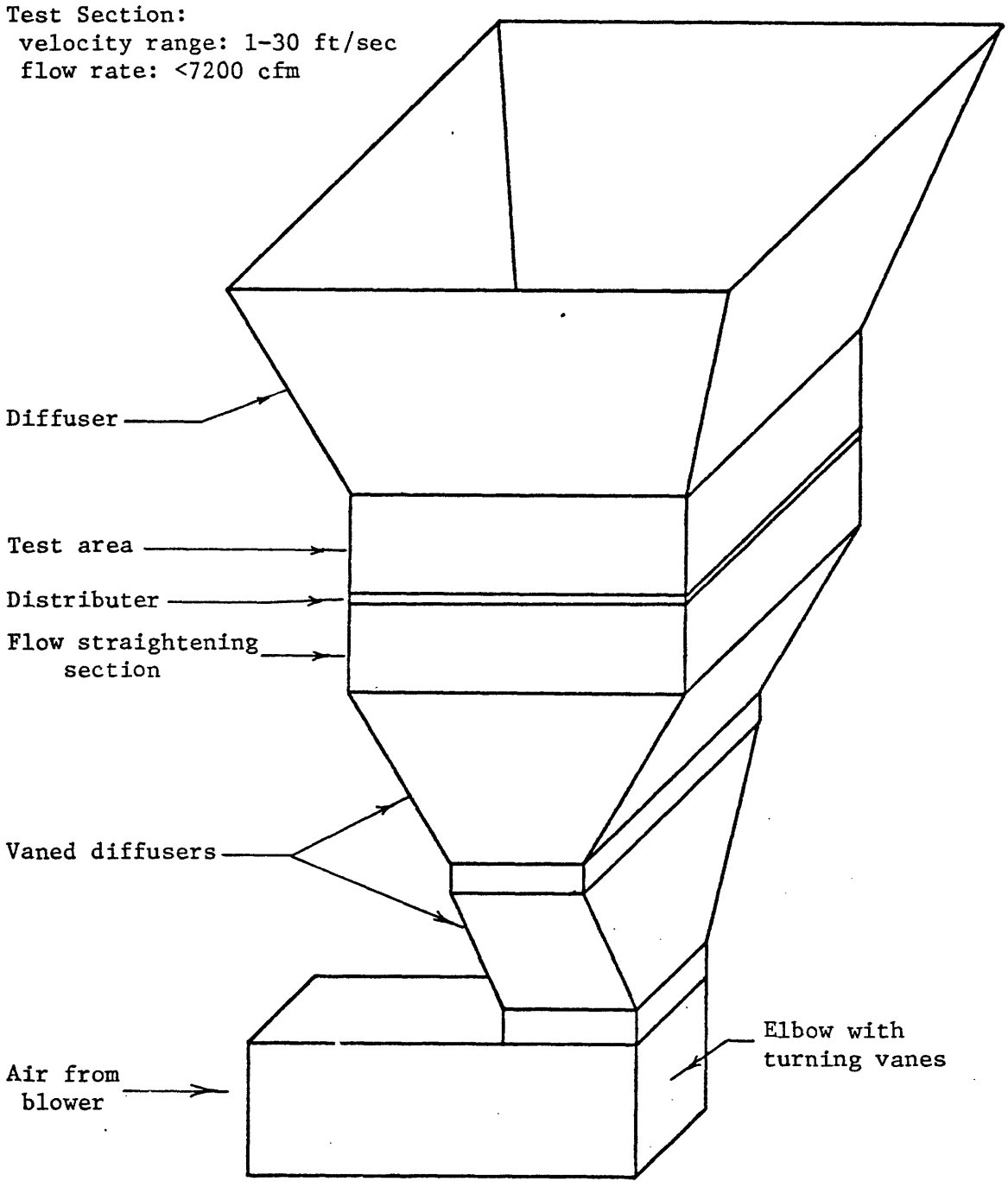

FLUIDIZED BED TEST SCHEMA

Figure 5

above the last diffuser was a flow straightening section, consisting of cloth restrictions, packed soda straws, and more screens. Air velocities across the flow straightening section were uniform to ± 6 - 8% when measured at velocities between 5 - 13 ft/sec. and measured by the hot wire probe. The distributer plate, located directly above the flow straightening section consisted of a 60 mesh brass wire cloth backed with one to two layers of cotton cloth. The cloth ensured an adequate pressure drop across the distributer to maintain bed stability. For tests on the effects of selective injection of air into the bed, areas of the distrubuter screen were blocked by placing masking tape on the upstream side of the screen. The unblocked sections formed slits, running the length of the tubes, immediately below the tubes. The distributer screen was exposed to both positive and negative vertical forces, as it is statically loaded by the weight of the sand when the blower is not in operation, and dynamically loaded by the flowing air when the blower is in operation. Rigidity was added to the screen by two means. Initially an "eggcrate" (fig. 6) made of 1" x 1/8" aluminum bar stock was placed immediately upstream of the screen, and the screen and its cloth backings strapped to the eggcrate structure by means of fine wire. Such a distributer performed well and was used for the uniform distributer tests, but changing screen blockage was a long and cumbersome process. Also with high blockage and high air velocities the strapping wire ruptured and the screen separated from the eggcrate. To provide greater rigidity under "dynamic" loading and easier screen access, the screen and backing cloths were sandwiched between steel bars (fig. 6). The three upper bars were kept thin (1/8" x 1/4") to minimize interaction with the fluidized particles. The three lower bars were 1/4" x 5/8" and provided the structural rigidity. Each upper bar was secured to the lower bar with five screws. This assembly

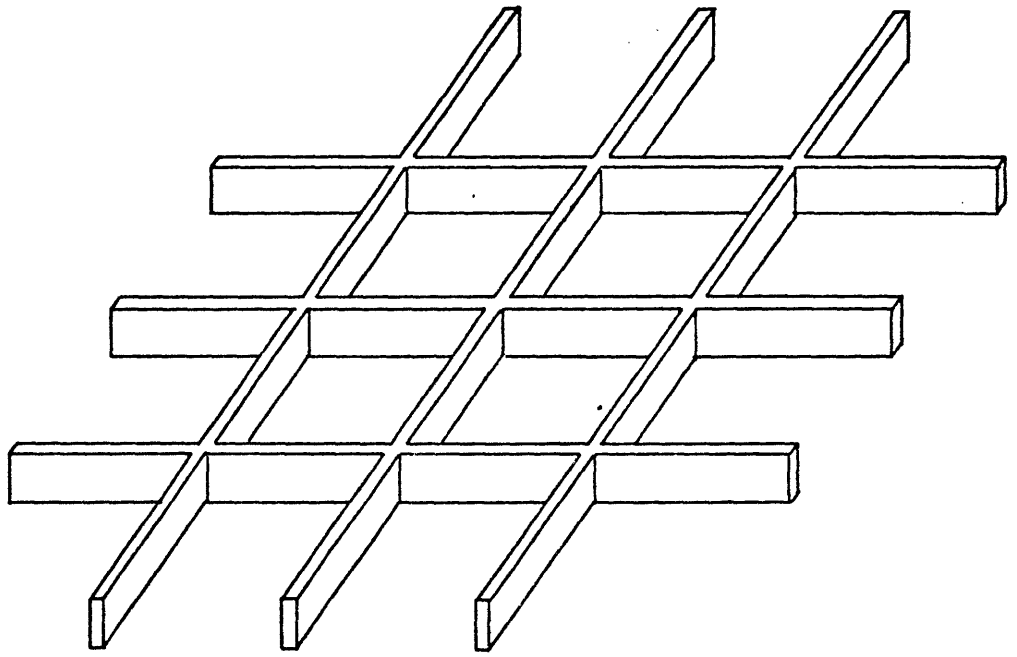

"Eggcrate"

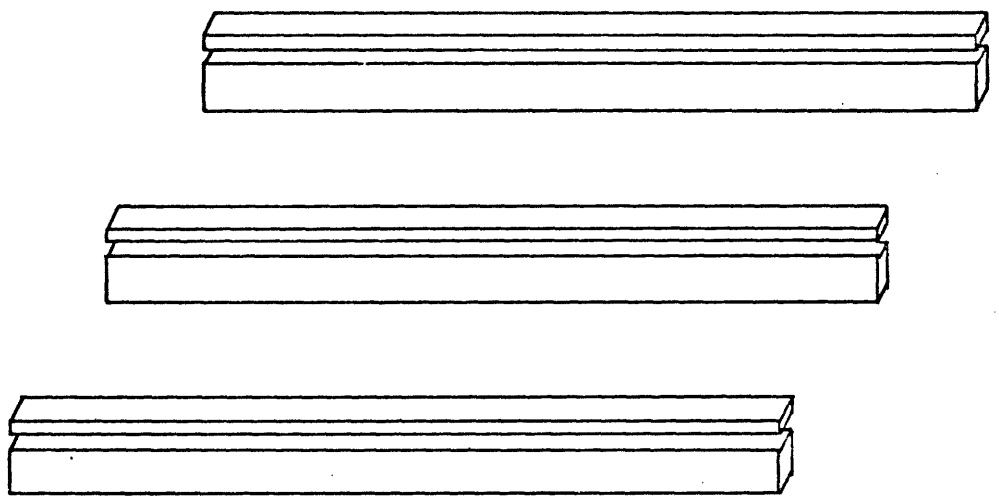

"Sandwich"

DISTRIBUTER SUPPORT STRUCTURES

Figure 6

provided adequate structural rigidity and allowed easy disassembly with a minimal interference with air or particle flow patterns. 3.1% of the test area is blocked by these supporting structures. In the second design, the bars were located beneath the blocked areas and no flow blockage occurred. The walls containing the fluidized bed were clear plastic. This allowed for easy and continual viewing of the bed's instabilities and flow patterns. Above the plastic walls was a third diffuser to catch entrained fines.

Fig. 7 illustrates the design of the instrumented heated tube used to measure the heat transfer coefficient in the fluidized bed. The tube is a full sized simulation of a pipe carrying water at 130-170°F; temperatures similar to those for a dry cooling tower. The tube length is divided into three sections. Each of the three sections is independently heated and instrumented, allowing the end sections to be used as guard heaters. To further provide thermal isolation, each section is separated by (1) a plastic spacer and (2) a steel spacer. The steel spacer provides structural continuity between the outer aluminum tubes and properly centers the ceramic heating core with a minimal amount of heat interaction. Less than 1% of the heat rejected to the bed is lost through both spacers. The tube is instrumented with a total of 19 thermocouples buried in the walls (9 in the center section), which lead out via groves on the interior of the aluminum tube. Fig. 8 illustrates the location of the 19 thermocouples in the instrumented tube. The instrumented tube can be readily removed and reinserted in the bed as all thermouples exit the tube from one end and electrical connections on the far end of the tube simply unplug.

Idealy, the instrumented tube should be at a uniform temperature.

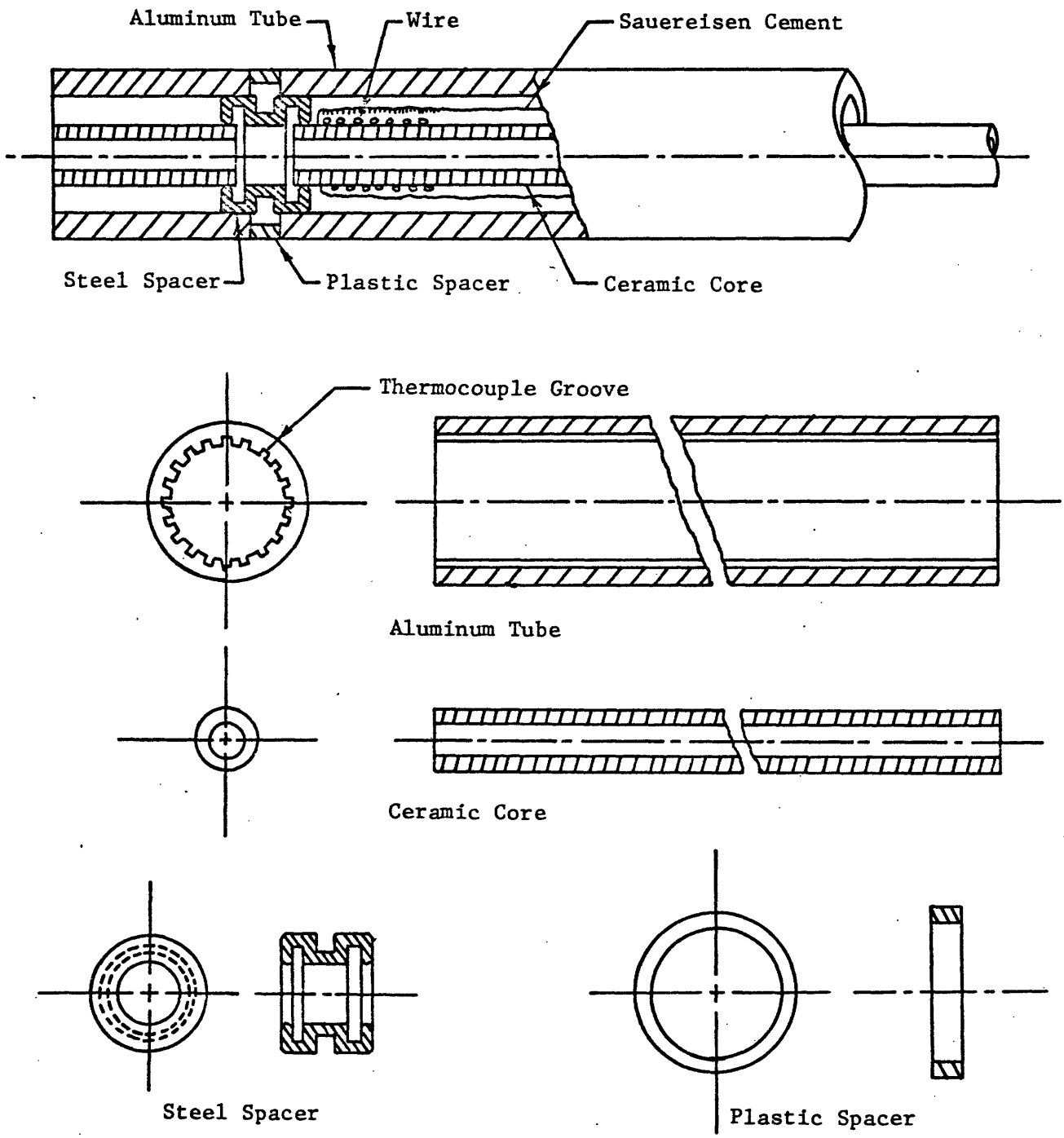

HORIZONTAL HEATED TUBE

-assembly drawing-

Figure 7

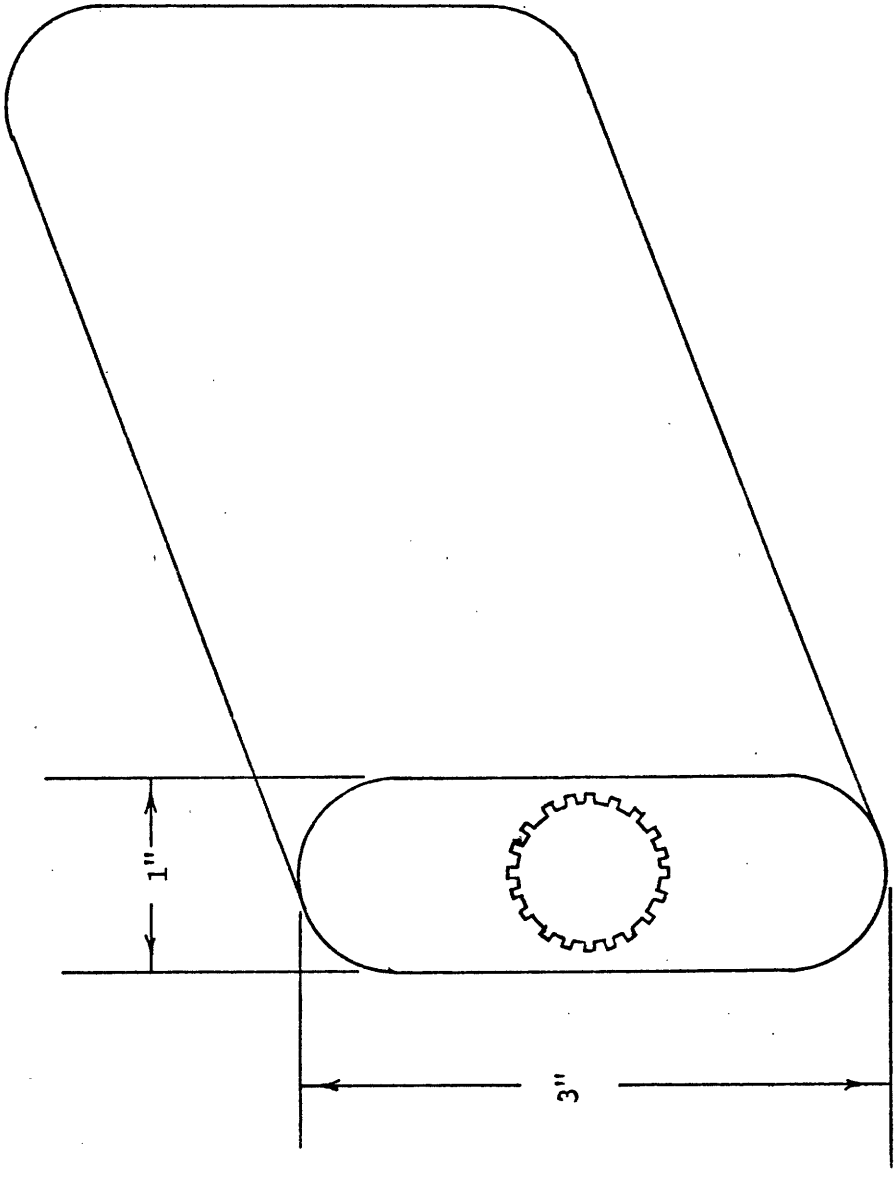

FLATTENED TUBE

Figure 8

This requires a small tube-to-bed Biot modulus (hL/k). The smaller the Biot modulus, the more isothermal the tube appears. A thick walled, high conductivity pipe was used to minimize the Biot modulus and consequently minimize any heating non-uniformities caused by the interior heating coils. Based on tube diameter and measured h's the Biot modulus is around 0.022. 3/4" schedule 80 pipe has an outer diameter of 1.050" and a wall thickness of 0.154". Thermocouple grooves are 0.050" deep, leaving a minimum wall thickness of .10". The flattened tube (fig. 8) used in later tests has the same interior details, but has overall dimensions of 1" x 3".

The electrical diagram for the section heaters is shown in fig. 9. Variacs allowed for individual adjustment of each section, and Simpson voltmeters and ammeters allowed for calculation of the wattage dissipated by the heaters, and subsequently the heat rejected to the bed.

The millivolt output of the 19 instrumented tube thermocouples and the thermocouple placed in the fluidized bed itself were measured by a Leeds & Northrup K-2 potentiometer.

The Disa 55A22 hot wire probe which was previously used for diffuser flow uniformity tests was placed upstream of the test section and calibrated to measure the superficial air velocity entering the test section. The hot wire was coupled with a Disa 55D05 CTA, and the voltage read on a precision voltmeter.

The fluidized particles consisted of Ottawa Standard sand, ASTM designation C-190 (20-30 mesh); and Graded Ottawa sand, ASTM designation C-109, which was graded to cuts of 30-40 mesh and 40-50 mesh. The mean diameter for these grades are .028", .020", and .014" respectively.

A simple water 'U' tube manometer measured pressure drops across the

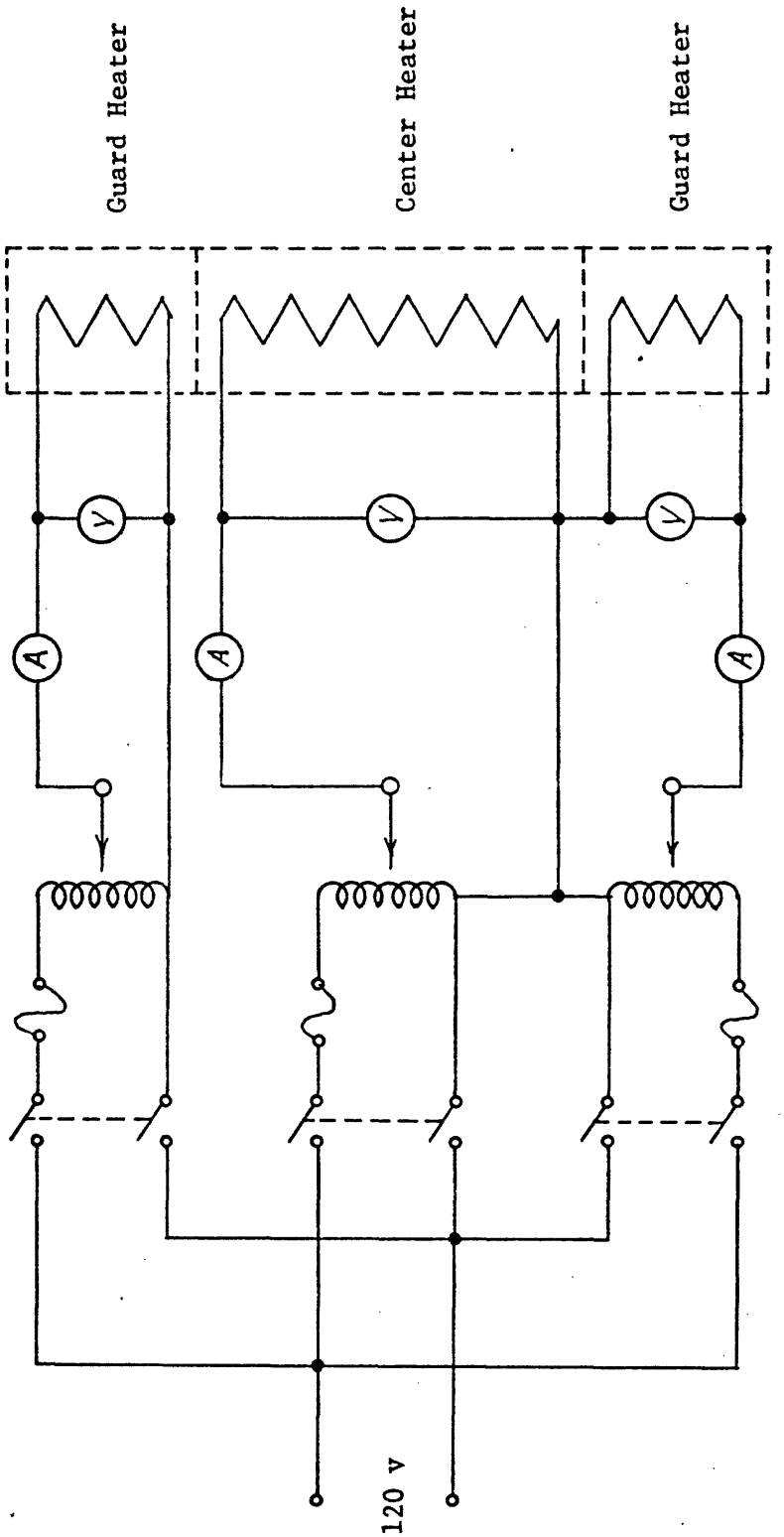

WIRING SCHEMA

Figure 9

distributer and fluidized bed. Pressure taps were located immediately upstream of the distributer, and in the plastic wall at a point above the level of the fluidized bed. Calibration runs were made without sand for each newly used distributer blockage and cloth backing combination so that the pressure drop resulting from the distributer could be separated from that resulting from the bed.

The calculation of a heat transfer coefficient is strongly dependent upon the temperature driving force, or the values of bed and wall temperature. If the bed is nonuniform in temperature, with temperature dropping with distance from the tube, the location of the bed thermocouple could affect the "measured" h. The closer to the tube, the lower the driving force, and the higher the h. Bed temperature was measured on either the far or near side of the adjacent dummy tube.

The temperature difference between these two locales was about 2°F. Comparing this temperature difference to the measured temperature difference between the tube and bed by $\Delta T/(T_w-T_b)$ shows that the measured h can vary by 4%, depending upon the location of the bed thermocouple. Assuming no bed mixing between tube regions, a simple energy balance indicated that for typical operating conditions the temperature difference between the two bed thermocouple locations should be 8-10°F. The presence of horizontal tubes are apparently not sufficient barriers to prevent particle motion, and the bed is, by in large, isothermal. Velocity distributions downstream of the bed were not measured due to the delicateness of the Disa hot wire probe. It was feared that sand particles impacting the probe would break the wire.

III.3 Calibration of Test Apparatus

Two items needed calibration: the hot wire probe and the distributer plate. It was also necessary to check the accuracy of the instrumented tube.

The hot wire was calibrated by placing it in a fully developed flow. Known velocities and fully developed flows were achieved by discharging a gasometer into a long straight tube. The tubular Disa probe has a maximum dimension of 7 mm, and tapers to the hot wire. The hot wire itself is stretched between two wire fingers extending from the tapered end. In order to minimize flow disturbances the tube flow area was made much larger than the maximum blockage caused by the probe body. With a tube inner diameter of 1.61" (2" pipe) this ratio of areas is slightly greater than 34:1. The probe was positioned axially along the tube to measure centerline velocity. Velocities were varied by changing the fall rate of the gasometer's displacement tank, and by varying the constriction resistance far upstream of the long tube. Flows were all in the turbulent regime, and centerline velocities were calculated using the relation

$$\frac{V}{V_{cl}} = \frac{2n^2}{(n+1)\ (2n+1)}$$

from reference 27. Here V is the average velocity, and n is a function of the Reynolds number. A curve fit of the data provides velocity as a function of the anemometer emf. As the hot wire was located in a narrower cross section upstream of the distributer, the hot wire was also calibrated to predict test section velocities from the higher upstream velocities. This was accomplished by correlating downstream anemometer emf's with upstream emf's.

Each distributer used was calibrated to determine its particular

pressure drop as a function of velocity. Since when running heat transfer measurements, the pressure drop measured was the sum of the bed and distributer pressure drops, such a calibration allows a separation of the two constituant pressure drops. Calibration was made by making runs without fluidized particles and measuring pressure drops for various velocities. Again, curve fitting pressure drop and velocity measurements allowed a continuous determination of pressure drop as a function of velocity.

The wire used for thermocouples was manufacturer precalibrated with an accuracy of $\pm$ .5% °F. In static tests at room temperature and in ovens, all thermocouples measured within .6 °F of each other.

The accuracy of the instrumented tube was checked by measuring natural and forced convection heat transfer coefficients and comparing them to accepted correlations for horizontal tubes.

With the low heat transfer coefficients achieved by natural or forced convection in air, the thermal resistance between tubes by the metal spacers, or out of the tube ends, is of the same order of magnitude as the resistance between the tube wall and the air stream. Hence heat leaks can easily and greatly affect the measurement of h's and the use of the two outside heaters as guard heaters to reduce the temperature difference between center and end sections is critical.

In the natural convection mode, the center section measured coefficient, corrected for radiation heat transfer, was 1.32 BTU/hr-ft^2-°F. Predicted convective heat transfer coefficients are 1.3 and 1.37 BTU/hr-ft^2-°F., using equations 8.67c and 8.63 of reference 28 respectively. These predictions straddle the measured value, and differ from it by less than 2 and 4%.

Measured values of h for forced convection correspond well with those predicted by equation 8.51 of reference 28. The measured convective h was 6.32 BTU/hr-ft^2-°F, while the predicted value was 6.23 BTU/hr-ft^2-°F; a descrepancy of less than 1.5%.

III.4 Test Procedure

The instrumented tube was placed in a row of dummy tubes in the test section. The dummy tubes generate the air and particle flow pattern of an actual operating tube row. A measured poundage of sand was added to the test section and the resulting nonfluidized bed depth measured. The blower was started, the superficial air velicity adjusted to desired levels, and anemometer EMF's recorded. The superficial air velocity is that velocity the air would have in the test area if no tubes or sand particles were present. Tube heaters were turned on and adjusted while approaching steady state such that temperature differences between the ends of the center tube and the adjoining ends of the guard heater sections were small. When no change in thermocouple output was observable for a period of time, steady state was assumed, and all thermocouple outputs were recorded. Also recorded were the pressure drop across the bed and distributer, and various bed depths. Bed depths were recorded as the maximum, mean and minimum height particles were achieving, as judged by the eye. The anemometer EMF was again recorded prior to system shutdown.

All tests were made with fluidization sufficient to cover the tubes. As the fluidized depth is a function of both sand poundage and void fraction, low sand poundage required larger voids (and thus larger velocities) for data taking. If poundage was sufficient to cover the bed in the non-fluidized state, data was taken at the lowest velocity which could sustain a uniformly active bed. Velocity was upper bound by elutriation of bed

particles and in some instances by vibrations set up by the motor-blower combination which corresponded to a natural frequency of the potientiometer's galvanometer.

Most of the heat leakage to the guard heaters is through the steel spacers. Due to the design of the spacers, the calculated resistance to heat transfer is 1.02 hr°F/BTU (see Appendix 3). Tests were made with a maximum discrepancy of 2°F between center and end tube thermocouples. Hence the heat leak per end was about 2 BTU/hr. Comparitively, assuming an air side h of 30, and a wall to bed temperature difference of 50°F, the heat rejected to the bed would be about 400 BTU/hr. The heat lost through both end spacers is about 1% of the heat rejected to the bed.

III.5 Estimation of Error

There exists a certain amount of inherent error in all measured data. Since h was determined by $h = q_{rej}/A(T_w-T_b)$, the error in the measured values of rejected heat, tube area, and wall and bed temperatures affect the error in the calculated h. Table 2 lists the errors in these variables, and of other measured quantities.

Error in q_{rej}

The accuracy of the meters measuring amperage and voltage (used in determining q_{rej}) is $\pm$ 2% of full scale deflection, or about 4% in the range of a half scale deflection, where runs were customarily made. Actually, q_{rej} = (amps x volts) - leaks, and as discussed in section III.4, the leaks were 1% of the product of amperage and voltage. By the method of reference 29 and as shown in appendix 4, the error in measured q_{rej} is 5.5%.

Error in tube area

Tube diameter as measured by a micrometer, varied by 0.4%, and consequently, the area has a 0.4% error band.

Error in $(T_w - T_b)$

Assuming both thermocouples have an accuracy of $\pm$ 1°F, by methods of reference 29, the temperature difference has an error of 1.4°F. Assuming a $(T_w - T_b)$ of 50°F, this is a 2.8% error. Including the additional variance of $\pm$ 1°F in the measurement of T_b (depending upon the thermocouple location), the error is 1.73°F, or 3.5% (see Appendix 4).

Net Error

The error of a result which is the product of several factors is the square root of the sum of the square of the errors in the individual factors (see Appendix 4). Consequently, the overall error in the measured h is:

$$\text{error} = (5.5^2 + 3.5^2 + 0.4^2)^{1/2} = 6.7\%$$

Error Induced by Local Variations in Wall Temperature

As discussed in the description of the test apparatus, the tube walls were made as thick as possible to maintain wall temperatures as uniform as possible. Testing the tube with natural convection, the wall temperatures were very uniform. The maximum temperature difference between any two thermocouples was 1°F, and seven of the nine were within 0.5°F. In a typical forced convection test, center section thermocouples had a maximum disparity of 4°F. Circumferentially, the thermocouples on the tube tops had an average temperature slightly higher than thermocouples on the tube side. Thermocouples on the tube bottom read 2-4°F lower than side or top thermocouples. In a typical fluidized bed run, the maximum disparity was 11°F, with typical difference from the averaged temperature of 3°F. As heat transfer coefficients rise and more wattage is dissipated through the heaters, heater anomalies and non-uniformities become more

evident.

The non-uniform temperature distribution is also due in part to variations in h's about the tube. One series of tests was made with the tube (1) operated in its normal position, and (2) rotated 90°. This maintained identical juxtaposition between thermocouples and heaters, but changed the orientation of the tube surface to the fluidized bed. Thermocouples previously on the top or bottom were now on the sides, and vice-versa. Thermocouples measuring a specific airstream location, say downstream tube temperature, measured different temperatures (by 2-4°F) than the thermocouple measuring the same airstream location with the tube rotated 90°. However, similar circumferential temperature distributions were apparent. Further, calculated h's were within 0.4 BTU/hr ft^2 °F, or 1.7% of each other, well within the error band.

Hence, temperature non-uniformities were due to (1) thermocouple error, (2) heater anomalies, and (3) variations in bed h's along the tube circumference. To include local variations in wall temperature in the estimated error, assume that this 1.7% error is due solely to an error in (T_w-T_b), and that it is additive to the other (T_w-T_b) errors. The error in (T_w-T_b) then becomes 5.2%, and the net error in h becomes

$$\text{error} = (4^2 + 4^2 + 5.2^2 + 4^2)^{1/2} = 7.7\%$$

The temperature non-uniformities were due to (1) thermocouple error, (2) heater anomalies, and (3) variations in bed h's along the tube surface. These errors are minimized by averaging the thermocouple temperatures, and maintaining wall temperature for the most part 50-60°F above the bed temperature.

Table 2

Error Sources

Item	Accuracy
Velocity	6-8%
Temperature	
Thermocouples	±1°F
Bed Location	±1°F
Wall Temperature Distribution	1.7%
Heat Rejection	
Amperage	2% (full scale)
Voltage	2% (full scale)
Leakage	1%
Tube Area	.4%
Pressure Drop Measurements	1/16 " of water

III.6 Data Reduction

Data was reduced by using the ME-CE Joint Computer Facility. The routine used reduced the raw data (thermocouple millivolt output, ammeter and voltmeter readings, anemometer voltage output, measured pressure drop, poundage of sand, and mean bed depth) to local wall temperatures, superficial velocities, fraction of pressure drop due to the distributer, test section friction power (hp/ft^2), and heat transfer coefficients. Conversion of thermocouple output was accomplished by using a curve fit of the tabulated values of copper-constantan's emf variation with temperature. A curve fit of anemometer emf variation with velocity was obtained by the hot wire calibration. The fraction of pressure drop due to the distributer was calculated by knowledge of the total pressure drop, the superficial velocity and the pressure drop across the distributer (without particles) for that velocity. The latter was obtained by calibration of each individual distributer. Friction power was determined, knowing the pressure drop, the air velocity, and the air side area. Heat transfer coefficients were determined using

$$h = \frac{q}{A_a (T_w - T_b)} \quad .$$

Here q is easily determined from heater wattage, and taking the circumferential average of tube temperature as T_w. Refering to fig. 10, the circumferential temperature average about the tube center would be

$$T_{w\ avg\ cent} = \frac{T_p + 2(T_{10}) + T_{11}}{4}$$

Radiation effects were taken into account, assuming an aluminum emmisivity of 0.09, but at the operating temperatures, such effects comprise less than 1% of the measured gross h, and are really insignificant. As discussed

in the error analysis, the confidence limits on h are 7.7%.

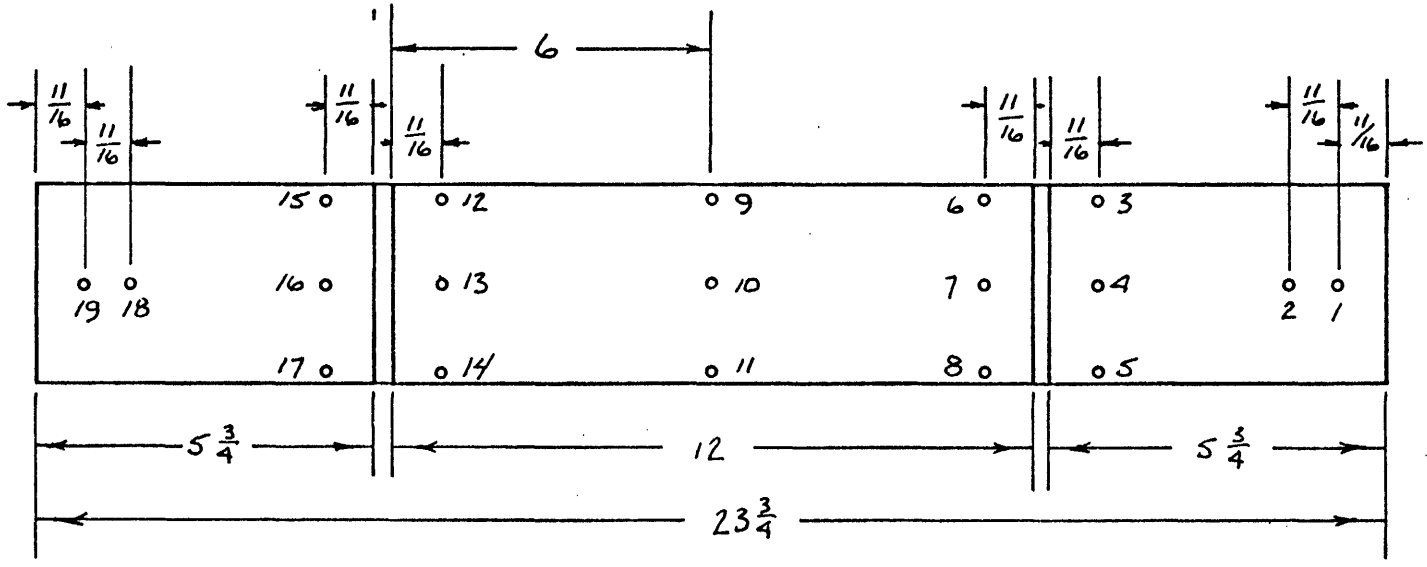

Guard Heater Center Heater Guard Heater

LOCATION OF THERMOCOUPLES

in test piece

Figure 10

IV Results of Experimental and Economic Studies

IV.1 Introduction

In this chapter are the results of the experimental phase. The sections deal with the reasons why various distributer and tube geometries were tested, qualitative results of these geometries, quantitatively with how h's measured from these different geometries varied between geometries and with the superficial velocity, and how experimental results compare with correlations. The last section deals with an economic evaluation of the use of a fluidized bed as a power plant dry cooling tower.

IV.2 Choice of Various Distributer Geometries and Qualitative Results

Initially data was taken with two rows of dummy tubes in a triangular stagger, with the instrumented tube in either the upper or lower rack. However, if all the tubes of one row were heated, the effectiveness would already be sufficiently large that doubling the number of heated tubes would not double the increase in the air temperature rise through the heat exchanger (see Appendix 5). Hence using two tube banks rather than one would effectively double the cost expenditure without doubling the net rate of heat rejection. Consequently, further experimental work was done with a single row of tubes, as it is more compatible with the heat capacity of the air.

As discussed in section II.3.2, the lower h's for horizontal tubes are attributed to particle stagnation areas on the top side of the tubes resulting in a smaller fraction of the surface area being exposed to the actively fluidized bed than is the case with a vertical wall. The problem is also heightened by the use of tube rows, as the blockage of flow area by multiple tubes increases local velocities. In the case of tubes with

a pitch of 2, the actual flow area is half the superficial area, and the resulting local velocity is twice the superficial velocity. The variation in local velocities makes for nonuniform fluidization. The areas between tubes are fluidized at a higher void (due to higher velocities) than areas above or below the tube row. Particles find it difficult to fall back through the high velocity region, increasing the accumulation in the stagnant region behind the tubes. Particles tend to get swept through the tube rack, and failing to fall back between the tubes, are lost from the active tube-particle system. Establishing a preferential path for particles to recirculate back below the tubes could reintroduce particles to the system and increase the measured h's. Four major efforts were made in attempting to enhance particle recirculation. These methods were tried separately and in combinations, and resulted in the use of seven distributers and geometries. Following is the reasoning behind the use of each case, and a qualitative analysis of the results. Quantitative results are encorporated in section IV.3.

1. Screen blockage (fig. 11). Areas of the distributer were blocked off, leaving air access only directly below the tubes. Measurements were made with 1/2 and 3/4 of the total distributer area blocked. It was hoped the screen blockage would be beneficial in three ways:

a. the selective injection of air directly beneath the tubes could increase particle action on the underside of the tubes.

b. the blockage below the tubes would result in more uniform maximum air velocities, at least below and between the tubes.

c. the introduction of air by separate slits may result in a non-uniform velocity distribution between tubes, with the higher velocities near

the tube wall. The lower velocity area may allow sand particles to fall between the tubes into the stagnant blocked area.

Visual observations indicated no improvement of particle recirculation. Mounds of stagnant particles did accrue above the blocked regions. Such regions merely add static weight to the bed, and increase the apparent mean bed voidage, but do nothing for h enhancement. Heat transfer measurements show no improvement of coefficients due to screen blockage.

2. Placing a corrugated screen above the tube row (fig. 12). Entrained particles striking the screen would be given a horizontal velocity component, while the air would be allowed to pass through the screen. This could result in a particle stagnation point at the apex of the corrugation, directly above the spacing between the tubes. From this stagnation point, particles could conceivably recirculate by falling between the tubes. This effect may be enhanced by simultaneously using distributer screen blockage.

By blocking the corrugated screen at the apex, a stagnation point can be assured and would result in more uniform maximum velocities above and between the tubes. Complete particle containment has a secondary advantage. If recirculation can be assured with increased air velocity, the increased velocity increases the heat capacity of the air, which is shown in Appendix 5 to be a limiting factor in the fluidized bed heat flux.

Corrugated screen tests were only run on Bowman's [25] small bed, and all visual results were indeterminant. No particle circulation paths were obviously developed. Neither blocking the screeen (either over the tubes or over the open area) nor reorienting the apex (so that the apex was over the tubes or over the open area) visually changed flow patterns.

Subsequently, increasing the air velocity to elutriation levels merely held the particles against the corrugated screen, increased the pressure drop, and deminished the particle fraction about the tube to zero.

3. Vanes between tubes (fig. 13). Vanes between tubes in conjunction with distributer screen blockage could definitely establish separate upward and downward particle flow regimes.

Unfortunately, vanes showed no real improvement on fluidization. Visual tests run on Bowman's small bed showed that vanes would sometimes fill with stagnant particles and not always be active. At other times vanes would not be stagnant, but no particle circulation pattern was definitely established. Using the corrugated screen in conjunction with vanes also made no visual improvement in particle circulation.

Visual observations while making h measurements with vanes confirmed the observations made on the small bed. Also the magnitude of some of the measured h's deteriorated rapidly with increased velocity (see section IV.3, Fig. 20) with the use of vanes indicating that if re-circulation was occuring, it was not occuring fast enough. Either particle mobility was deminished by the presence of the vanes, or particle densities were deminished due to particle stagnation in the vanes.

4. Flattened tubes (fig. 14). Flattening the tubes should make them appear more as verticle walls. It does so by reducing the fraction of the tube relegated to the top, or stagnant area. Further, if one keeps the same air side area to frontal area ratio, the plane area blocked by the tubes is reduced. For the same superficial velocity, this reduces the between tube velocity, and should aid recirculation by making it easier for particles to fall between tubes.

Due to size considerations of the heating elements, the flattened instrumented tube had the same interior dimensions as the round tube, and externally was 1" wide and 3" high. Measured h's were the same magnitude as that for 1" diameter round tubes.

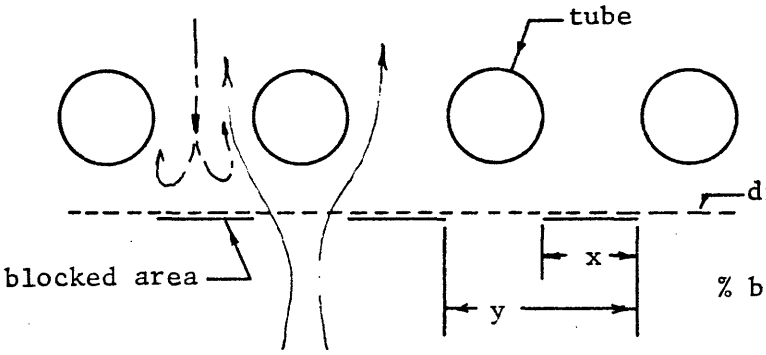

Figure 11

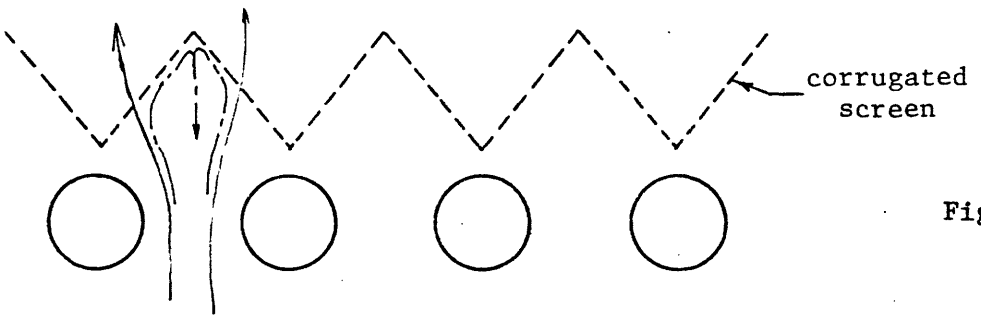

Figure 12

Figure 13

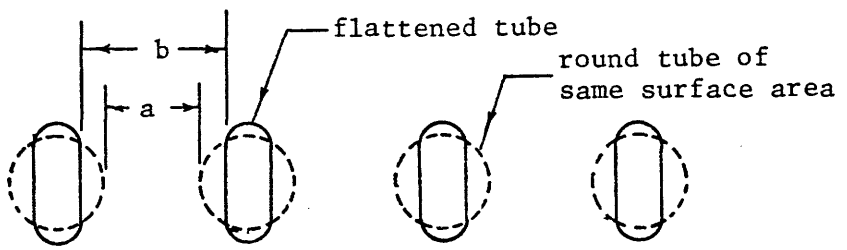

Figure 14

$$\frac{\text{Velocity between flattened tubes}}{\text{Velocity between round tubes}} = \frac{a}{b}$$

air path ————————————

particle path —— - —— - ——

GEOMETRIES USED TO TRY AND ENHANCE
FLUIDIZED BED HEAT TRANSFER COEFFICIENTS

IV.3 Heat Transfer Coefficients as a Function of Velocity

Measured h's are plotted versus superficial air velocities in figures 15 - 21. The data is subdivided into these seven figures in accordance with distributer and tube geometries used for the measurements. The seven distributer and tube geometries are listed in Table 3.

In general, for particles .028" in diameter, heat transfer coefficients rise from a level of about 20 BTU/hr ft^2 °F at low velocities, and reach a maximum h of about 28 - 32 BTU/hr ft^2 °F which is maintained for a range of velocities. Further velocity increases causes the h to fall. The width of this velocity range in which h is roughly constant was directly proportional to the size of the tested particles. For the largest particle size (.028") no significant decrease in h was measured at the high velocity levels. The h's for the smallest particles (.014") on the other hand, peaked and fell within a fairly small span of velocities.

With geometry 1, (fig. 15) the self imposed requirement that all tubes be covered with fluidized particles meant that low velocities could not be tested with the sand poundage used. For the velocities and particles tested, h's were substantially uniform.

With geometry 2 (fig. 16), since only 1 tube row was used, tubes could be covered with particles at air velocities low enough so the finest particles could be used. Coefficients for the small particles (0.014") rose and fell within a narrow range of velocities. A test with 25 lbs. of sand, being half coarse particles (0.028") and half fine particles (0.014") yielded h's in the range of the test with only the fine particles. By observation, the test with a mixture of particles sizes was strongly stratified, with the finer particles actively fluidized, and

the coarser particles generally stagnant and beneath the fines. The coarse particles behaved more as an additional distributer, lifting the fines higher about the tubes. This bed of mixed particle sizes yielded h's which were lower than the maximum h with only fine particles, but were less susceptible to changes in velocities. This indicates that some of the coarse particles must have been fluidized, as their presence would aid in the containment, or prevention of the elutriation, of the finer particles. Collisions between fine particles experiencing near elutriation velocities and coarse particles experiencing substantially sub-elutriation velocities will tend to contain the fines, and will require larger than normal velocities to elutriate the fines.

The coarse particles by themselves in geometry 2 (fig. 16), as in geometry 1 (fig. 15) illustrated constant h's with increasing velocities. However, the coefficients are about 11% lower than those in geometry 1. The presence of the second, staggered, tube row reduces the area of stagnant particles on the downstream side of the tube by forcing the flow of air to more closely follow the contours of the tube. This is evidenced by tube wall temperatures. In geometry 1, tube wall temperatures were about uniform, while in geometry 2, the tube top temperatures were generally greater than other temperatures by 2-8°F. Geometry 2 has a greater amount of stagnant particles on the tube top, acting as an insulation rather than an h enhancement.

With the distributer 3/4 blocked (geometry 3, fig. 17), the tests made with large quantities of particles yield results substantially the same as in geometry 2. However, with a smaller quantity of particles,

h's rise and fall over a smaller span of velocities. With the distributer 3/4 blocked, piles of particles accumulate in the dead regions over the blocked areas of the distributer. Such stagnant particles are essentially lost to the system, and comprise a larger percent of the total particle weight as the total weight is decreased. The low h's for low weights are then the result of poor and nonuniform fluidization because of the distributer blockage.

By halving the distance in geometry 3 between the tube surface and the distributer (geometry 4, fig. 18), there is a substantial increase in the heat transfer coefficient at the higher velocities. This is noticeable even with smaller quantities of particles. Lowering the tubes toward the distributer should increase h because of two effects:
(1) The lowering deflects more air into the previously stagnant region above the blocked areas of the distributer. This reduces the stagnant area, and increases the percent of bed particles in active fluidization.
(2) The lowering allows a more direct impingement of air flow upon the leading edge of the tube. As discussed in the section on heat transfer mechanism, this upstream side is a region of low particle density, and local h's are subsequentiy increased by the reduction of the thermal boundary layer by the air impingement.

As was the case in geometry 3, a small quantity of particles and/or low air velocities leads to low h's. As before, this is due to low particle fractions about the tube because of particles lost to the system in the stagnant, blocked region. This is evidenced in fig. 18 by the data for 10 lbs. of sand, and the lower velocity in the 20 pound

load case. There is also an indication that coefficients rise and fall as the number of particles in the bed is increased. In fig. 18, heat transfer coefficients for the bed weight of 48.5 pounds are less than the measured h's for the bed weight of 30 pounds. This effect is also evident in geometry 5. The air velocity distribution downstream of the tubes is strongly nonuniform, with low yelocities in the wakes of the tubes. Perhaps with larger loads of particles, more particles become trapped in the stagnant region in the lee of the tubes. This would lead to either a deeper or larger stagnation area on the tube tops, and consequently, a reduction of the over-all tube heat transfer coefficient. This mechanism is partially borne out by experimental data: the tube top temperature relative to the other wall temperatures is 1-2°F higher in the tests with a 48.5 pound load than with a 30 pound load.

Experimental data of geometry 5 (fig. 19) illustrates roughly the same effects: coarse particles have a stable h for a relatively large range of velocity, while the coefficients for fine particles rise and fall over a short range; h's for coarse particles peak and fall with an increasing load of particles; poor fluidization and consequently low h's are exhibited with low particle loads. In connection with the last effect, note that not only do low particle loads tend to exhibit low h's at low velocities, indicating poor fluidization (4 points) but that low loads reach their heat transfer coefficient plateau at higher velocities than large loads. This can be seen in both the coarse and medium sized particle data. As this effect is only apparent in cases of blocked distributers, it is probably a direct result of the fraction of particle

load which is stagnant above the blocked distributer areas. The turbulence of higher velocities tends to activate more and more of these stagnant particles.

The results of attempting to create preferential particle recirculation paths using vanes (geometry 6) as described in section IV.2 is shown in fig. 20. In general, coefficients have deteriorated, and at best, are about the same as other geometries. With the distributer 3/4 blocked, there is a quick peaking of h with respect to velocity. Apparently vanes lower the particle densities about the tubes as too many particles are lost to the recirculating system, and are stagnant between vanes and above blocked areas.

Definitive conclusions or trends of the flattened tubes (geometry 7, fig. 21) are difficult to determine from the limited tests made. The flattened tube h seems to be a fairly strong function of particle load, and tube pitch. Also, the highest heat transfer coefficients for coarse particles were achieved with the flattened tube, but they were not of the hoped for level. Because of this failure to substantially improve the h by the use of flattened tubes, further tests were not made with this geometry.

The failure to measure high h's for flattened tubes may be a problem of scale. Vreedenberg's relation (equation 72) indicated that h's increase with a decrease in characteristic tube diameter. Further tests should be made with flattened tubes, but with test sections that are smaller and more in proportion to realistic sizes.

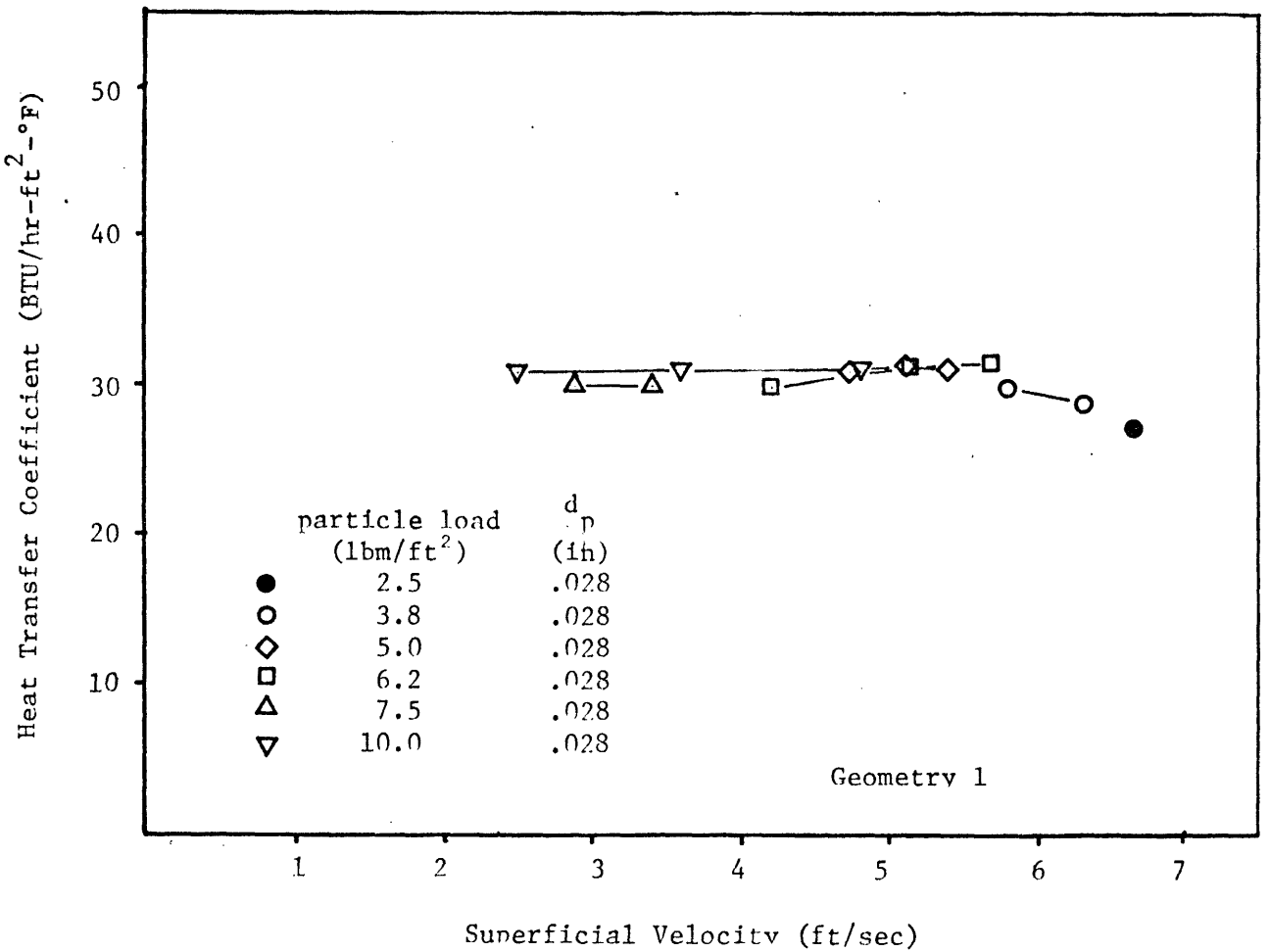

HEAT TRANSFER COEFFICIENT VS. SUPERFICIAL VELOCITY

Figure 15

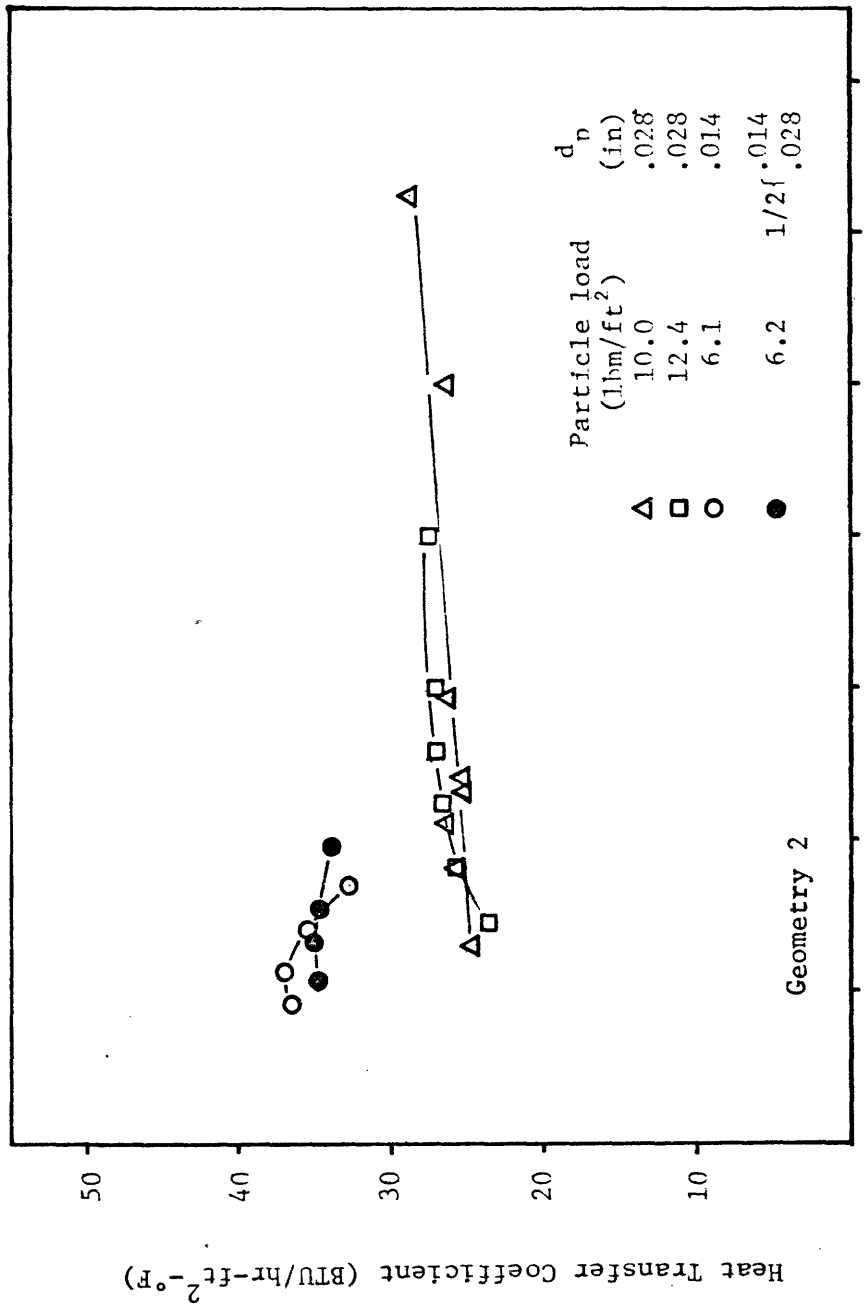

HEAT TRANSFER COEFFICIENT VS. SUPERFICIAL VELOCITY

Figure 16

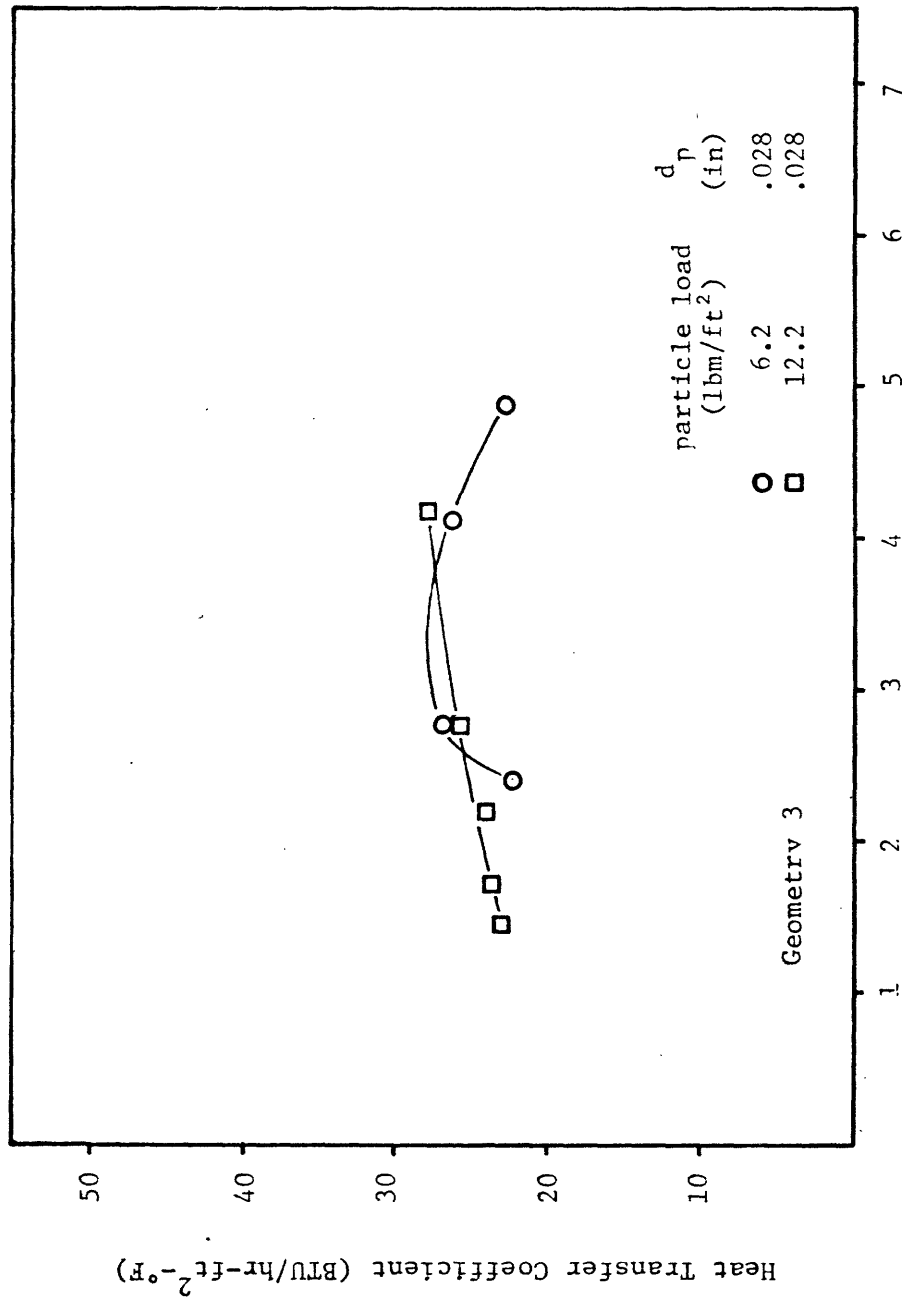

HEAT TRANSFER COEFFICIENT VS. SUPERFICIAL VELOCITY

Figure 17

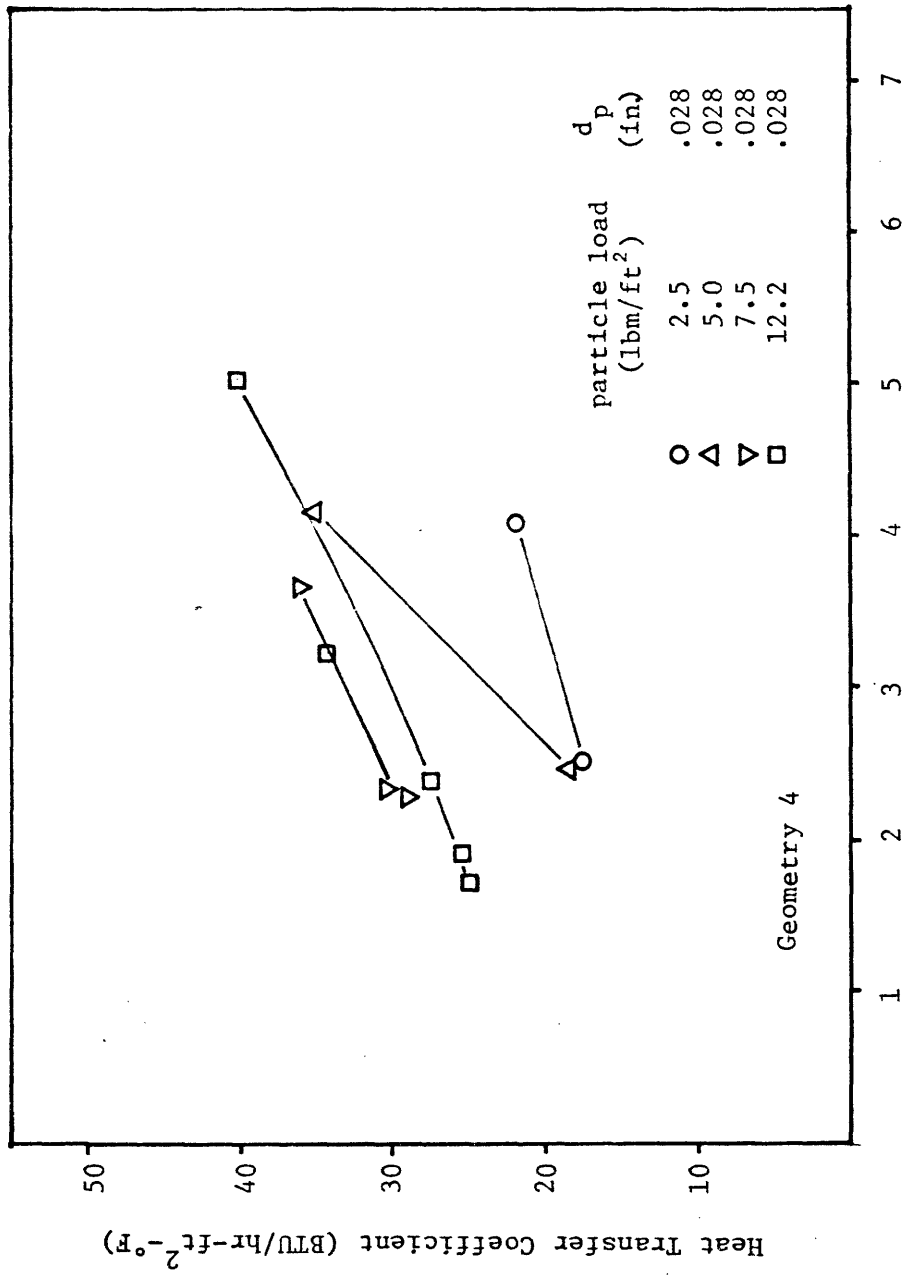

HEAT TRANSFER COEFFICIENT VS. SUPERFICIAL VELOCITY

Figure 18

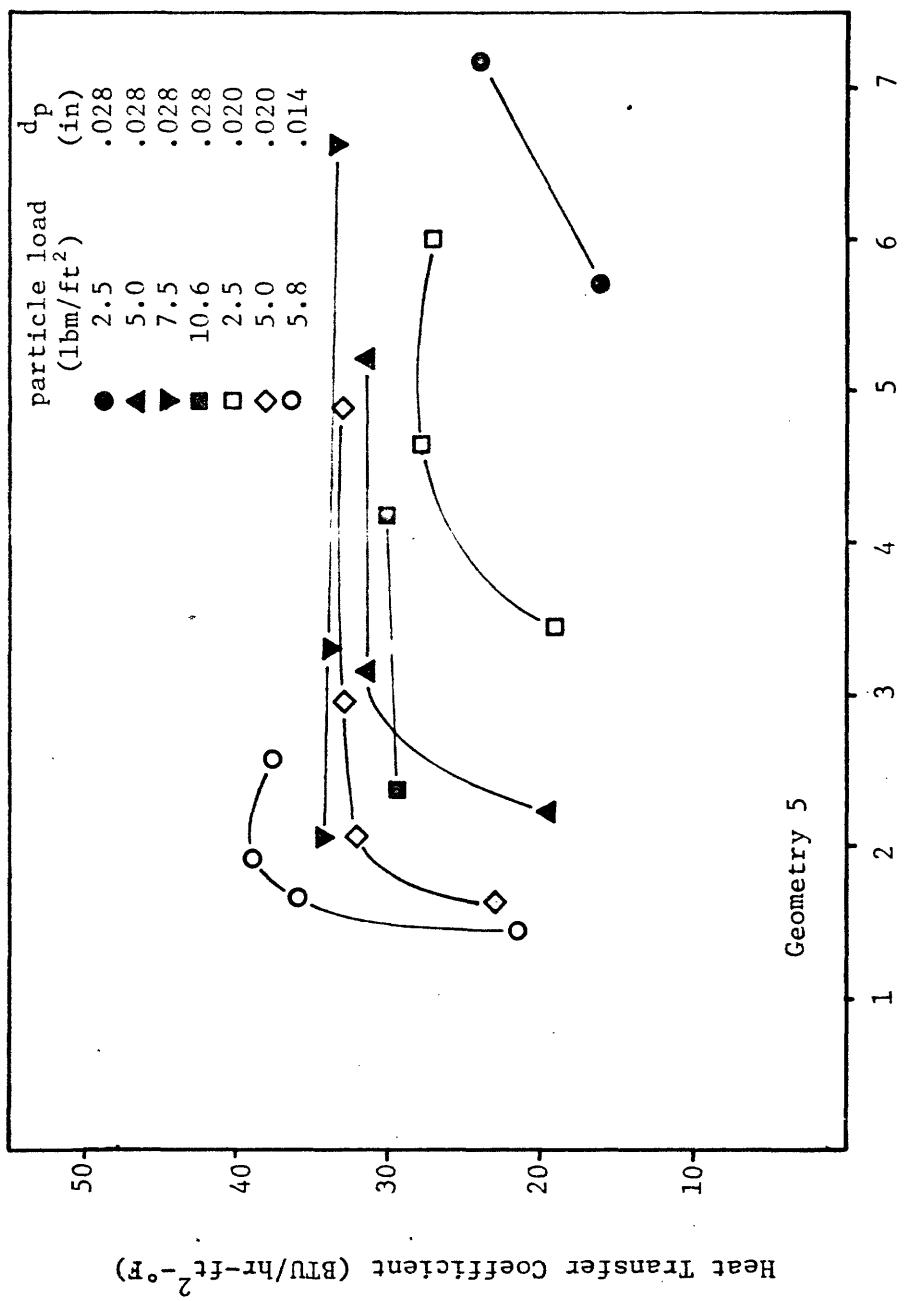

HEAT TRANSFER COEFFICIENT VS. SUPERFICIAL VELOCITY

Figure 19

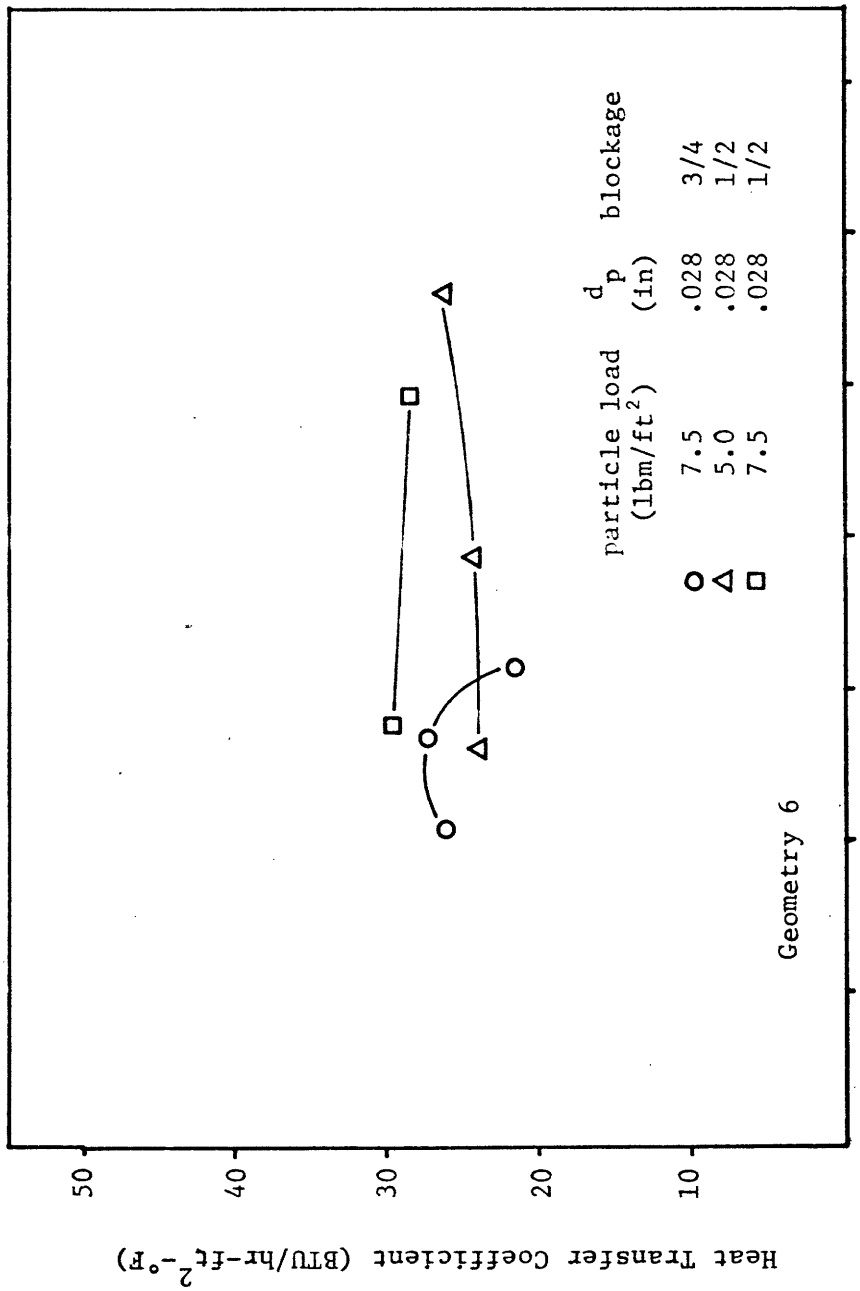

HEAT TRANSFER COEFFICIENT VS. SUPERFICIAL VELOCITY

Figure 20

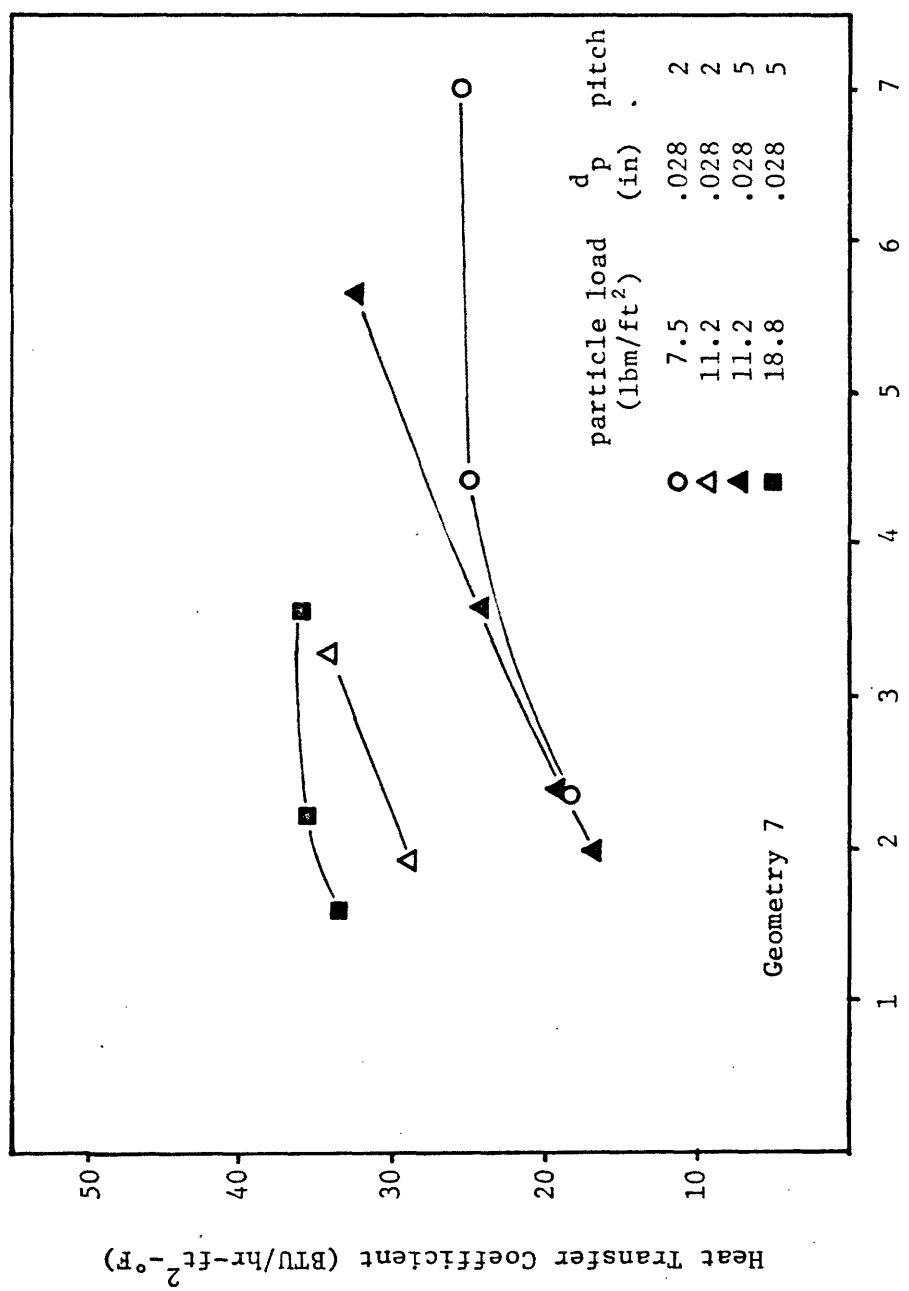

HEAT TRANSFER COEFFICIENT VS. SUPERFICIAL VELOCITY

Figure 21

Table 3

Distributer Configurations & Geometries

Geometry #	Refered to as	Description
1	Δ-uniform	2 banks of staggered tube rows, uniform distributer, α=1/2", P=2
2	uniform	1 row of tubes, uniform distributer α= 1/2", P=2
3	3/4 blocked α=1/2	1 row of tubes, distributer 3/4 blocked, α=1/2", P=2.
4	3/4 blocked α=1/4	1 row of tubes, distributer 3/4 blocked, α=1/4", P=2
5	1/2 blocked	1 row of tubes, distributer 1/2 blocked, α=1/2", P=2
6	vaned	1 row of tubes, vanes between tubes, distributer 1/2 or 3/4 blocked, α= 1/2", P=2
7	flattened	1 row of flattened tubes, distributer 1/2 blocked, α=1/2", P= 2 or 5

α = minimum spacing between tube surface and distributer

P = tube pitch, ie., ratio of centerline distance between tubes to tube diameter

IV.4 Comparison of Experimental Data With Correlations

IV.4.1 Scope

In this section, the data obtained with the experimental apparatus described in section III.2 is compared with the correlations of Wender-Cooper, Ainshtien, Vreedenberg, and the model of section II.2.6. The correlations are described in section II.3.1. In those correlations requiring the particle or void fraction ($1 - \varepsilon$, ε), it has been calculated from Leva's [16] relation for void

$$\frac{\varepsilon^3}{(1 - \varepsilon)} = 200 \frac{V_g \mu}{d_p^2 (\rho_p - \rho_g) g} \tag{76}$$

or a linearization of this relation:

$$\varepsilon = \left[0.4 + \left[200 \frac{V_g \mu}{d_p^2 (\rho_p - \rho_g) g} \right]^{1/3}\right] \frac{1}{2.1} \tag{77}$$

Equation 77 differs from equation 76 by less than 7% for ε's between .45 and .80.

Voidage could also be determined by using experimentally measured bed heights and assuming uniform voidage. This was not done for several reasons. First, the presence of tubes and the subsequent high between-tube velocities caused the bed to 'spout' between the tubes. This led to a non-definitive bed height, and any bed height measurement had to be 'eyeballed'. Since these are shallow bed experiments, error introduced by this visual measurement is sizable -- up to about 30%. Secondly, with the use of distributer blockage, and the subsequent buildup of stagnant particles over the blocked area, a void determination from bed height

measurement includes these stagnant particles in the average void. Because of this, the actual void about the tubes would be greater than the measured void. Note that the largest error on void determination by these effects occurs with low particle loads in the bed. Here a greater percent of the total load is lost to the blocked distributer regions, and as the bed is among the shallowest tested, the eyeball error is the greatest.

The void calculated for unblocked distributer (geometries 1 & 2) by optical measurements is compared to Leva's prediction in fig. 22. The scatter in fig. 22 is due primarily to the inability to optically discern the bed height.

Leva's void relations was used as a means to provide a consistant and relatively accurate determination of void. Air properties in these correlations were evaluated by using the average of the wall and bed temperature, $(T_w - T_b)/2$.

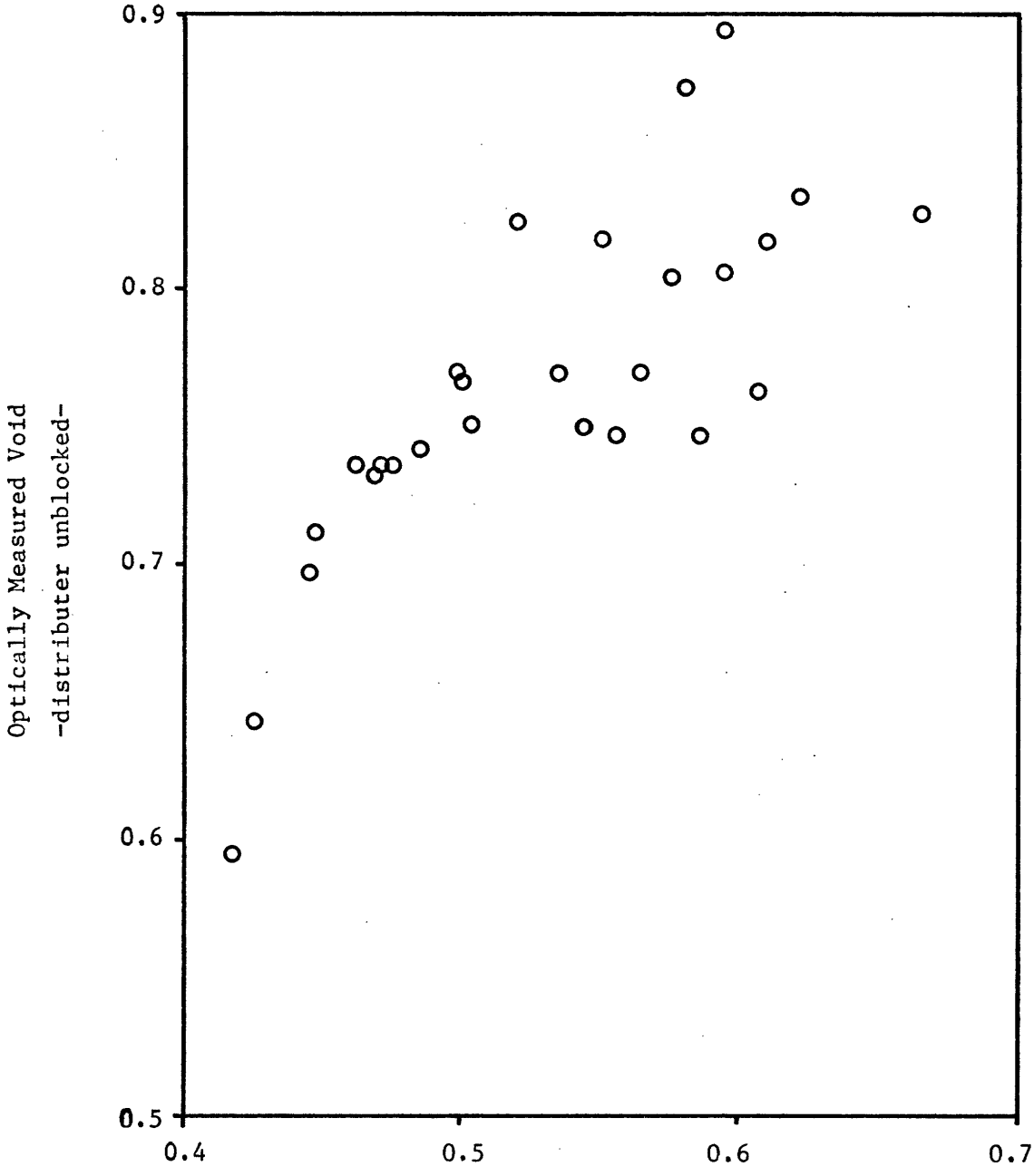

OPTICALLY MEASURED VOID VS. LEVA'S RELATION

Figure 22

IV.4.2 Wender-Cooper Correlation of Data

Cr, the correction factor in equation 75 was assumed to be 1.4, This is an average value of those proposed by Wender and Cooper [18] for vertical tubes. The correlation goes through the data as a whole, as can be seen in figures 23 - 28, and is strongly segmented into narrow bands along the horizontal axis in accordance with particle size. As in section IV.3, data is plotted in different figures according to the distributer and geometry used. The velocity used in determining ε and G in these figures is the superficial air velocity. As the properties of the fluidized bed may be better determined by the actual air velocity, the data was also compared to the correlation assuming the air velocity is equal to the superficial velocity divided by the fraction of the distributer which is unblocked, or

$$V_g = V_s/(1 - \text{Blockage}) \qquad (78)$$

Table 4 lists the root mean square (RMS) deviation of data from the Wender-Cooper correlation for each distributer case and both air velocities. Table 4 also lists the RMS deviation of Vreedenberg's data [15] from the Wender-Cooper correlation.

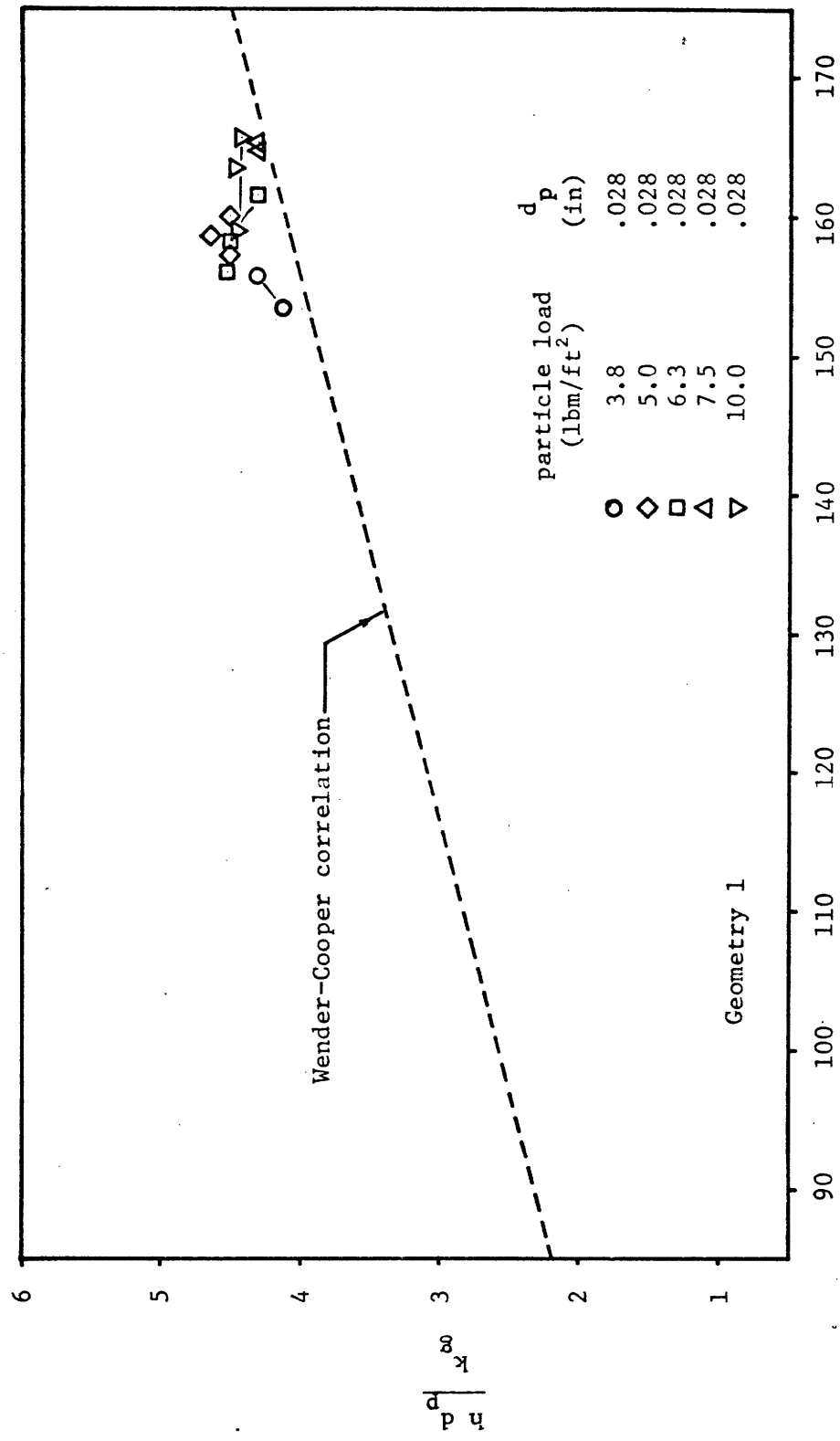

DATA PLOTTED WITH WENDER-COOPER PARAMETERS

Figure 23

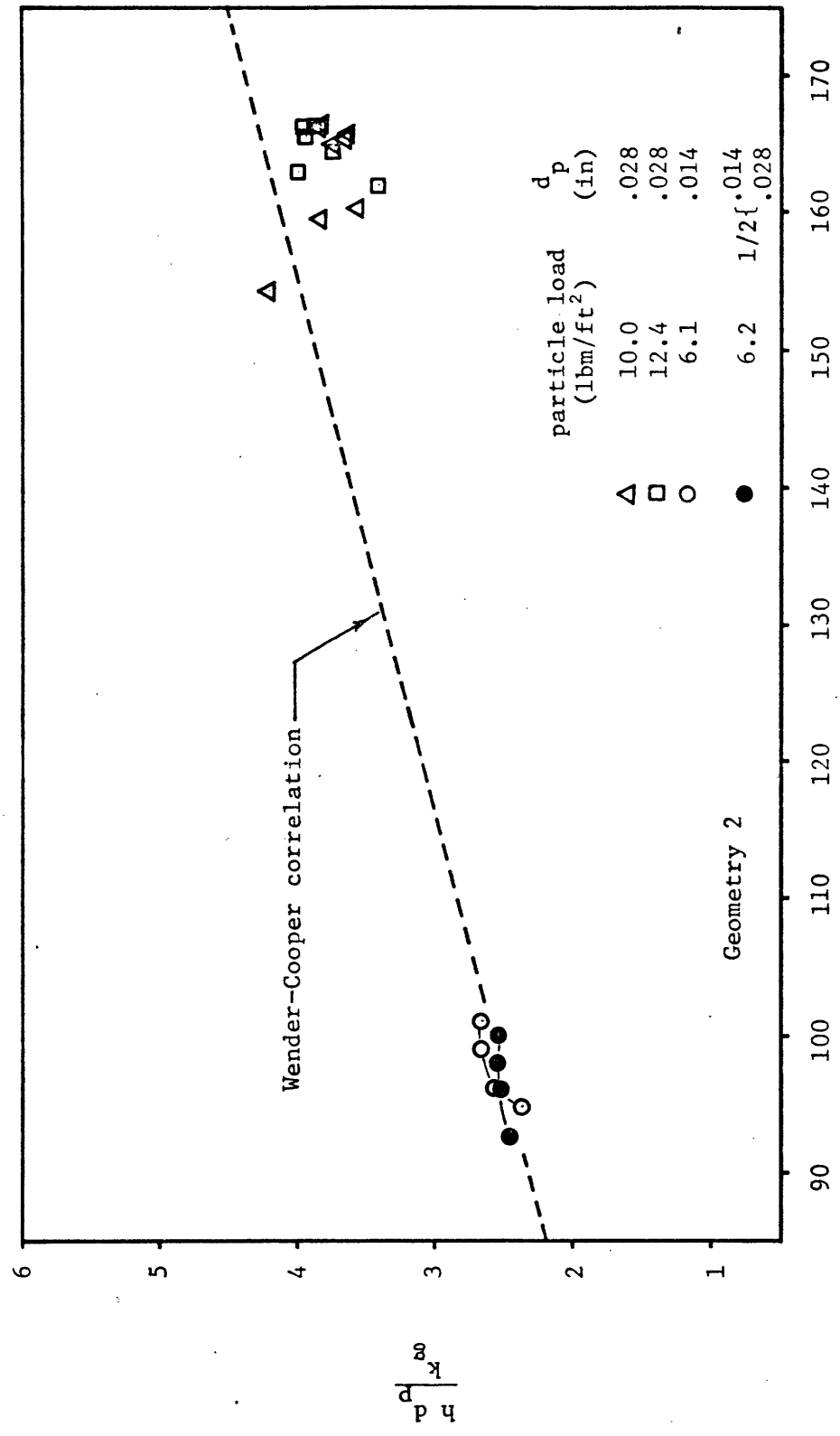

DATA PLOTTED WITH WENDER-COOPER PARAMETERS

Figure 24

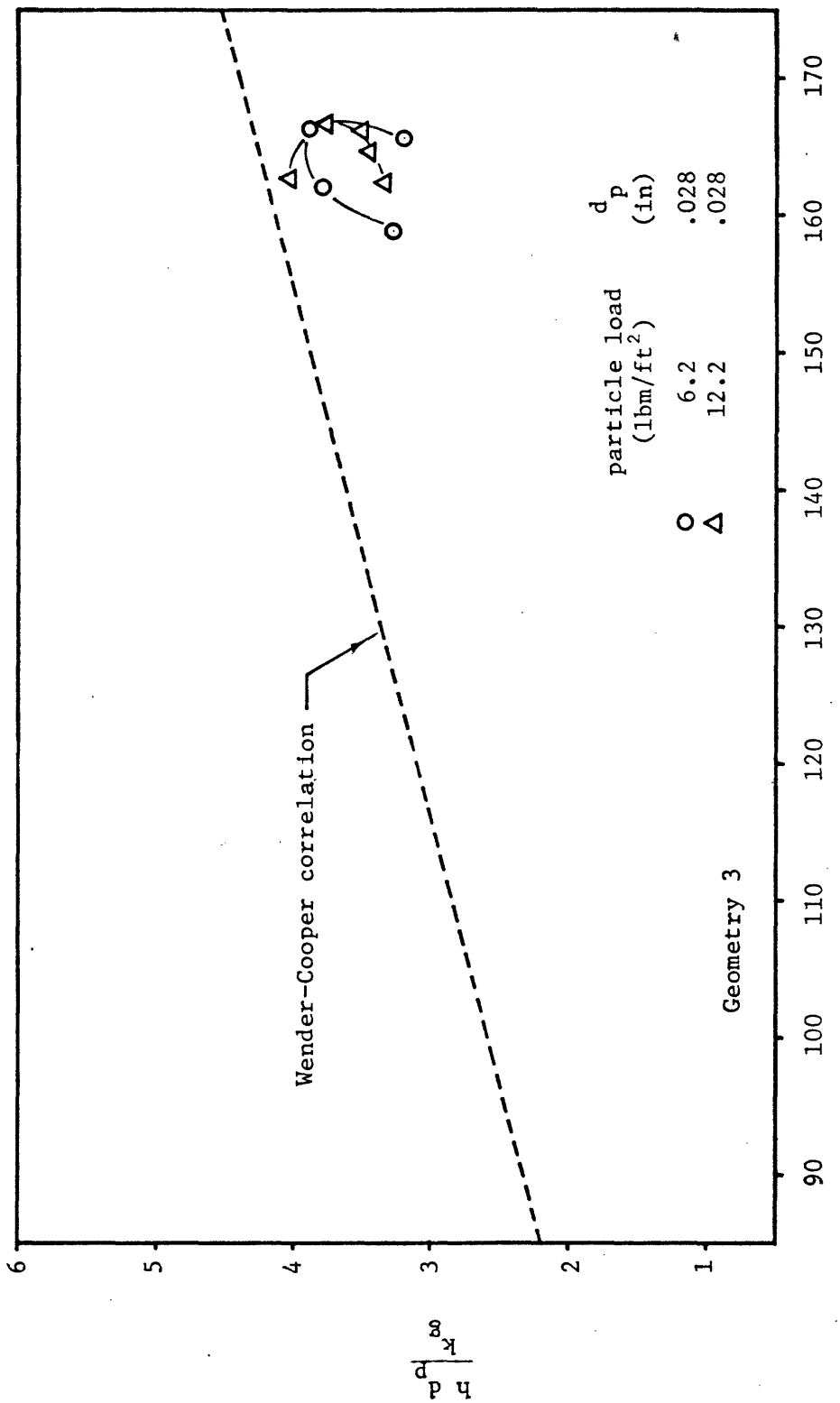

DATA PLOTTED WITH WENDER-COOPER PARAMETERS

Figure 25

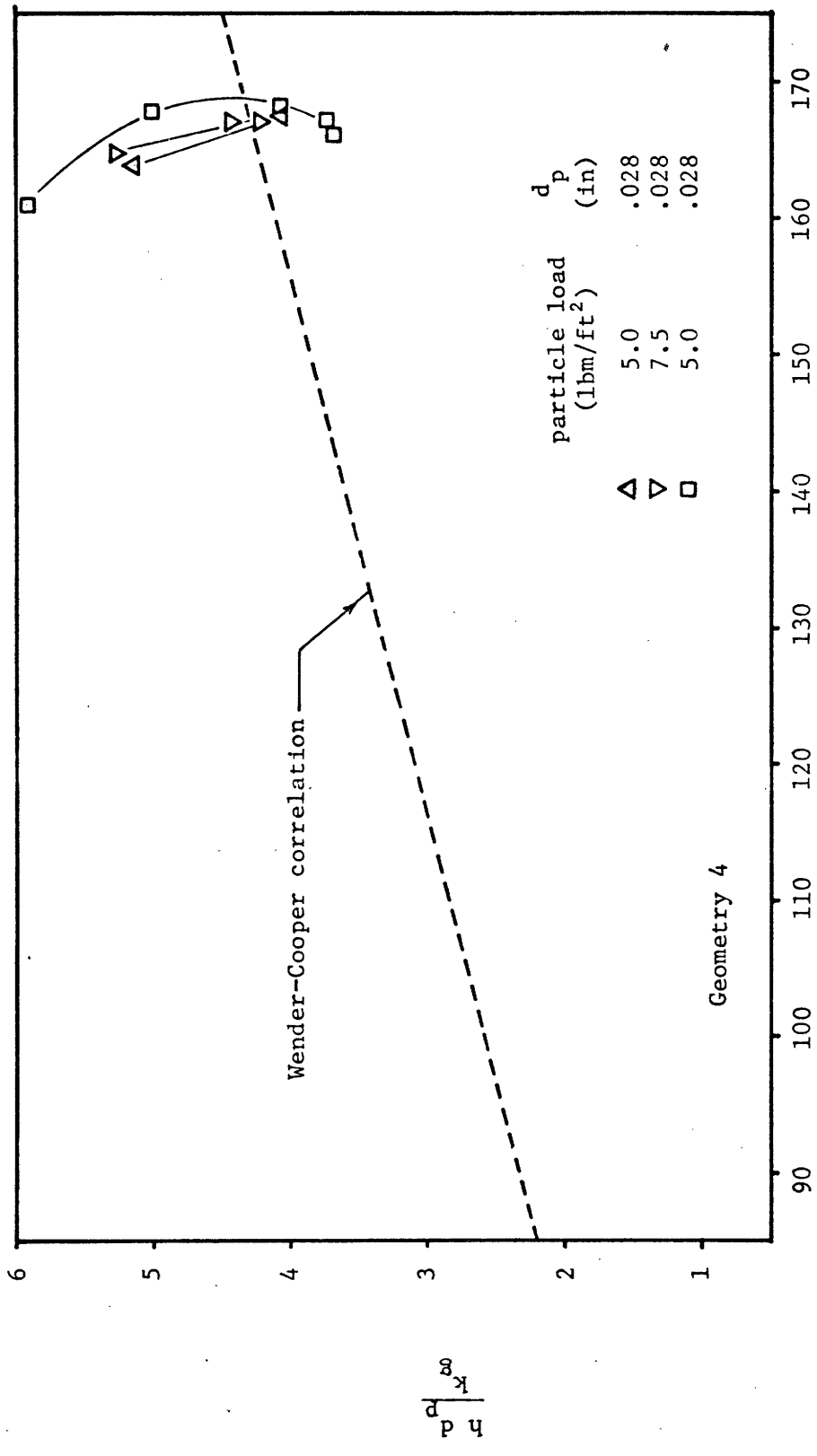

DATA PLOTTED WITH WENDER-COOPER PARAMETERS

Figure 26

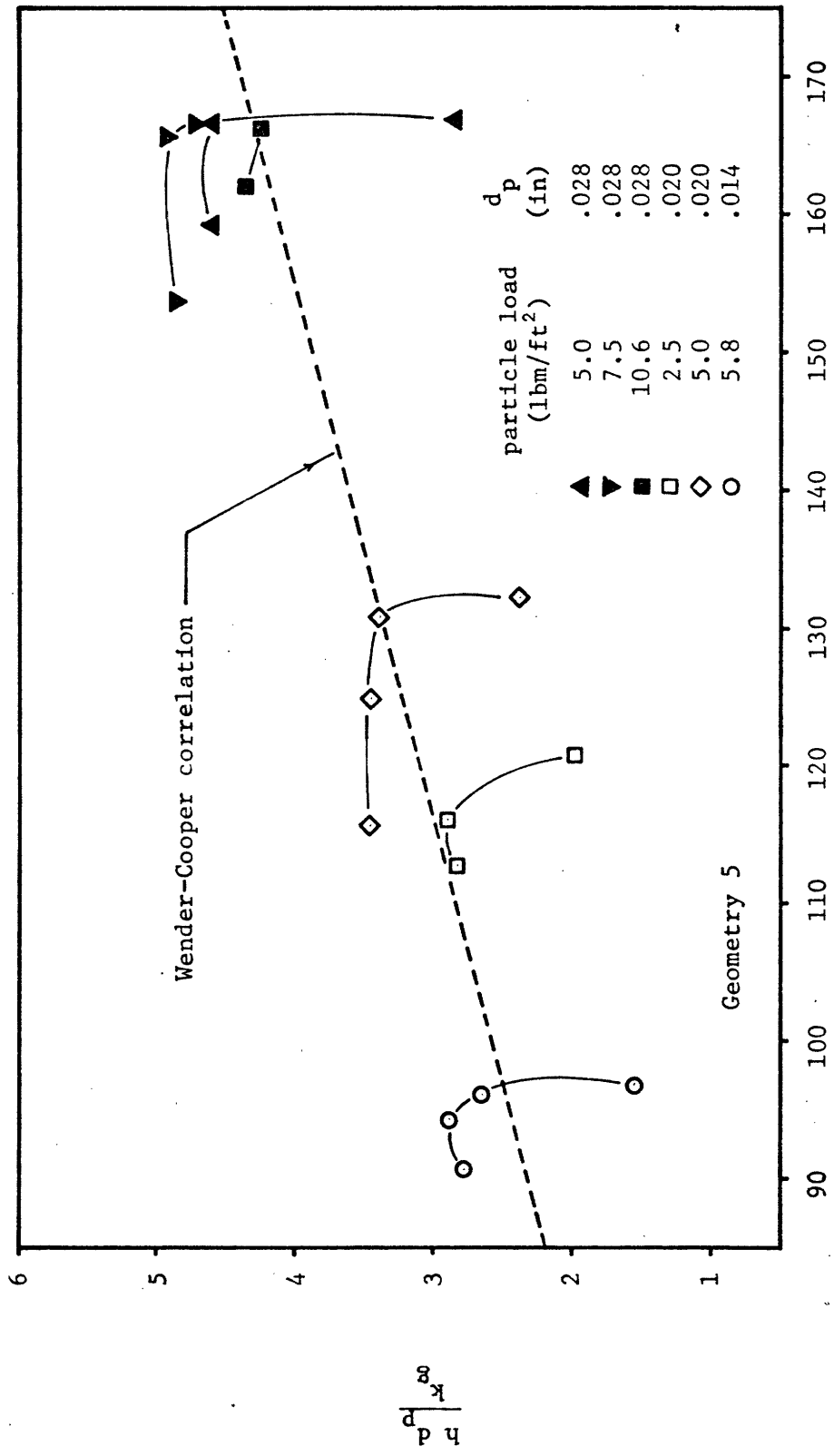

DATA PLOTTED WITH WENDER-COOPER PARAMETERS

Figure 27

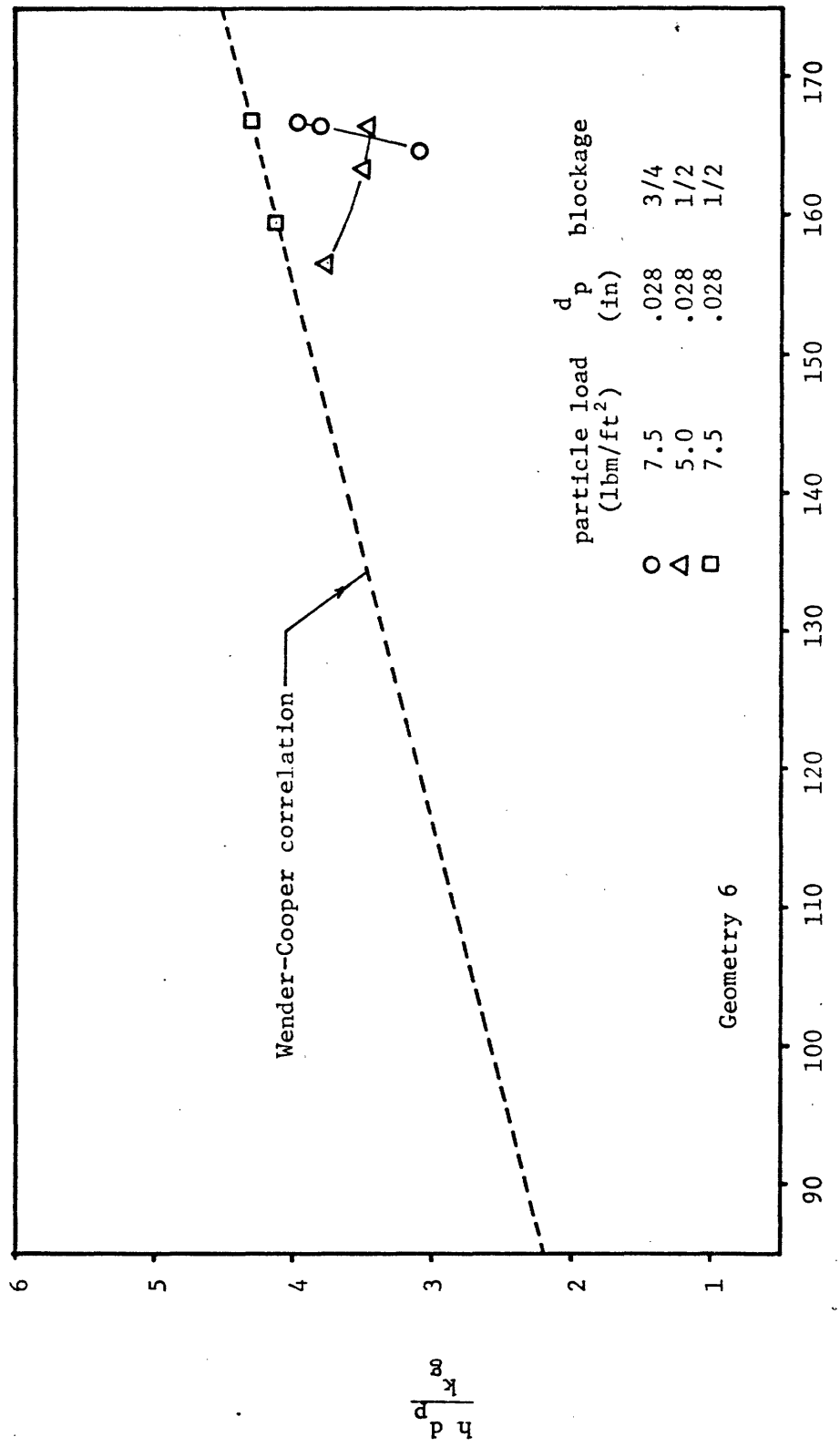

DATA PLOTTED WITH WENDER-COOPER PARAMETERS

Figure 28

Table 4

RMS Deviation of Data from Wender-Cooper Correlation

Geometry/Data	Assuming $V_g = V_s$ * (%)	Assuming $V_g = V_s/(1-\text{blockage})$ (%)
Δ-uniform	7.9	7.9
uniform	9.3	9.3
3/4 blocked, α=1/2	16.7	39.1
3/4 blocked, α=1/4	18.4	81.4
1/2 blocked	19.1	40.5
Sum of above	14.6	40.4
vaned	14.3	27.2
Vreedenberg data	30.8	--

* data graphed in figures 23-28

IV.4.3 Ainshtein's Correlation of Data

Ainshtein's correlation predicts a decrease in h as the tube approaches the distributer. However, as discussed in section IV.3, an opposite effect was observed. Consequently, data was also compared to Ainshtein's correlation by dropping the α/d_b factor and curve fitting Ainshtein's parameters as determined by data by a least squares routine to determine a coefficient and power for the Reynolds group in equation 74. This yielded the correlation:

$$\frac{h\, d_p}{6(1-\varepsilon)\, k_g} = .487\left(\frac{G\, d_p}{\mu\, \varepsilon}\right)^{.277} Pr^{.33} \qquad (79)$$

Data is compared to the above correlation in figures 29-34, according to the distributer and geometry used. Note that the correlation collapses the data well for any one particle size, but that different particle sizes seem to be collapsing to a different line (albeit, the same slope). This would indicate some dependency of particle size which is not included in the correlation. Table 5 lists the RMS deviation of data from both formulations of the Ainshtein correlation (equations 74 & 79) in accordance with the distributer geometry. The table also includes the RMS deviation of Vreedenberg's data from equation 79.

The air velocity used in these correlations is the superficial air velocity. The use of ε in the denominator of the Reynolds group raises the velocity value to the actual local velocity.

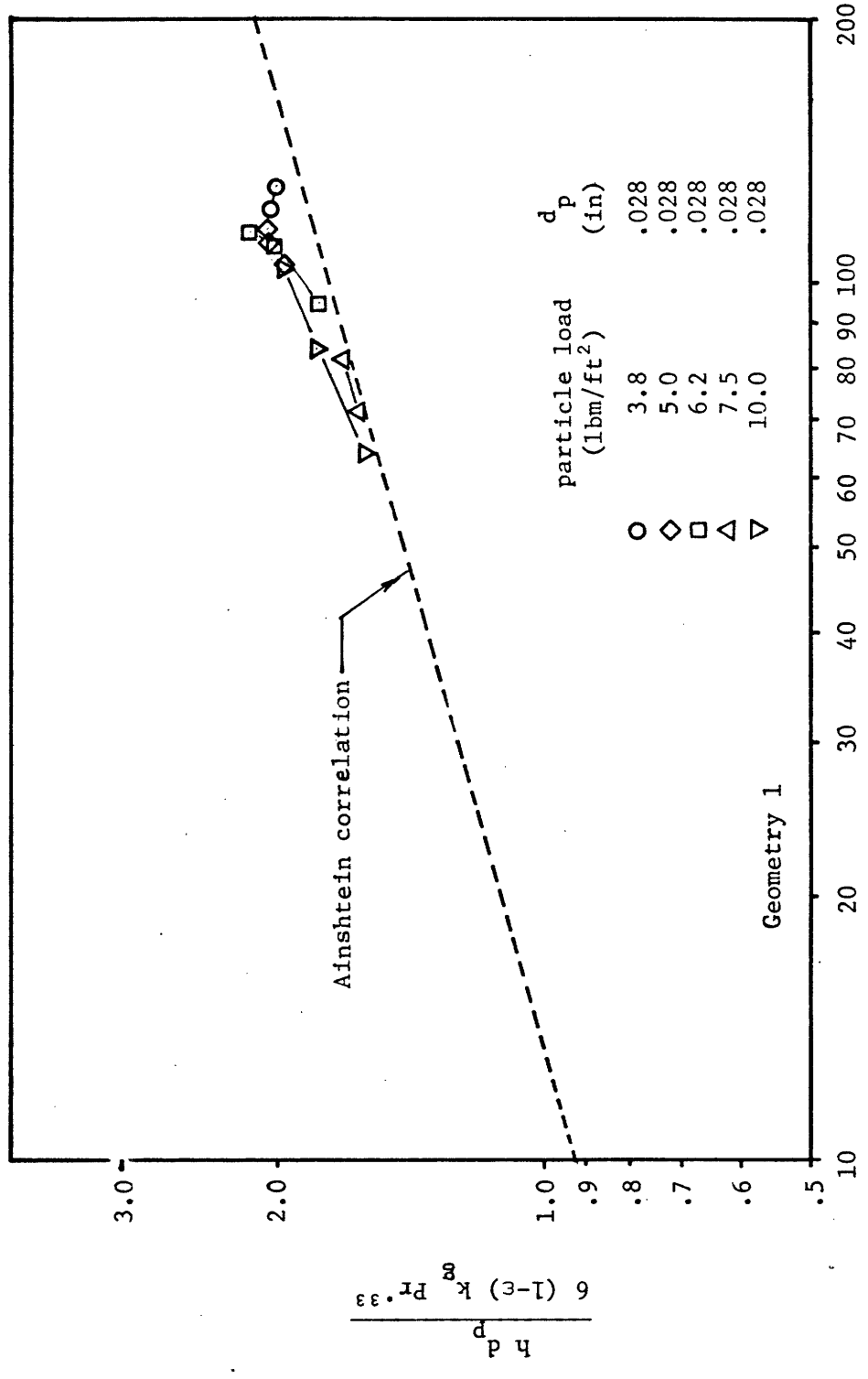

DATA PLOTTED WITH AINSHTEIN PARAMETERS

Figure 29

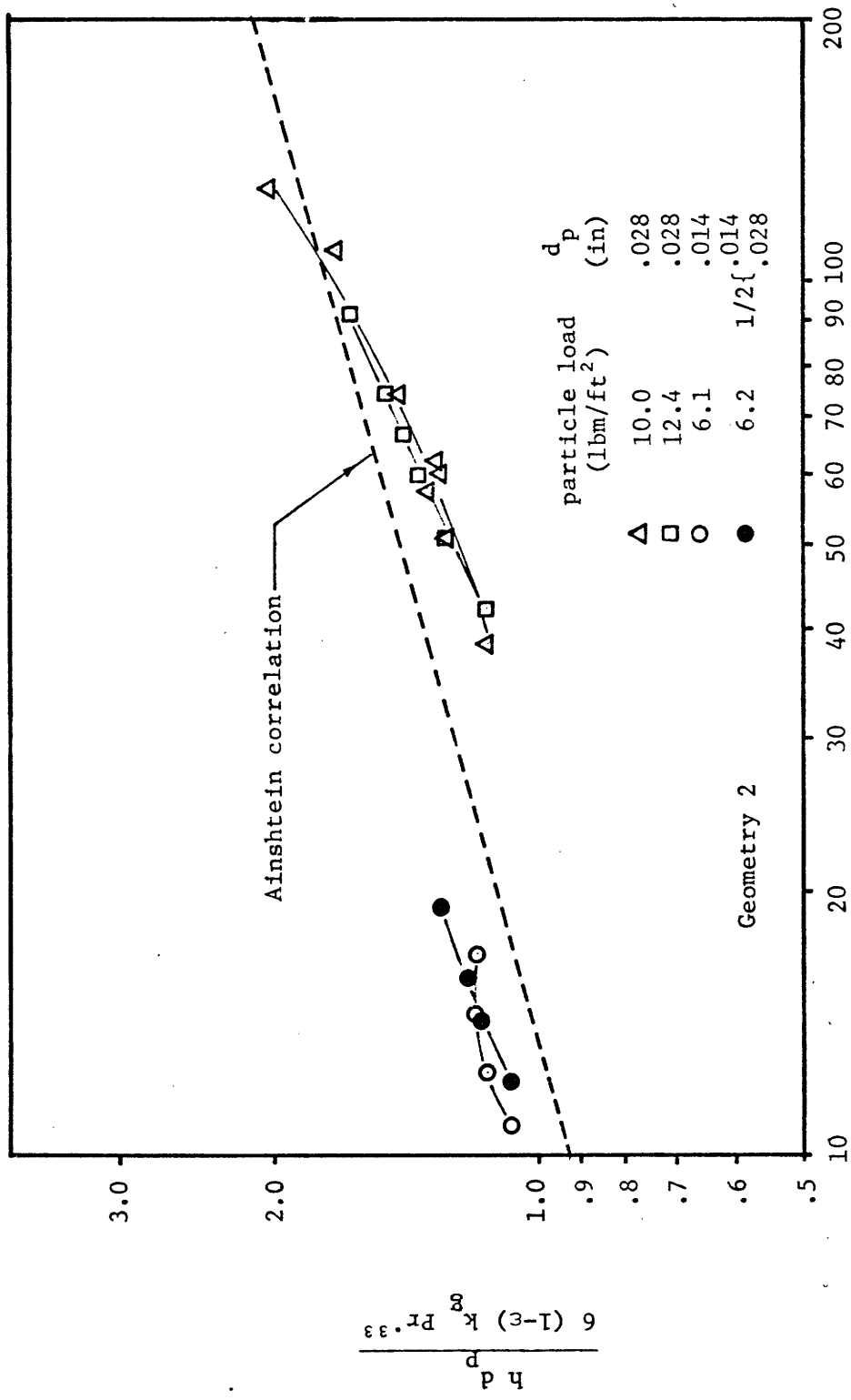

DATA PLOTTED WITH AINSHTEIN PARAMETERS

Figure 30

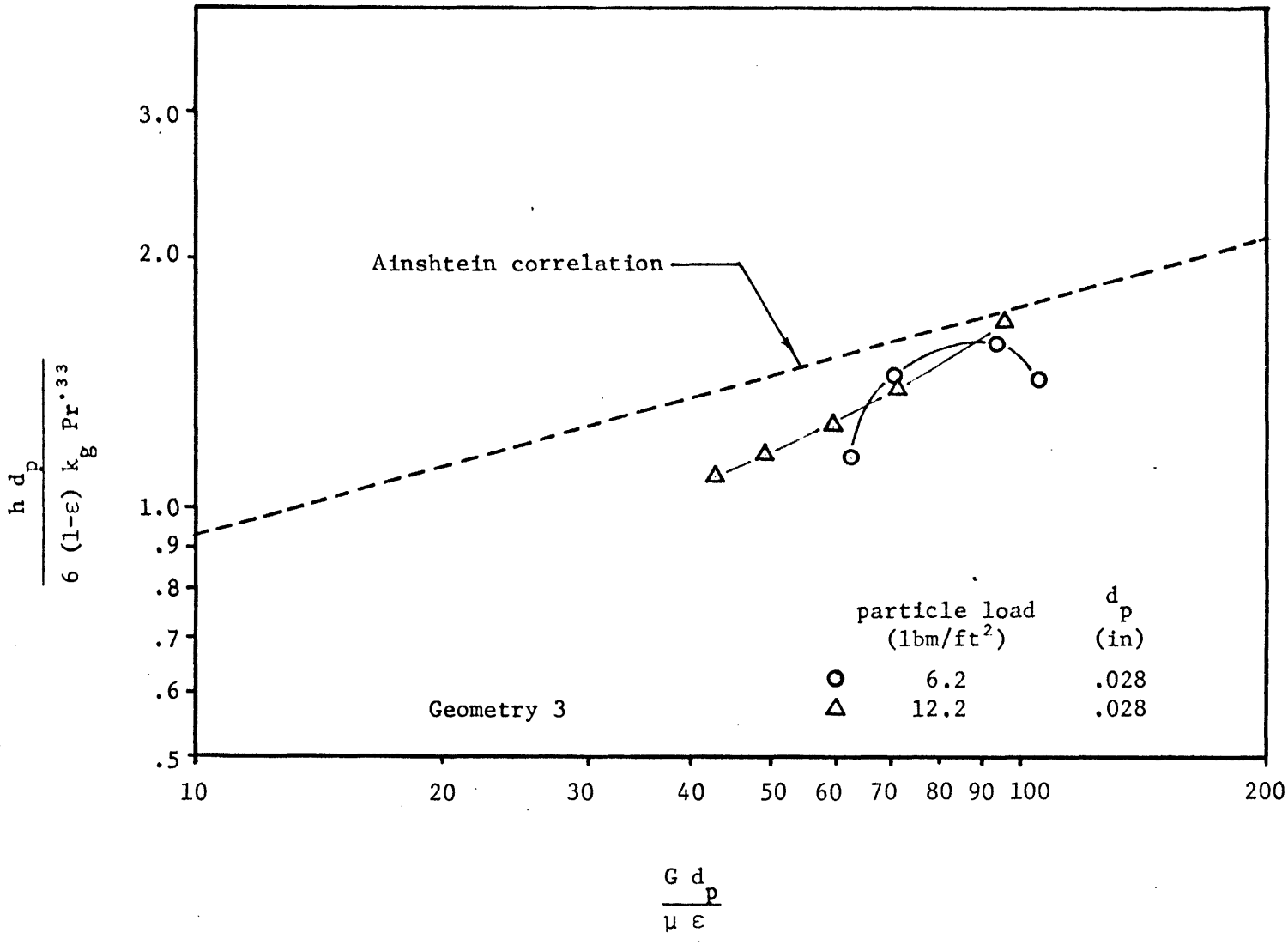

DATA PLOTTED WITH AINSHTEIN PARAMETERS

Figure 31

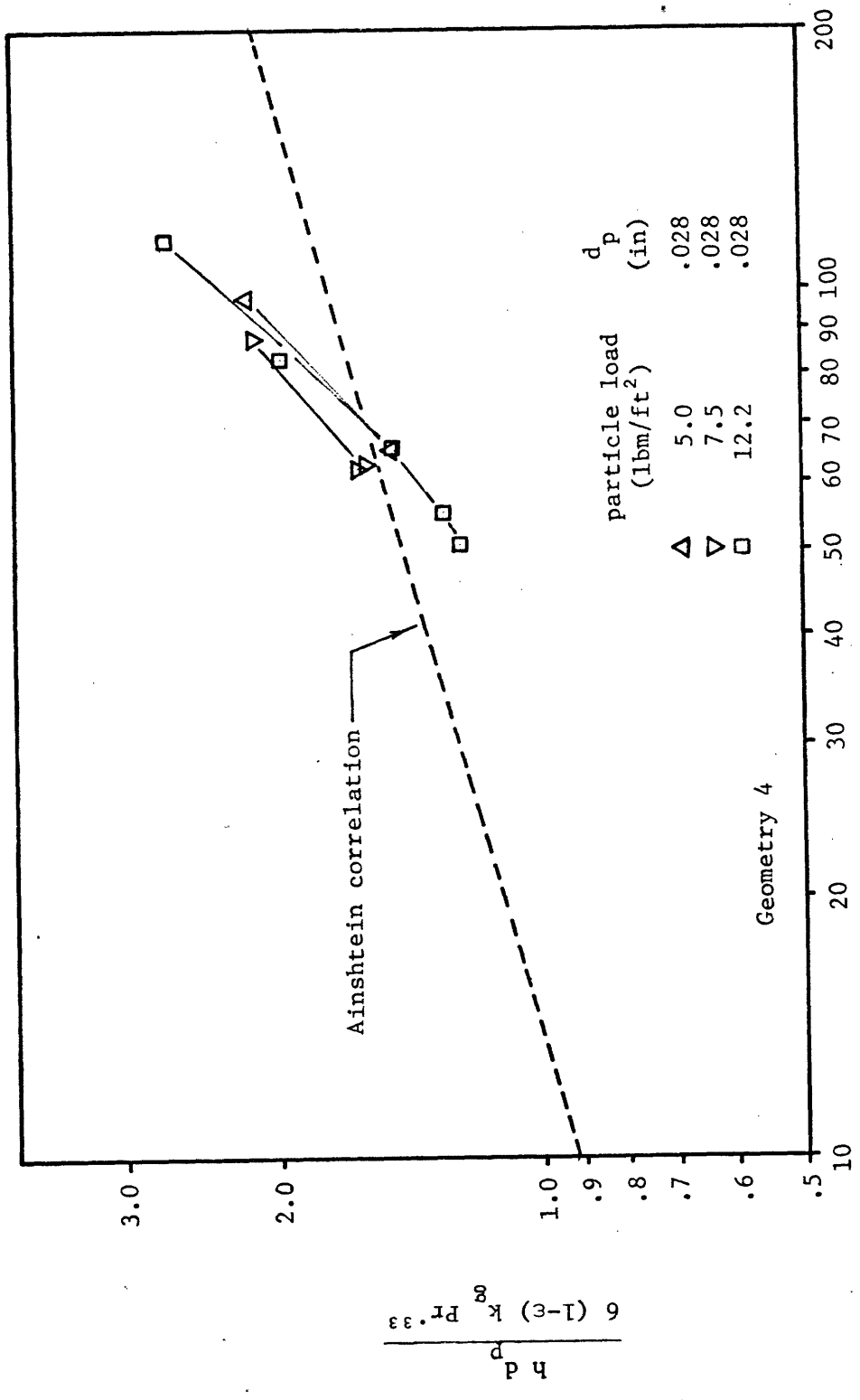

DATA PLOTTED WITH AINSHTEIN PARAMETERS

Figure 32

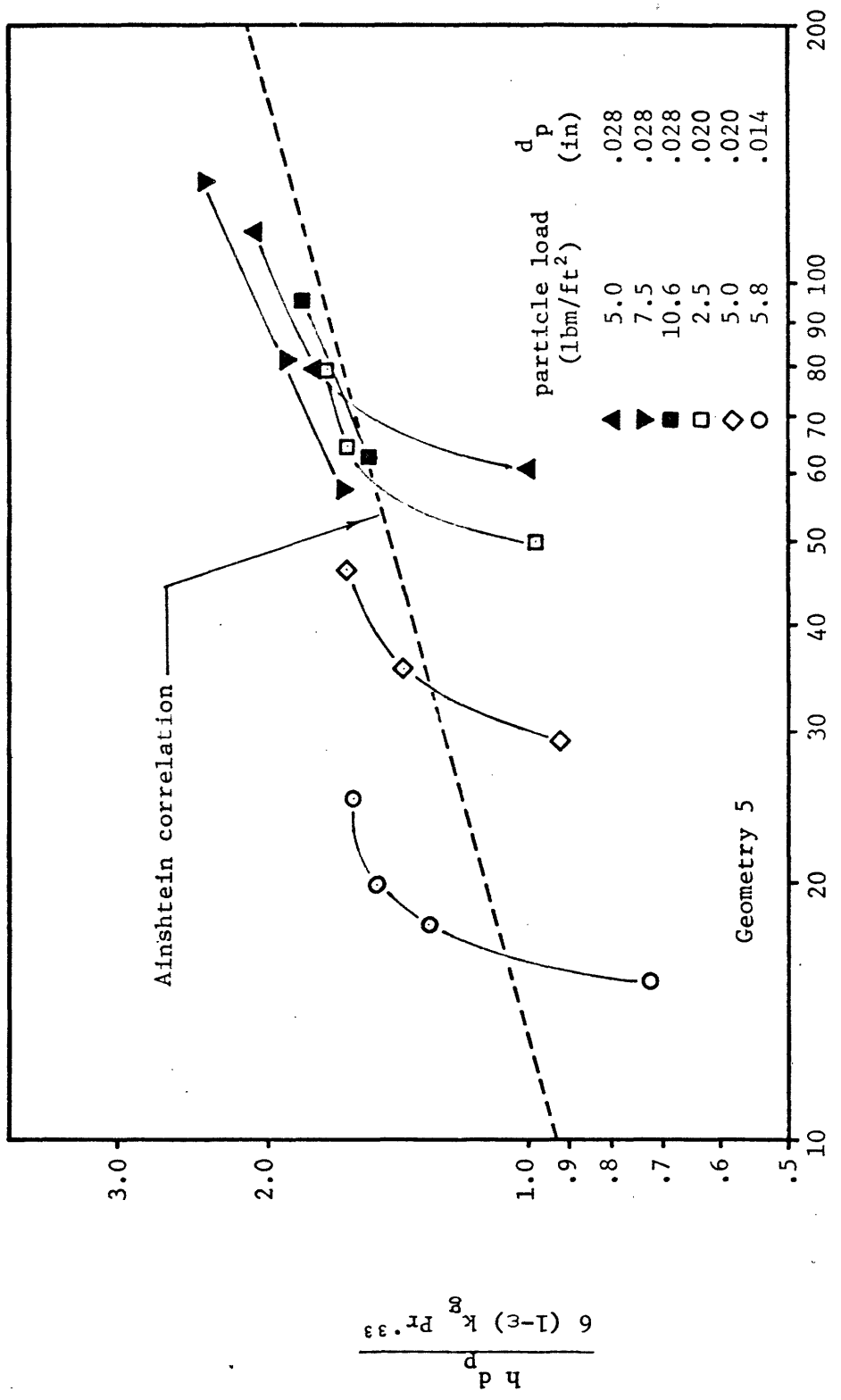

DATA PLOTTED WITH AINSHTEIN PARAMETERS

Figure 33

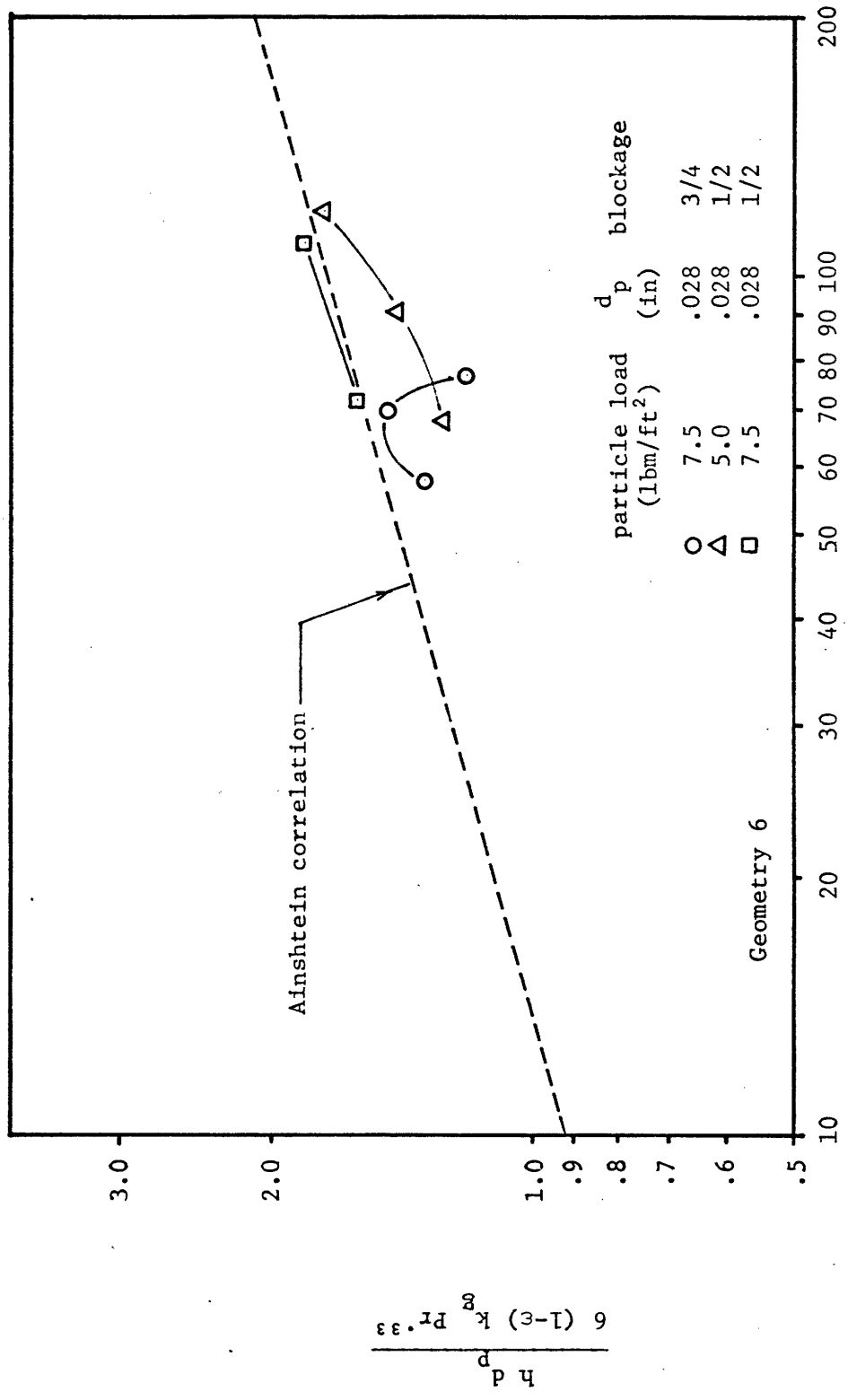

DATA PLOTTED WITH AINSHTEIN PARAMETERS

Figure 34

Table 5

RMS Deviation of Data from Ainshtein Correlation

Geometry/Data	from equation 74 (%)	from equation 79 * (%)
Δ-uniform	23.6	9.3
uniform	28.6	12.5
3/4 blocked, α=1/2"	39.0	16.8
3/4 blocked, α=1/4"	19.2	12.2
1/2 blocked	27.5	21.3
Sum of above	27.9	16.4
vaned	36.7	14.2
Vreedenberg data	--	34.2

* data graphed in figures 29-34

IV.4.4 Vreedenberg's Correlation of Data

Vreedenberg's correlation (equation 72) correlates low void data well. However, as the void increases as a result of increased velocity, and the h decreases (in accordance with theory), Vreedenberg's correlation predicts a continual rise in h or Nu. In order to include the effect of decreased particle fraction, the Vreedenberg parameters as determined by the data and modified by $(1 - \varepsilon)$ were curve fit by a least squares routine to yield a new coefficient and power:

$$\frac{h\, d_t/k_g}{(C_g\, \mu/k_g)^{.3}} = 900\ (1 - \varepsilon)\ \left(\frac{G\, d_t\, \rho_p}{\rho_g \mu}\ \frac{\mu^2}{d_p^3\, \rho_p^2\, g}\right)^{.326} \qquad (80)$$

The comparison of data to equations 72 & 80 are shown if Figures 35A & B - 40 A & B. 'A' figures employ Vreedenberg's original correlation (equation 72) and 'B' figures employ the modified Vreedenberg correlation (equation 80). Note that the inclusion of $(1 - \varepsilon)$ raises the high void data to the modified correlation, greatly improving the correspondance between data and correlation. This can be seen in figures 41 A and 41 B, where the total data scatter about both the original and modified Vreedenberg correlation is illustrated. Figure 42 A and 42 B illustrate how Vreedenberg's initial data compares with the original and modified correlations. Although the modified correlation with the inclusion of $(1 - \varepsilon)$ has a smaller RMS deviation from data than the original correlation, the void range is sufficiently small to make any such judgements questionable. The effect of $(1 - \varepsilon)$ is only starting to become apparent. More important is the change of slope of the lines. In the modified correlation, each case has

an increasing slope with increasing air velocity, while in the original correlation lines have both positive and negative slopes. Data from Petrie et al [23] can also be compared to equations 72 & 80. Petrie found reasonable agreement between his data and Vreedenberg's original correlation. Figures 43 A and 43B show the comparison of Petrie's data, when fluid properties are based on film temperatures, to the original and modified Vreedenberg correlations. Again, better agreement at the higher Reynolds group values are observed in the modified correlation.

The air velocity and void used in these correlations is based upon the superficial air velocity, and as in section IV.4.2, the data was also compared to the correlations assuming $V_g = V_s/(1 - \text{Blockage})$. Further, assuming this velocity variation, the Vreedenberg parameters were again curve fit by the least square routine to yield

$$\frac{Nu_t}{Pr^{.3}} = 981\ (1 - \varepsilon)\ (Re_t/Ar)^{.36} \qquad (81)$$

Table 6 lists the RMS deviation of data from these correlations, and the assumed air velocities, in accordance with the distributer and geometry. Table 6 also includes the RMS deviation of Vreedenberg's data from the correlation.

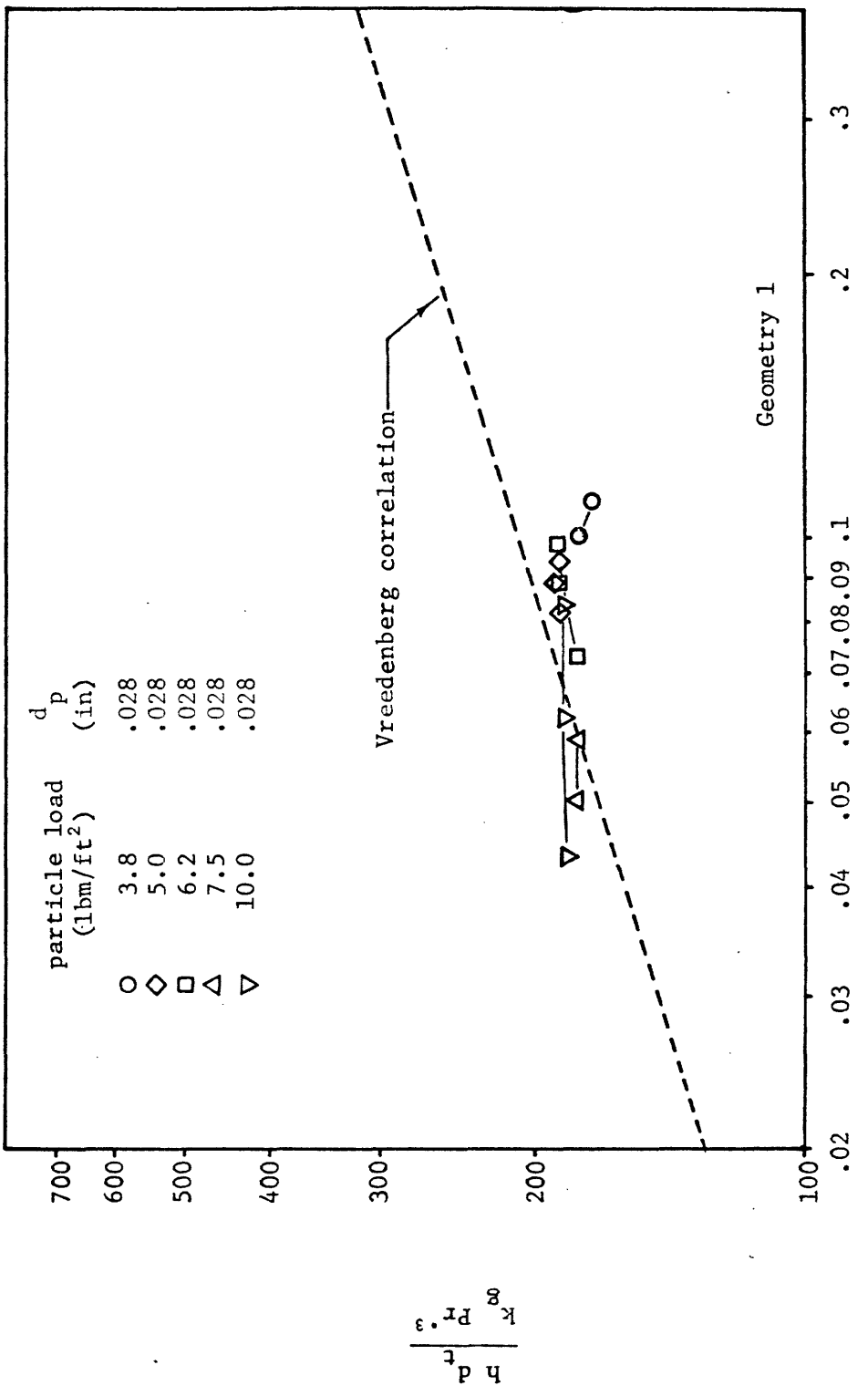

DATA PLOTTED WITH VREEDENBERG PARAMETERS

Figure 35A

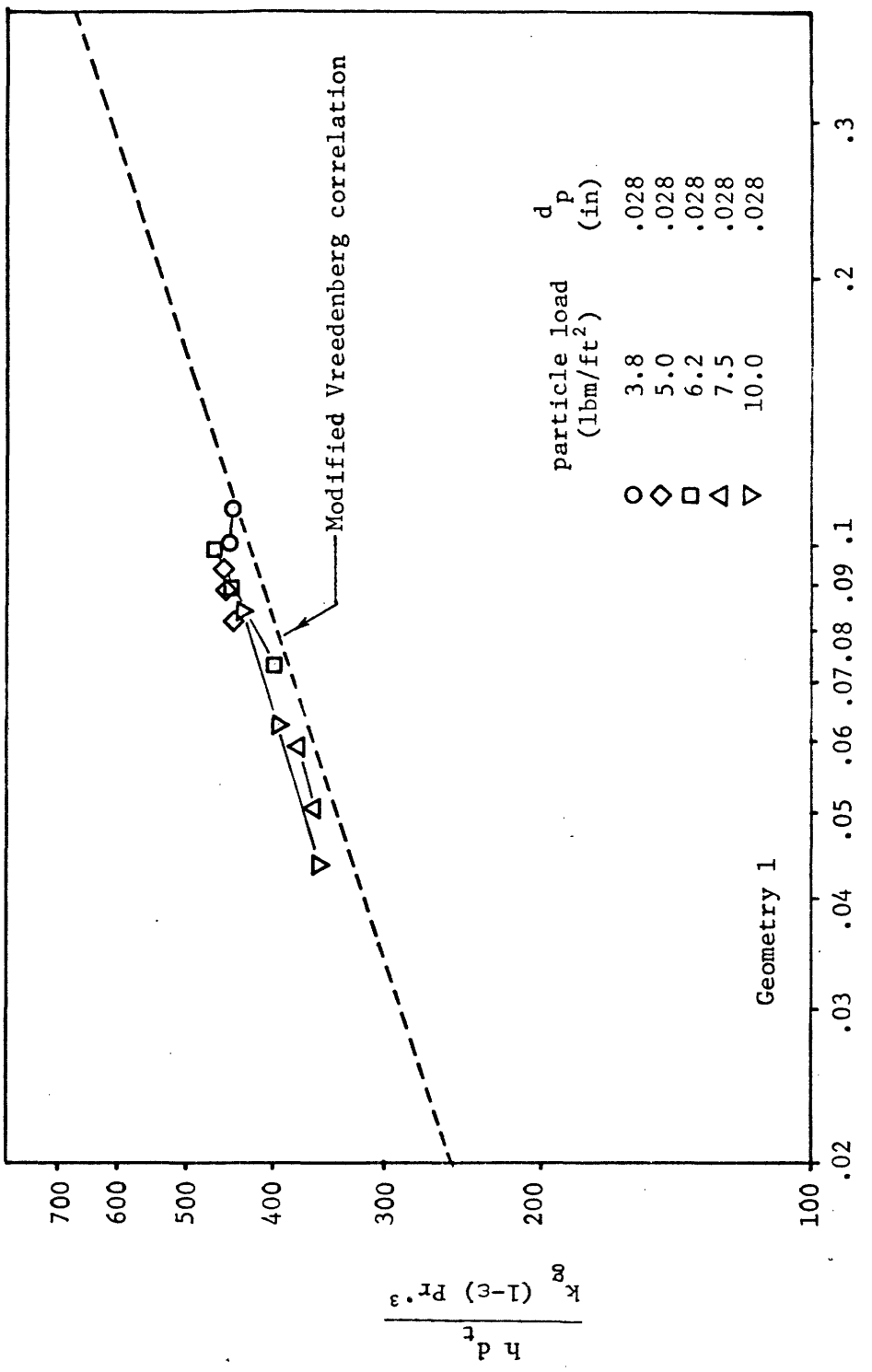

DATA PLOTTED WITH MODIFIED VREEDENBERG PARAMETERS

Figure 35B

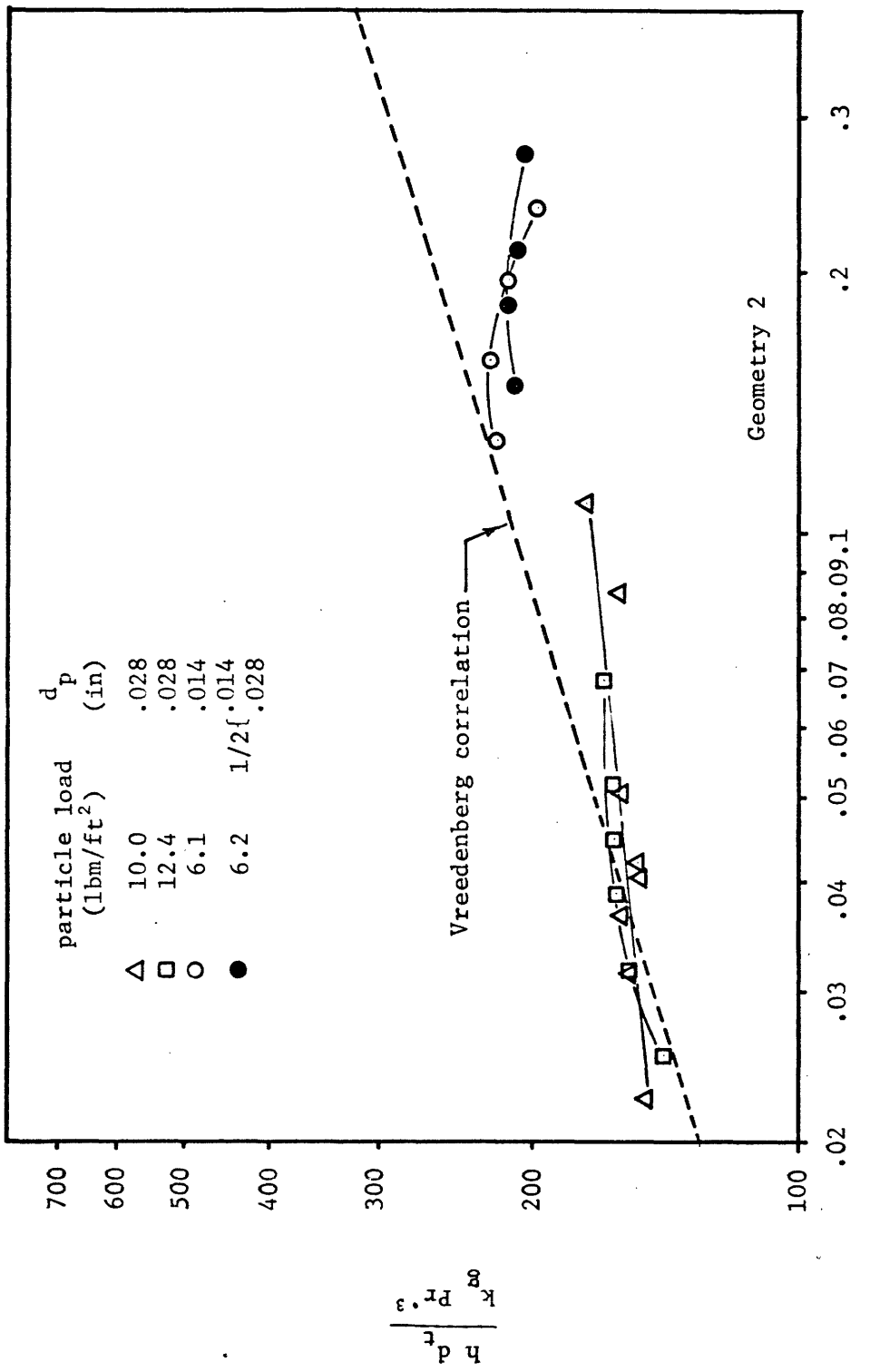

DATA PLOTTED WITH VREEDENBERG PARAMETERS

Figure 36A

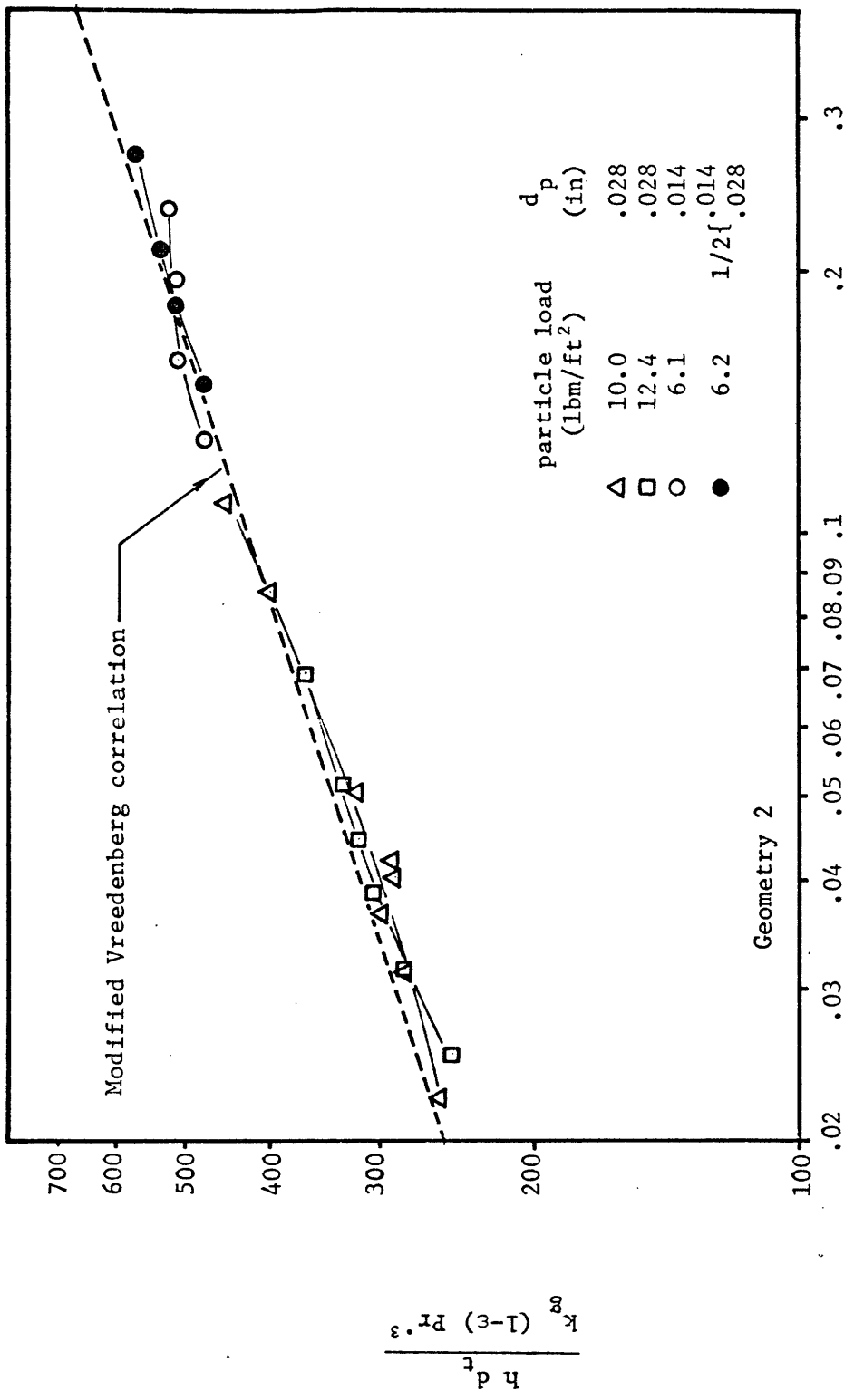

DATA PLOTTED WITH MODIFIED VREEDENBERG PARAMETERS

Figure 36B

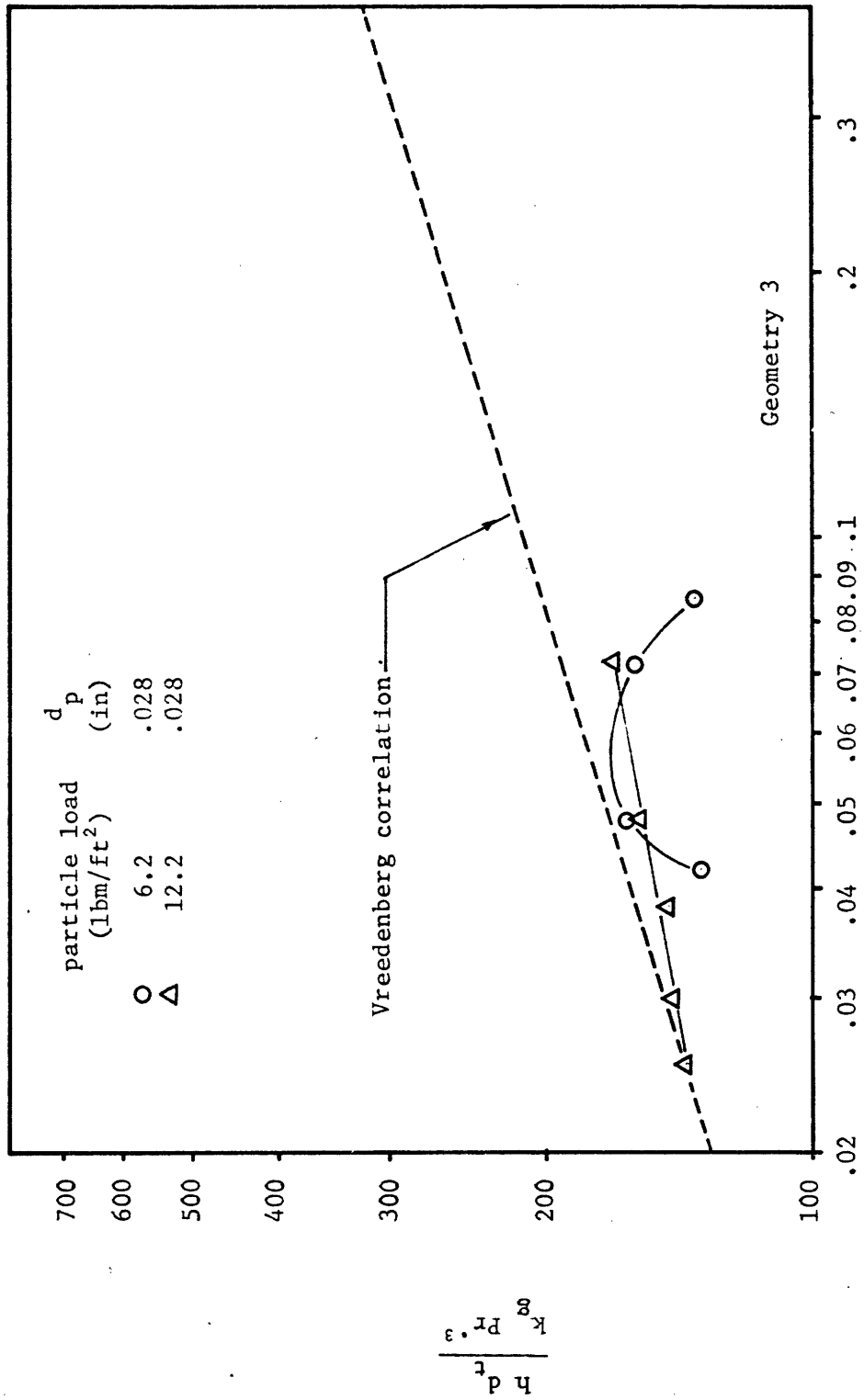

DATA PLOTTED WITH VREEDENBERG PARAMETERS

Figure 37A

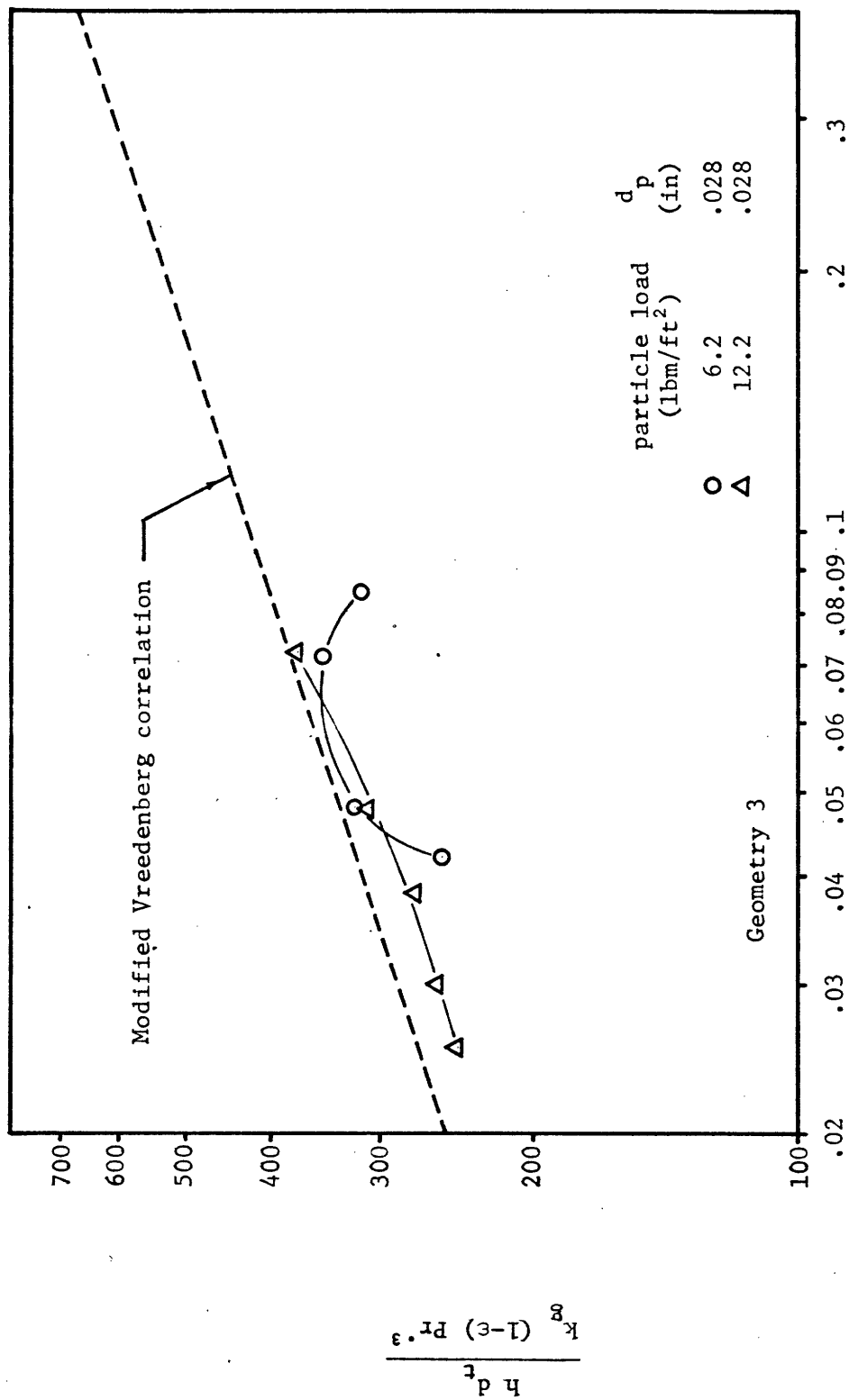

DATA PLOTTED WITH MODIFIED VREEDENBERG PARAMETERS

Figure 37B

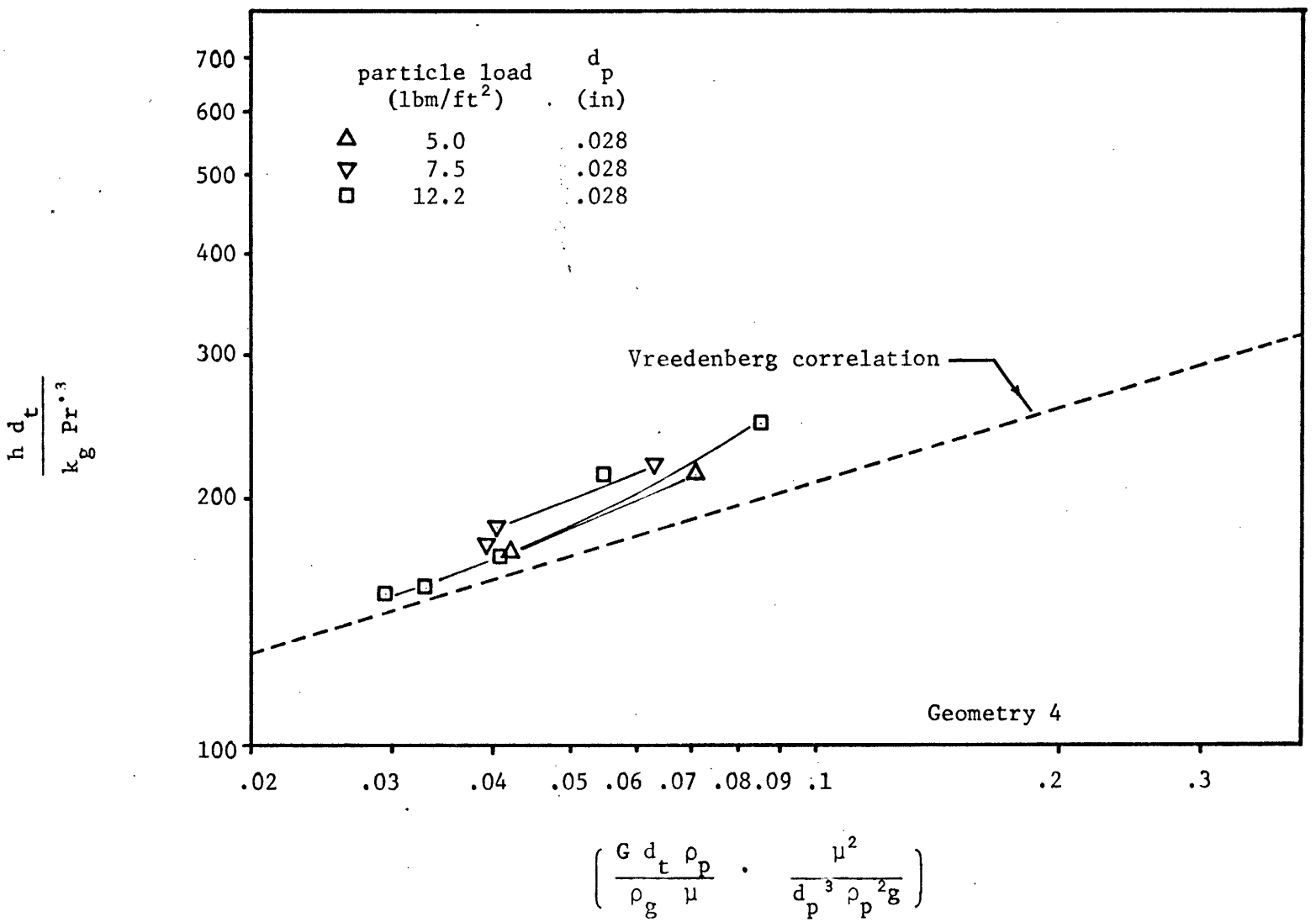

DATA PLOTTED WITH VREEDENBERG PARAMETERS

Figure 38A

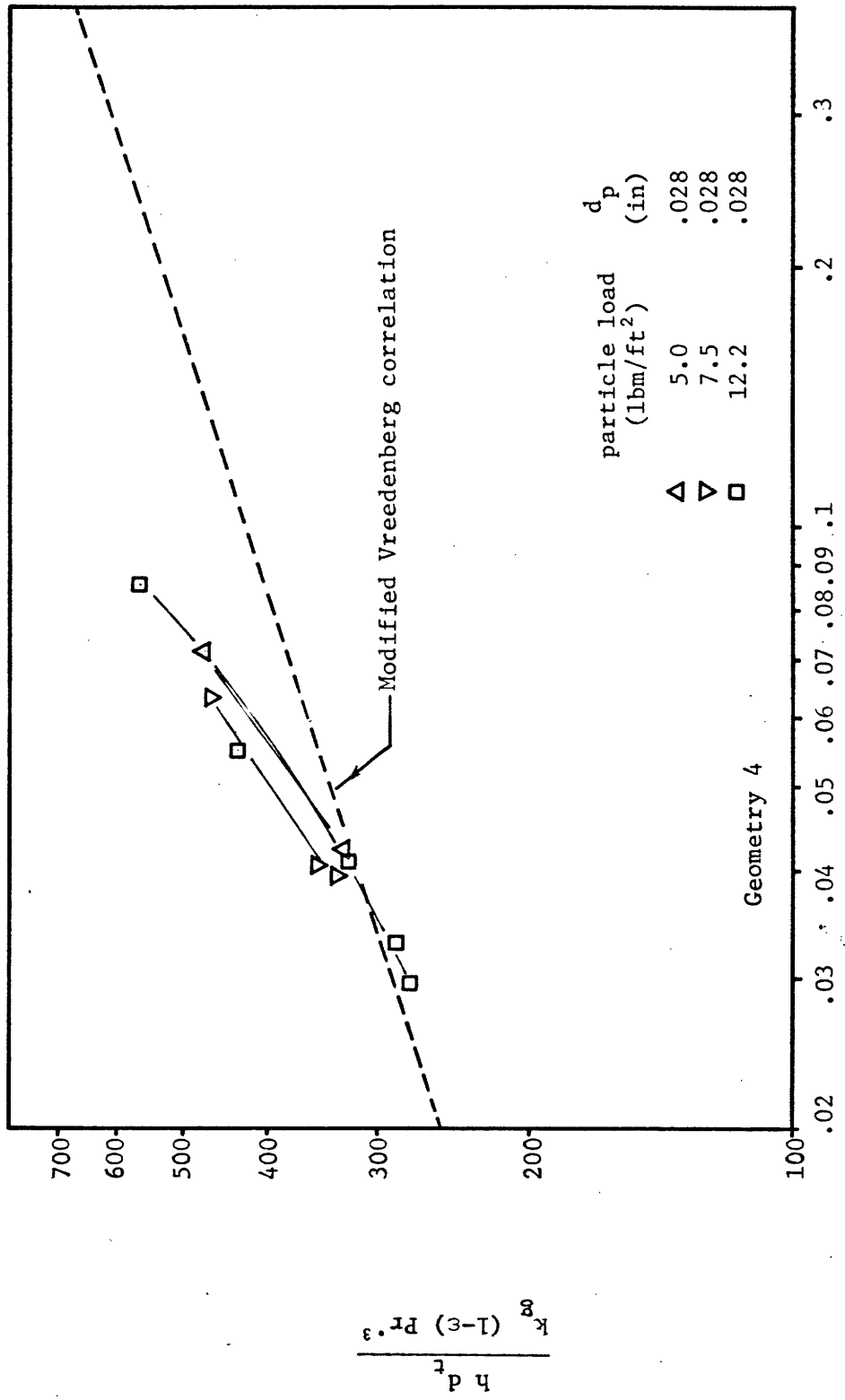

DATA PLOTTED WITH MODIFIED VREEDENBERG PARAMETERS

Figure 38B

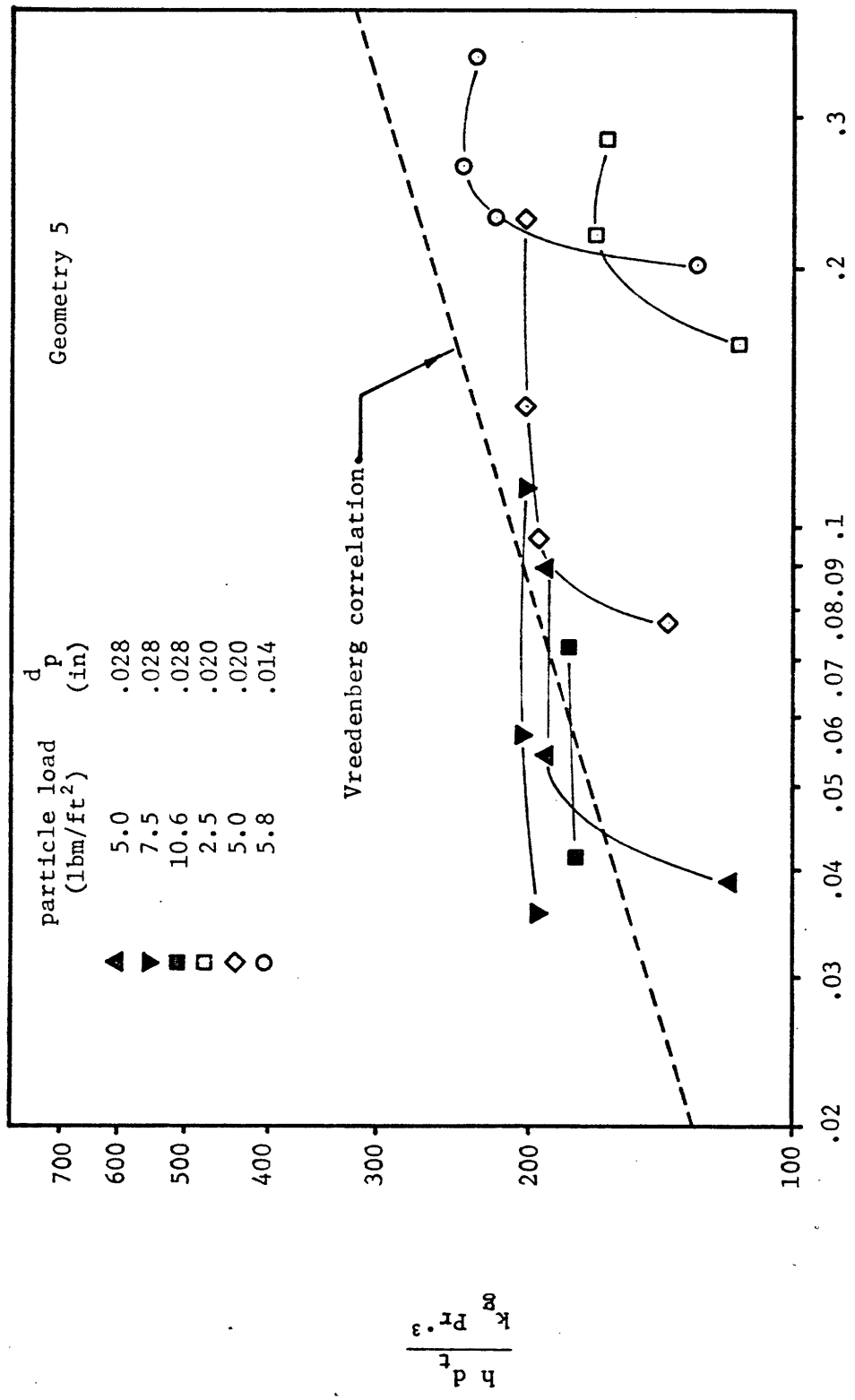

DATA PLOTTED WITH VREEDENBERG PARAMETERS

Figure 39A

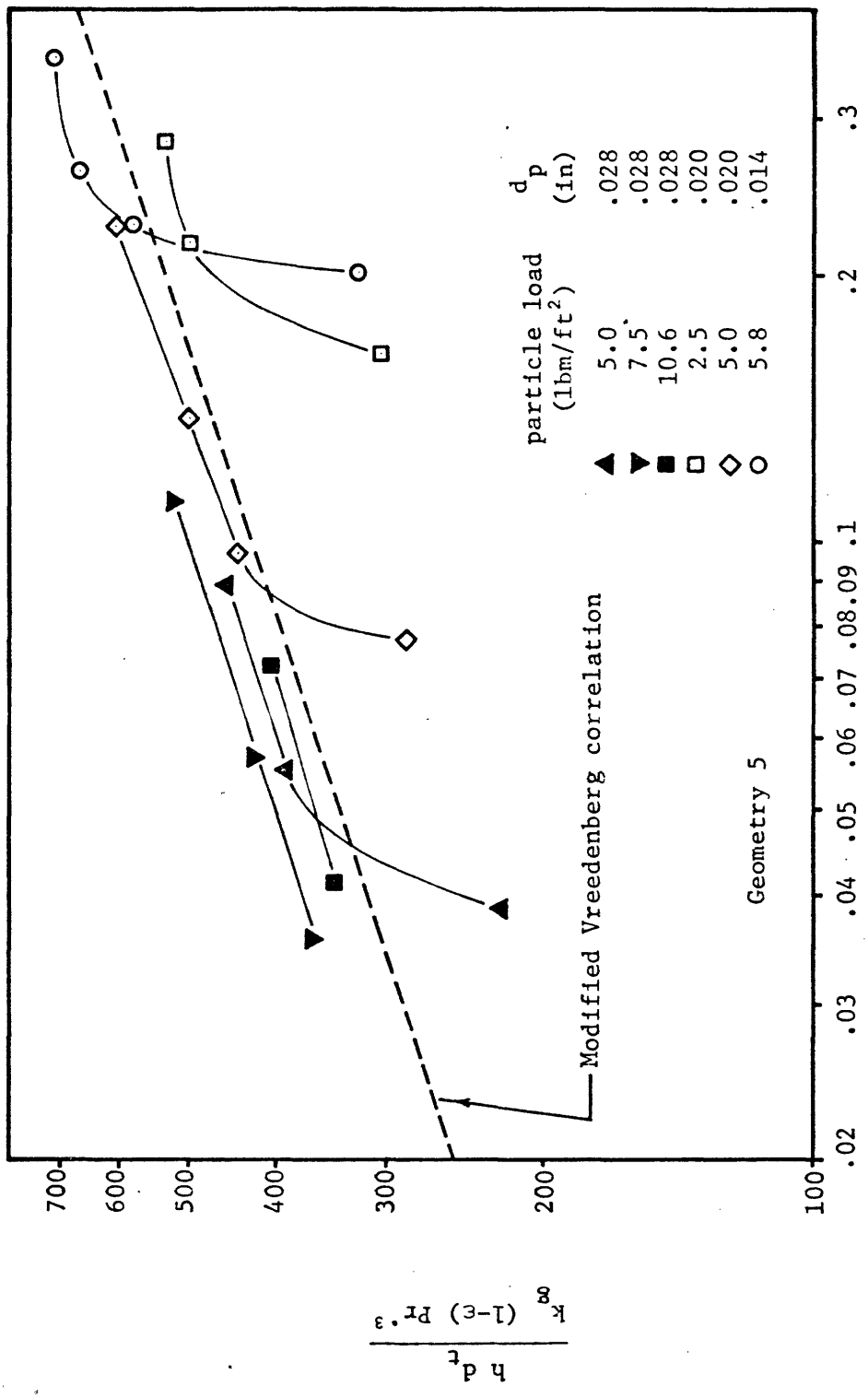

DATA PLOTTED WITH MODIFIED VREEDENBERG PARAMETERS

Figure 39B

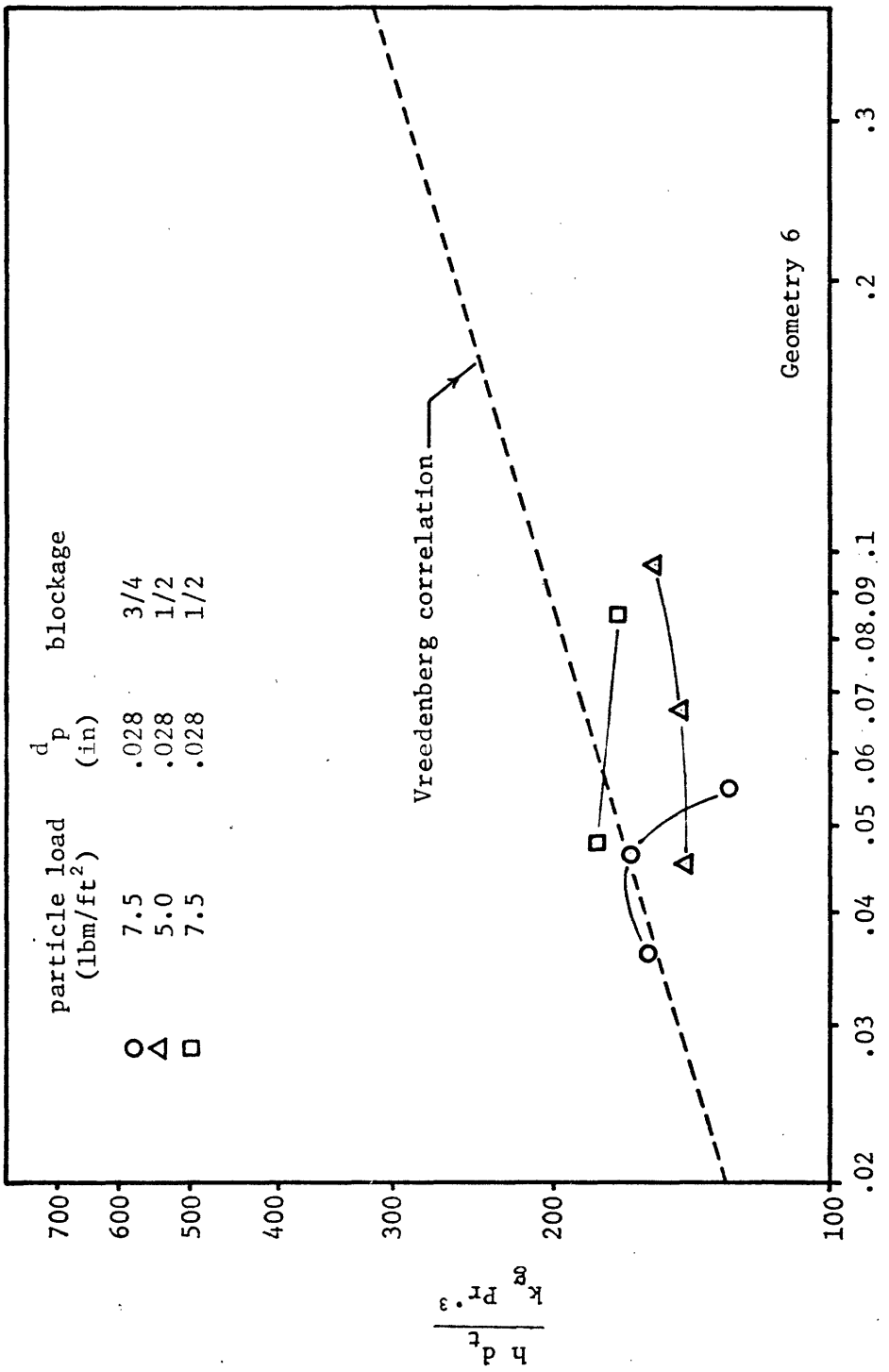

DATA PLOTTED WITH VREEDENBERG PARAMETERS

Figure 40A

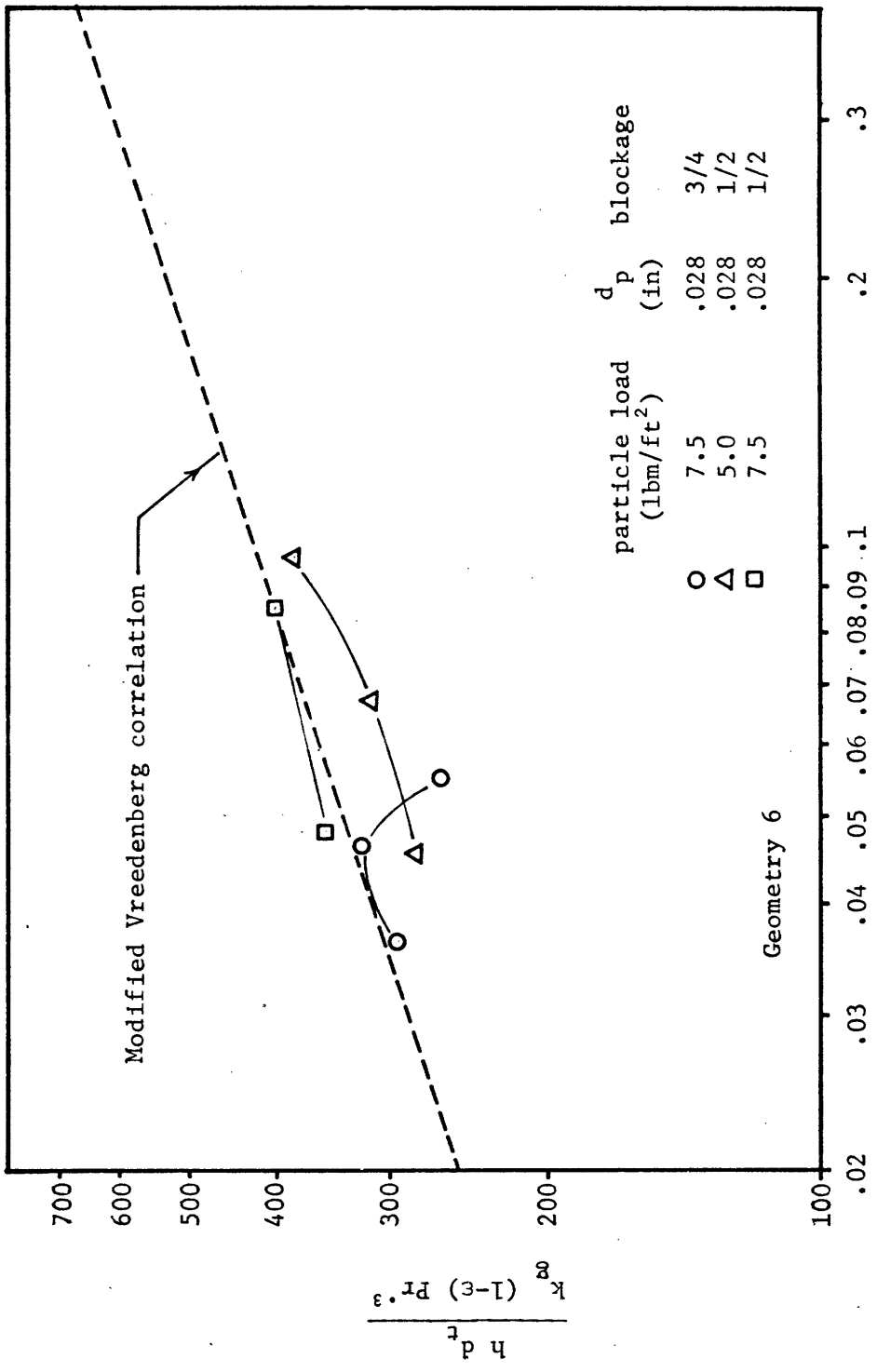

DATA PLOTTED WITH MODIFIED VREEDENBERG PARAMETERS

Figure 40B

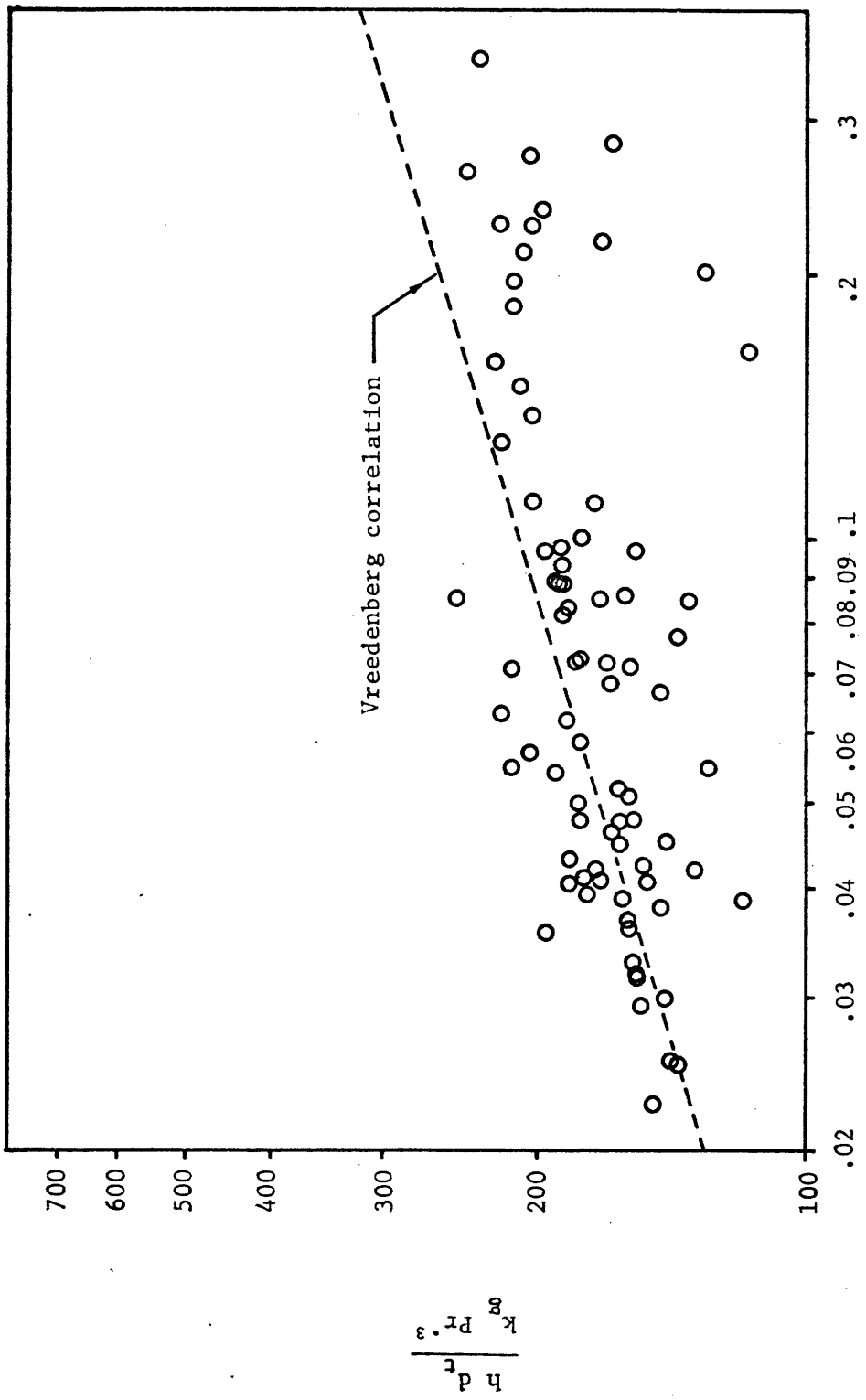

DATA PLOTTED WITH VREEDENBERG PARAMETERS

Figure 41A

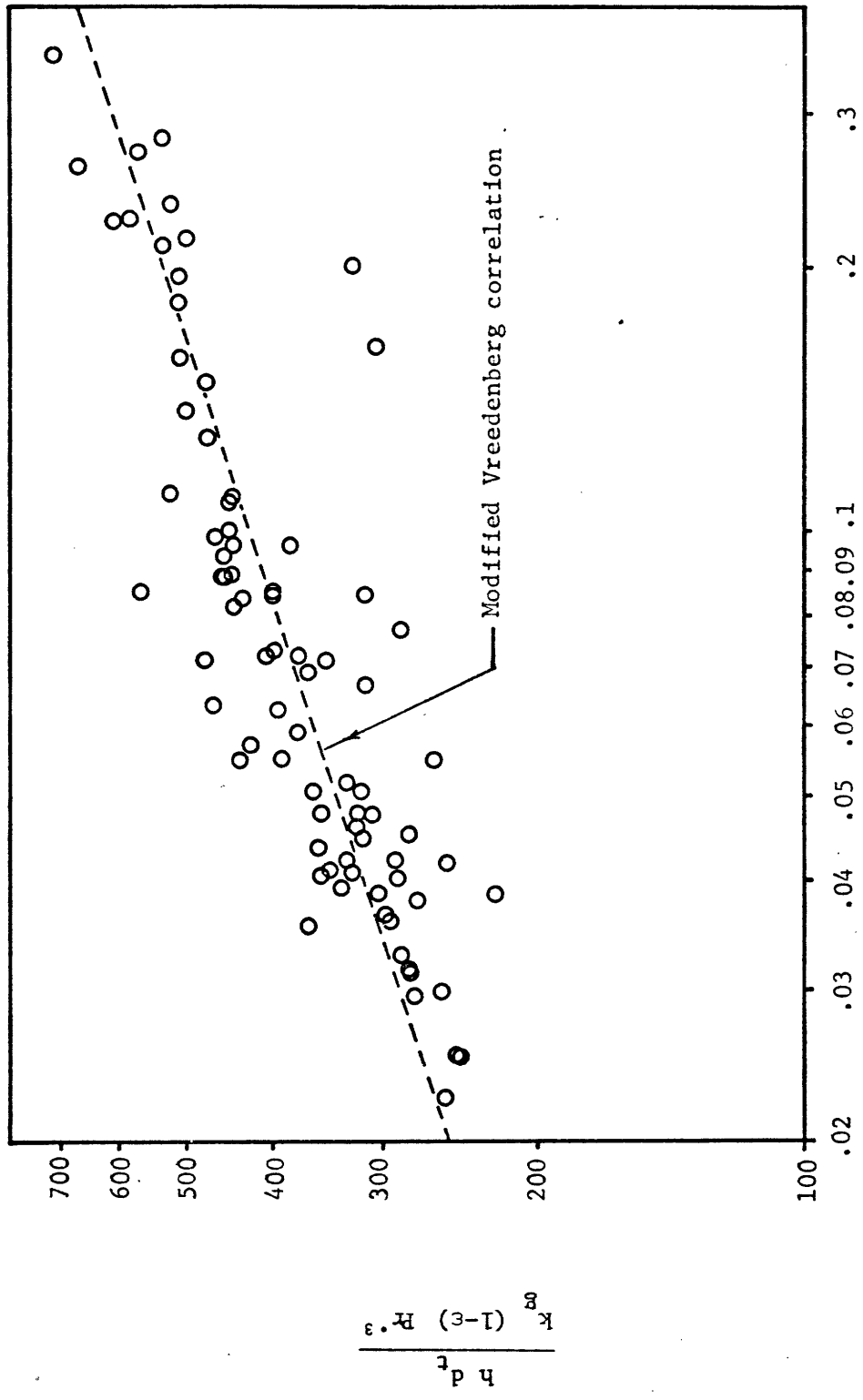

DATA PLOTTED WITH MODIFIED VREEDENBERG PARAMETERS

Figure 41B

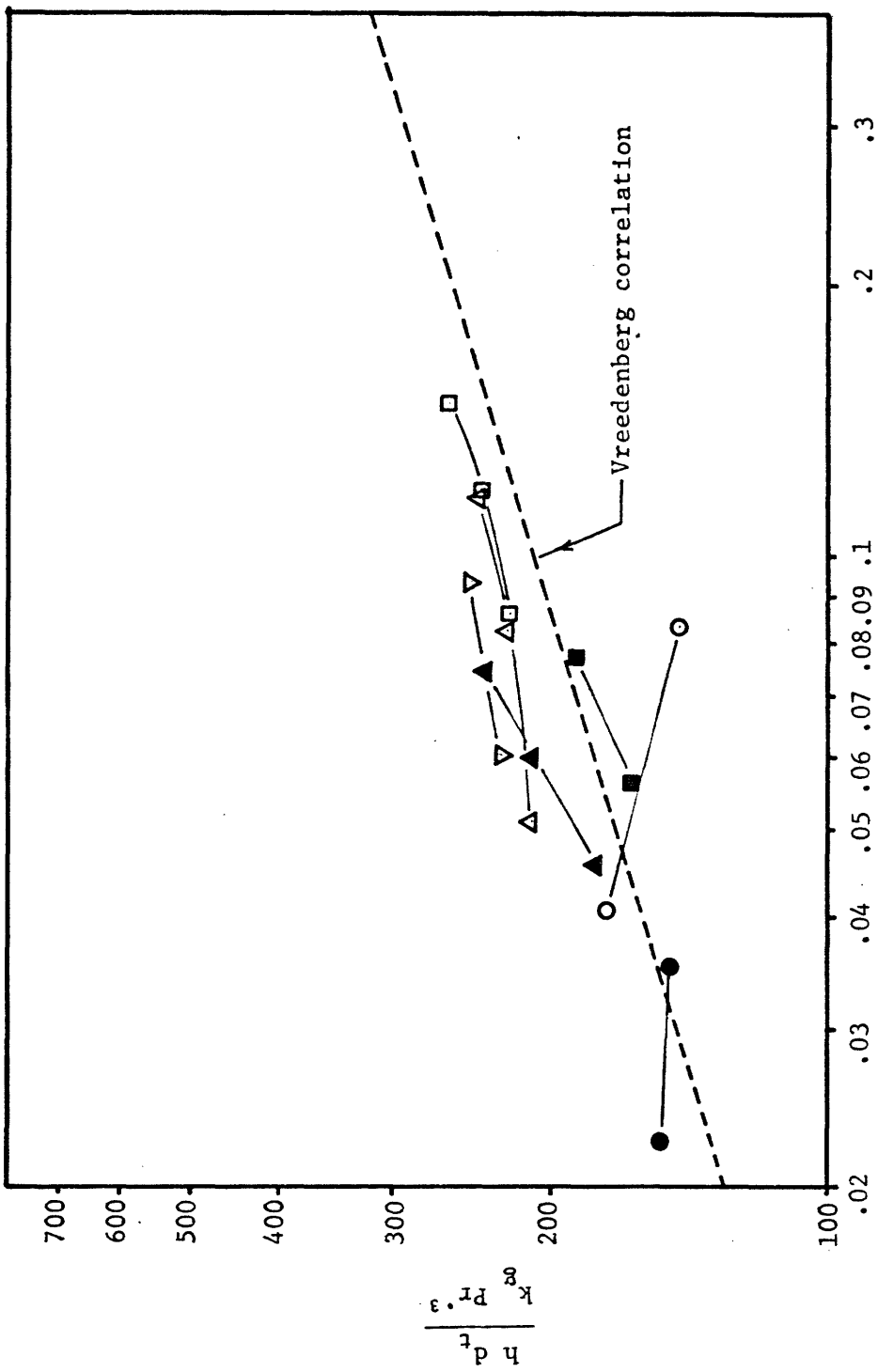

VREEDENBERG'S DATA PLOTTED WITH VREEDENBERG PARAMETERS

Figure 42A

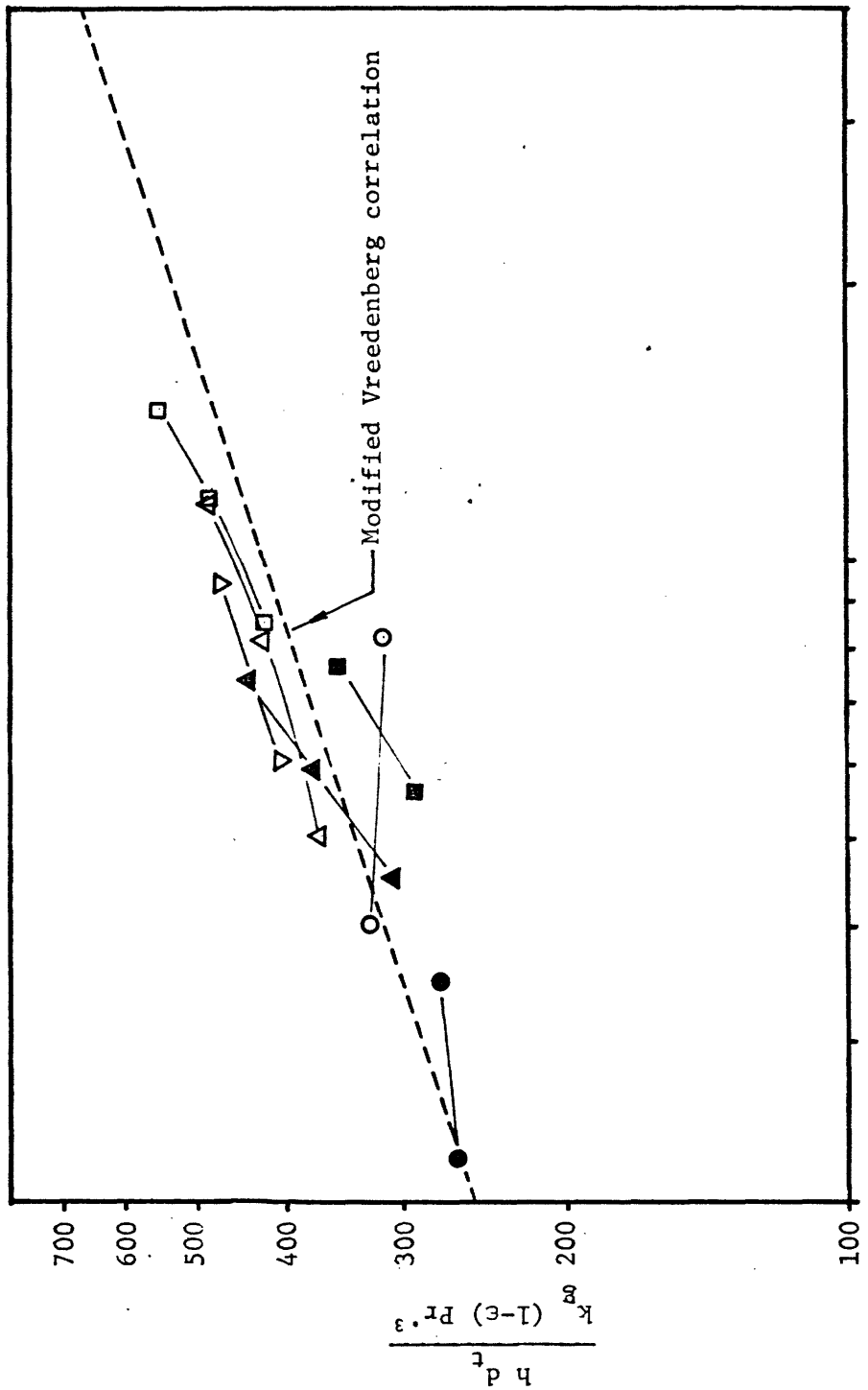

VREEDENBERG'S DATA PLOTTED WITH MODIFIED VREEDENBERG PARAMETERS

Figure 42B

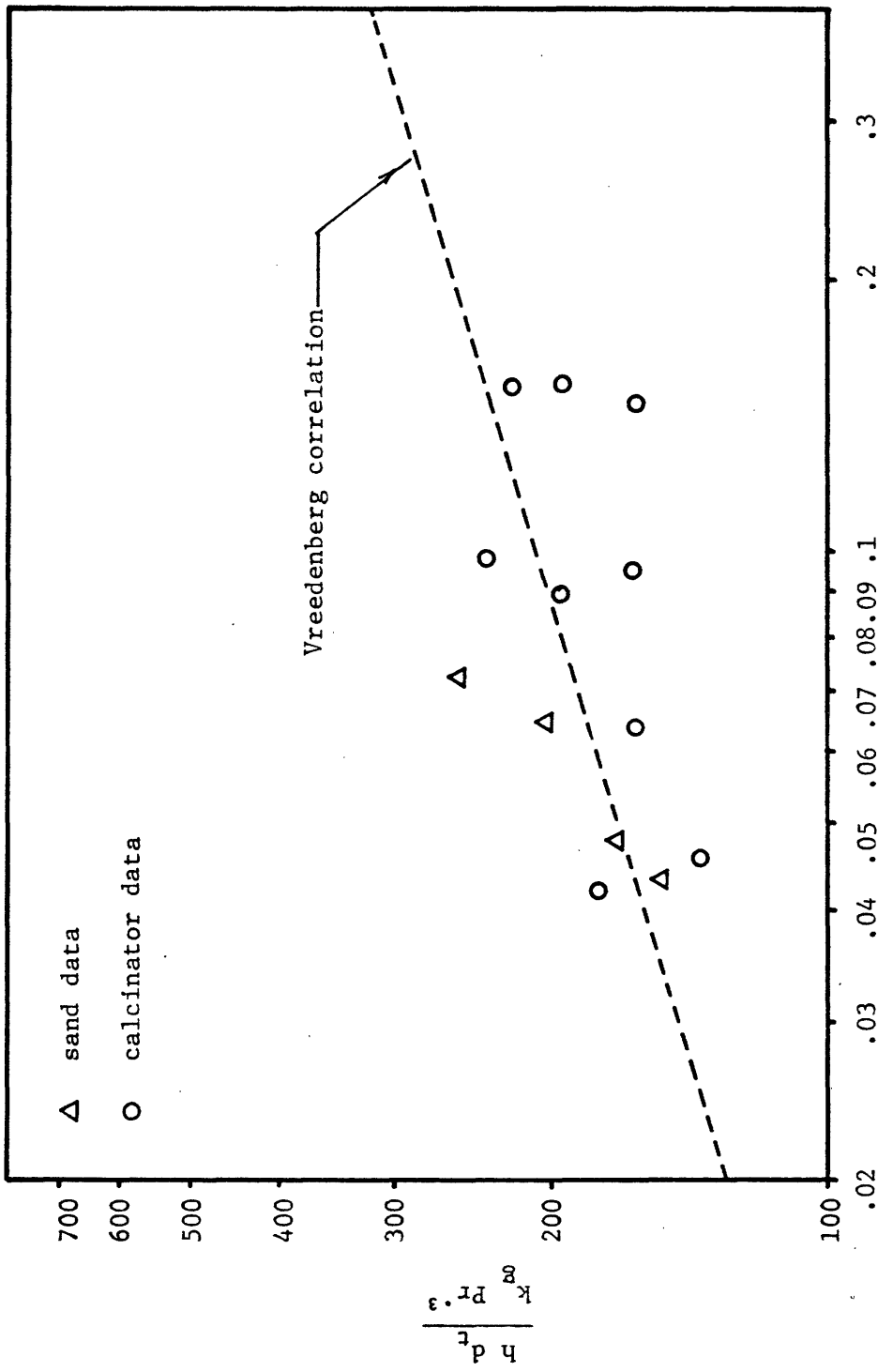

PETRIE'S DATA PLOTTED WITH VREEDENBERG PARAMETERS

Figure 43A

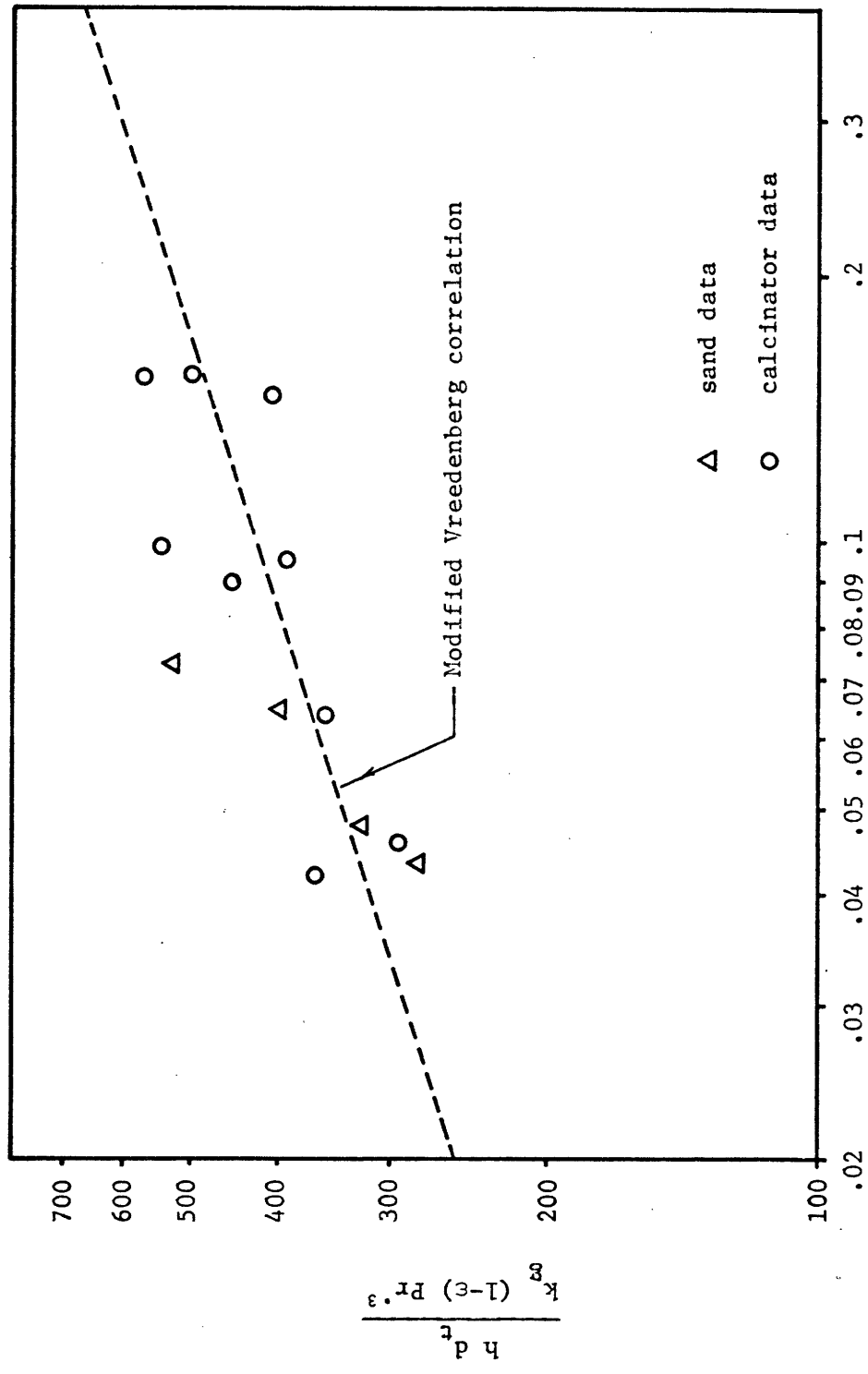

PETRIE'S DATA PLOTTED WITH MODIFIED VREEDENBERG PARAMETERS

Figure 43B

Table 6

RMS Deviation of Data from Vreedenberg Type Correlations

Geometry/Data	Equation 72		Equation 80		Equation 81
	$V_g=V_s$* (%)	$V_g=V_s/(1-\text{blockage})$ (%)	$V_g=V_s$† (%)	$V_g=V_s/(1-\text{blockage})$ (%)	$V_g=V_s/(1-\text{blockage})$ (%)
Δ-uniform	9.7	9.7	8.1	8.1	8.5
uniform	13.4	13.4	4.8	4.8	4.4
3/4 blocked, $\alpha = 1/2$	14.5	41.8	12.2	12.0	13.5
3/4 blocked $\alpha = 1/4$	14.3	26.2	20.2	27.2	23.7
1/2 blocked	26.4	35.8	19.0	20.5	19.4
Sum of above	17.5	26.7	13.8	15.9	14.8
vaned	16.8	35.0	12.1	11.2	12.3
Vreedenberg data	14.9	--	11.2	--	--

* data graphed in figures 35A - 42A

† data graphed in figures 35B - 42B

IV.4.5 Correlation of Data to The Model of Section II.2.6

The h predicted by the model of section II.2.6 was the sum of equations 66, 18, and 25. Or nondimensionalized:

$$\frac{h_{net}\, d_p}{k_g} = 1.17\ (1-\varepsilon)^{2/3}\ \ln\left[\frac{5.27}{(1-\varepsilon)} + 1\right] + .03\ (1-\varepsilon)^{1/8}\left[\frac{V_p\ \rho_p\ d_p}{\mu}\right]^{.625} + 1.13\left[\frac{d_p\ V_p}{\alpha}\right]^{1/2} \qquad (82)$$

Implicit in the development of this model was that the velocity of the particle (V_p) was the root mean square of the fluctuational velocity ($V_p = \tilde{v}' = (g\ \nu\ V_a)^{1/4}$). Experimental data is compared to equation 82 in figures 44 - 49. In the figures, the void and particle velocites are based upon the superficial air velocity. Table 7 lists the RMS deviation of data from equation 82 both for this case and the case where void and particle velocity are based on $V_a = V_s/(1 - \text{blockage})$.

Like the Wender-Cooper case, the model strongly segments data into narrow bands in accordance with particle size, but is within 10-20% of the measured h. The form of the data curves as compared to the form of the model is not as consistant as the Vreedenberg form, but it is far better than the non-existant form of the data when plotted with the Wender-Cooper parameters.

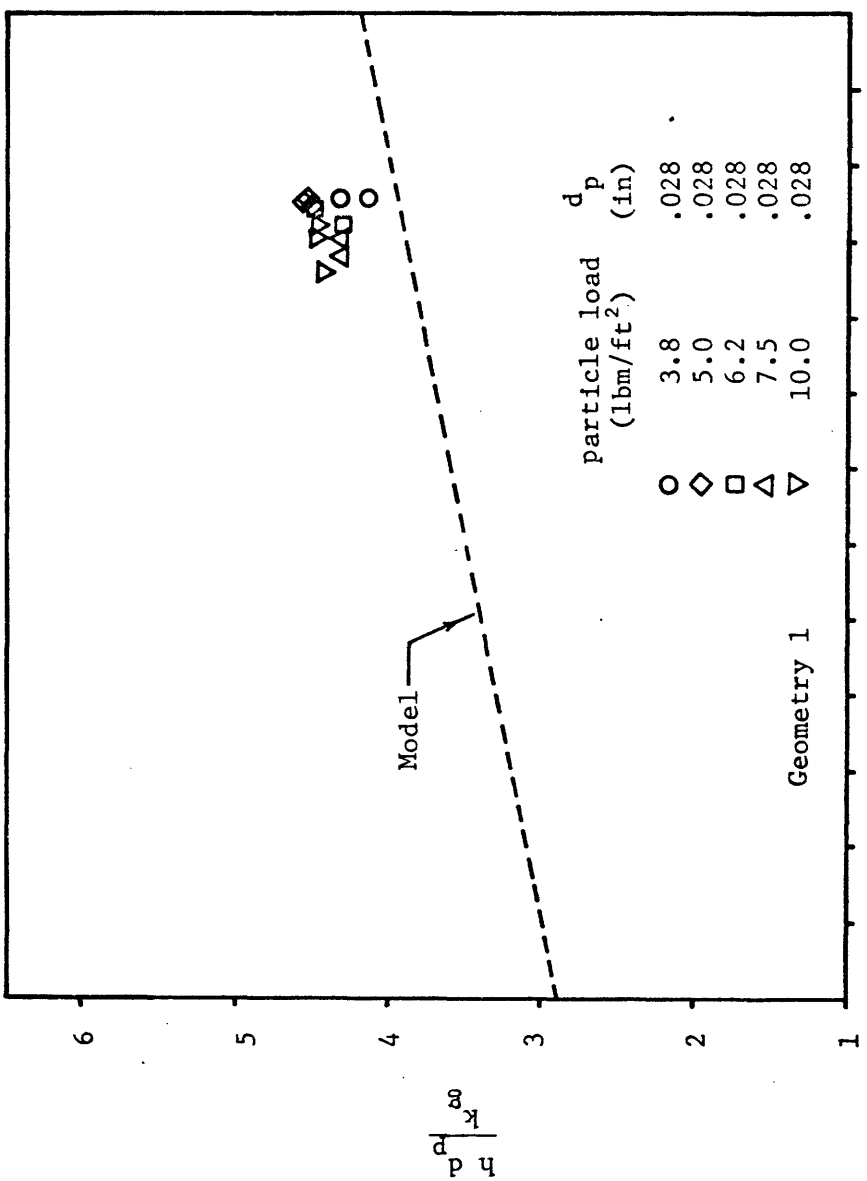

COMPARISON OF DATA WITH MODEL OF SECTION II.2.6

Figure 44

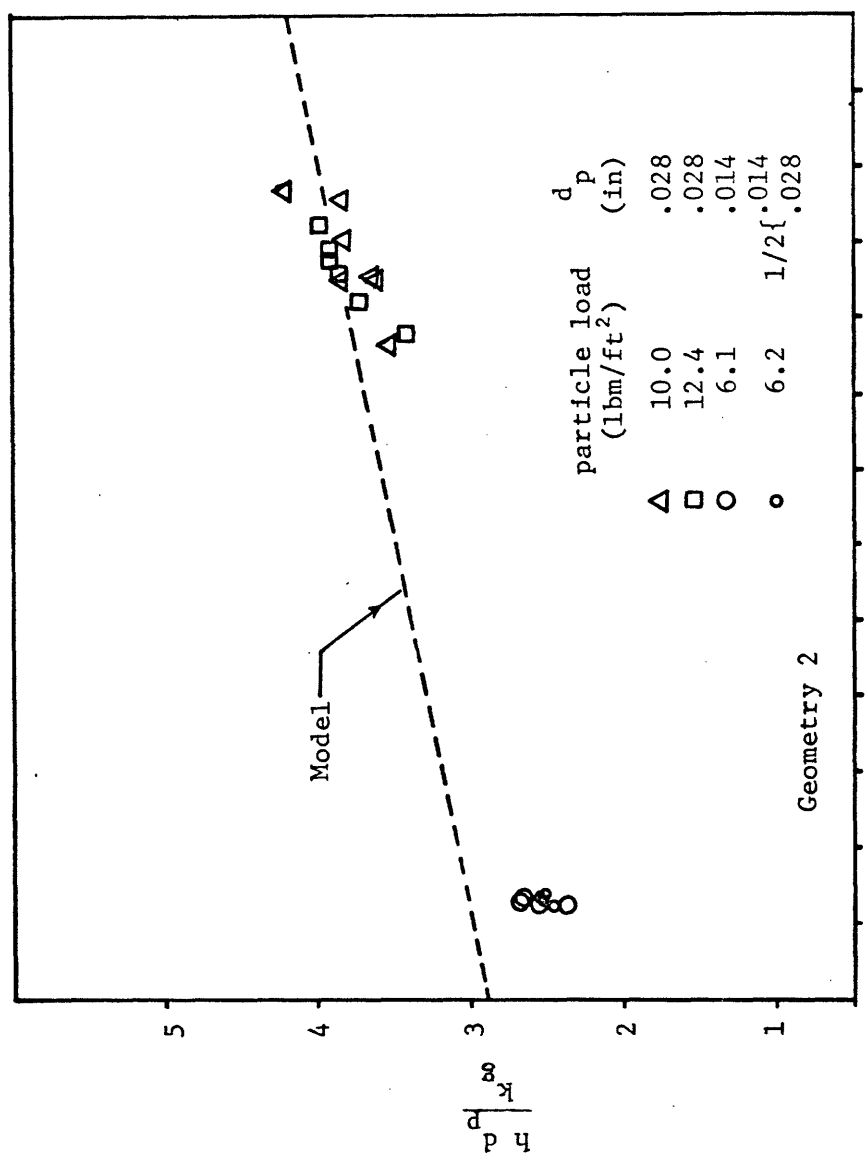

COMPARISON OF DATA WITH MODEL OF SECTION II.2.6

Figure 45

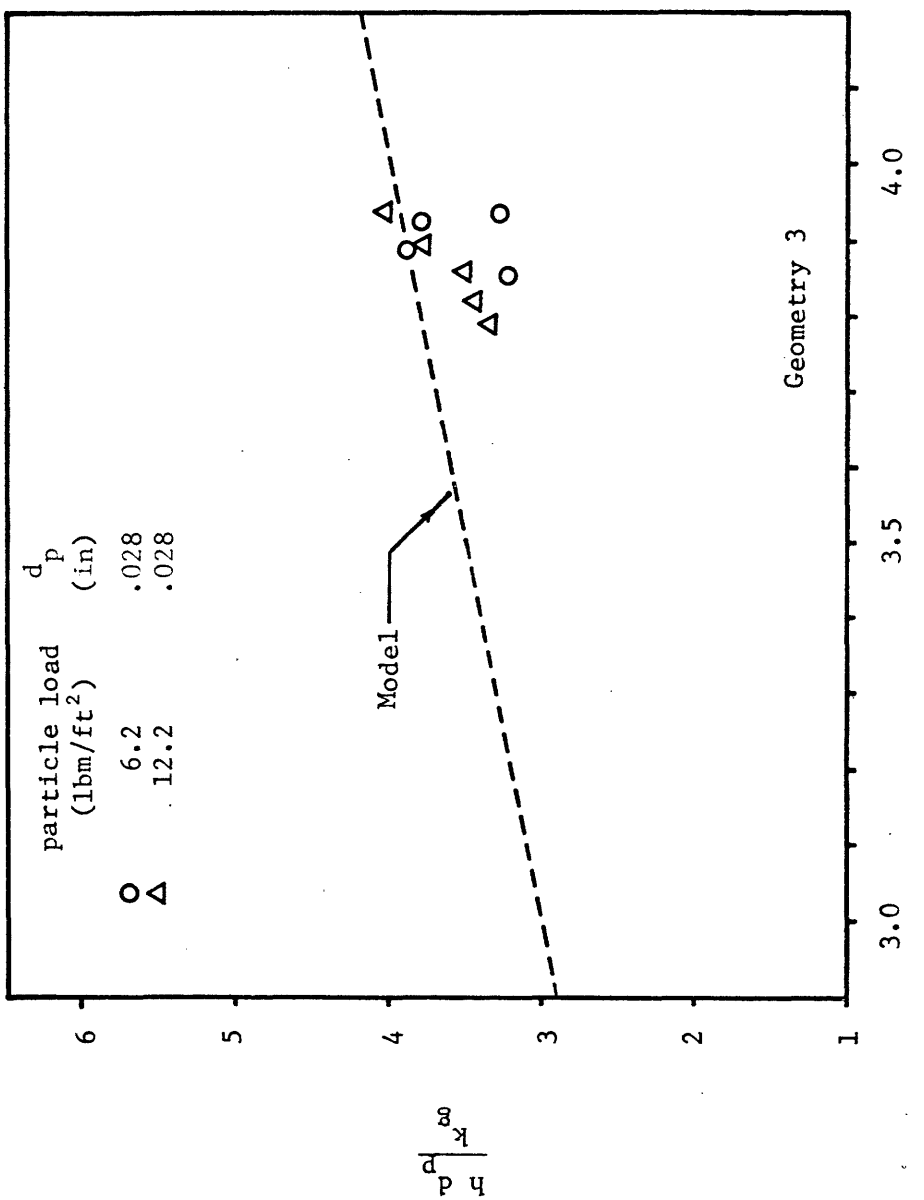

COMPARISON OF DATA WITH MODEL OF SECTION II.2.6

Figure 46

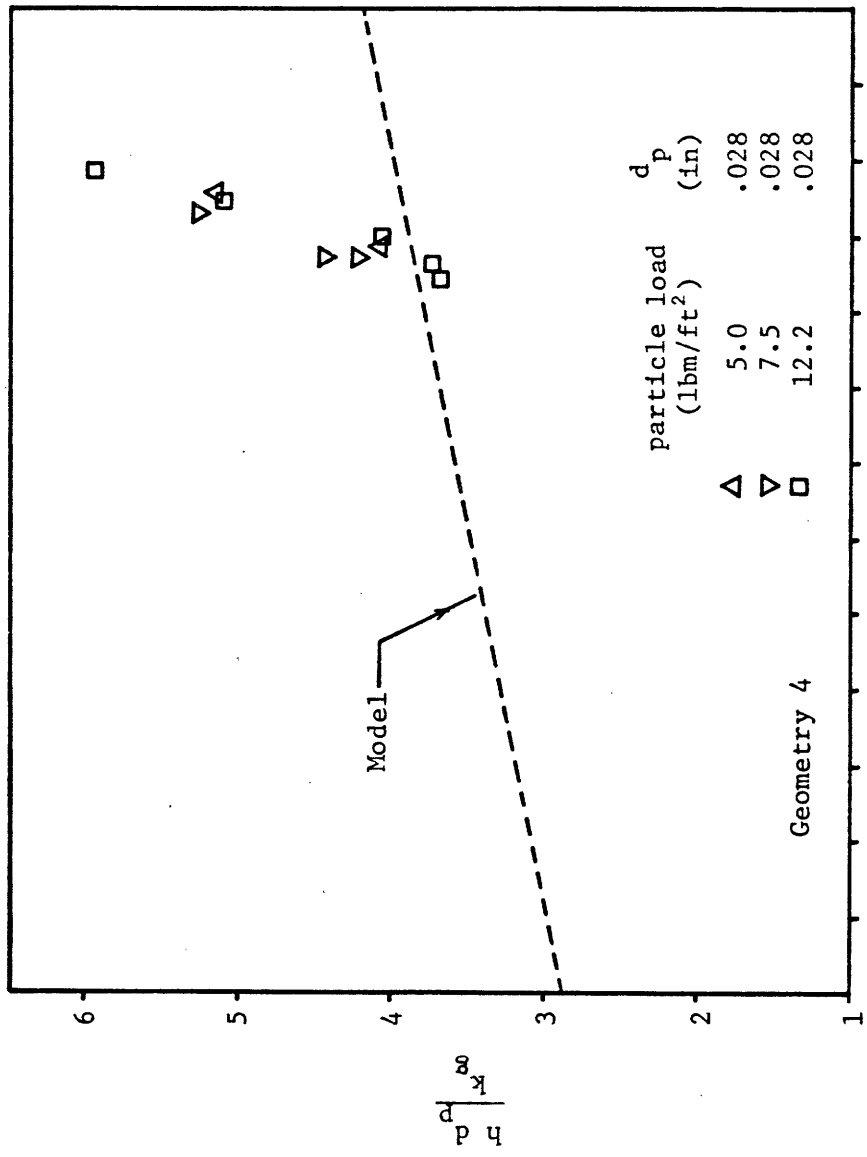

COMPARISON OF DATA WITH MODEL OF SECTION II.2.6

Figure 47

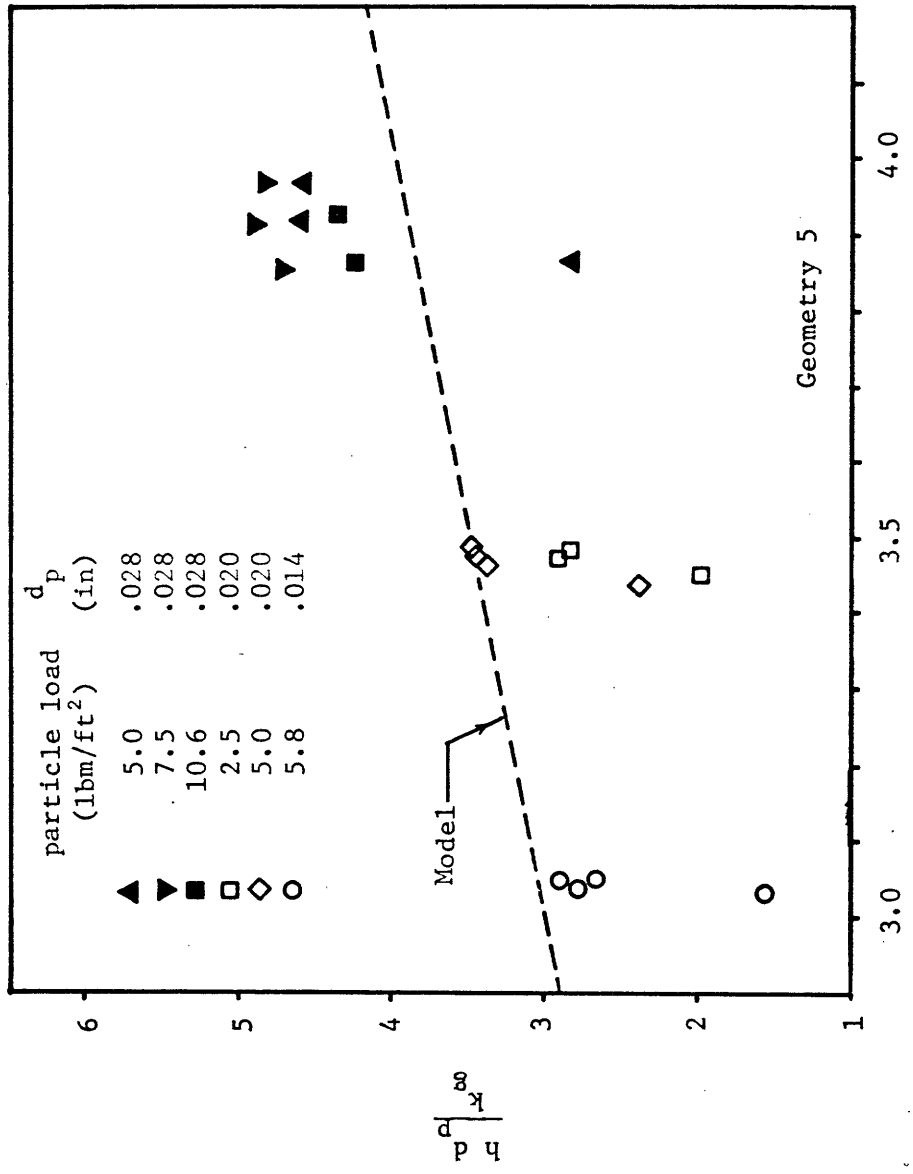

COMPARISON OF DATA WITH MODEL OF SECTION II.2.6

Figure 48

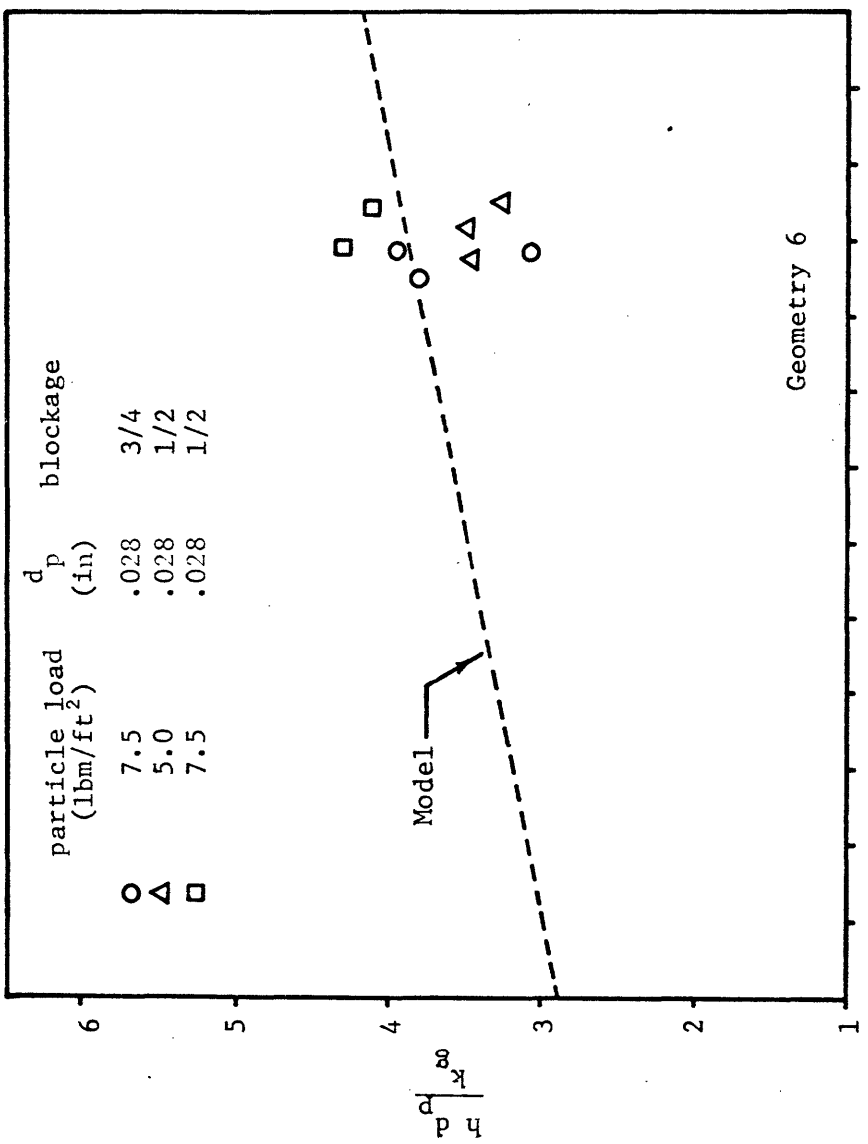

COMPARISON OF DATA WITH MODEL OF SECTION II.2.6

Figure 49

Table 7

RMS Deviation of Data from Model of Section II.2.6

Geometry/Data	Assuming $V_g=V_s$ * (%)	Assuming $V_g=V_s/(1-\text{blockage})$ (%)
Δ-uniform	12.8	12.8
uniform	10.5	10.5
3/4 blocked, α=1/2	10.1	12.6
3/4 blocked, α=1/4	23.4	20.4
1/2 blocked	22.0	21.5
Sum of above	16.7	16.2
vaned	10.0	11.1

* data graphed in figures 44 - 49

IV.4.6 Comparison of Correlations

By comparing tables 4-7, it is evident that the best correlation is obtained by the Vreedenberg correlation modified to encorporate $(1-\varepsilon)$ and using $V_g = V_s$. Data from all particle sizes and distributer geometries match this modified correlation in magnitude as well as form. In contrast, the Ainshtein correlation seems to lack the proper variable relationships, as data collapsed well for different particle sizes, but failed to collapse together as a whole. The correlation goes through the individual data, but the form of the data curves are different than the correlation's. The Wender-Cooper correlation also yielded good agreement with data, but also lacks any consistancy between the shape of the curves formed by data and the correlation. The scatter of data points about the correlation is almost random. Further, the correlation factor Cr has no real significance for horizontal tubes as they aren't axially alligned.

The fact that data compares favorably with the model of section II.2.6 is exciting. Predicted values derived solely from theoretical assumptions are within 10-20% of experimental data. This is particularly pleasing when the model was derived for a vertical wall, and hence has no dependency on d_t. As far as is known, this is the first time data has been so well correlated by a first principle analysis. No empirically determined constants are in equation 82.

None of the correlations take into account effects of closeness to the distributer, presence of other tubes, and the like, However, these effects are small, at least until the distances start to approach the order of magnitude of the particle size or the mean free path of the

particles. This was noted by Lese & Kermode as discussed in section II.3.2, and by the dropping of the horizontal tube very close to the distributer, as in geometry 4.

With this effect, modified Vreedenberg correlation is poorest (with an RMS deviation of about 20%) in predicting values of h when the distributer is 3/4 blocked and the distance between the tube and the distributer is 1/4". As discussed in section IV.3, this is probably due to a more direct impingement of air on the upstream side of the tube, and an interaction with the stagnant particles behind the blocked areas of the distributer.

The Vreedenberg correlation is almost as poor for the 1/2 blocked distributer (geometry 5). However, four experimental data points, as discussed in section IV.3, exhibit low h's due to poor fluidization and low particle loads. Eliminating these four points from the RMS deviation drops the deviation for the original Vreedenberg correlation to 20.7% and the deviation from the modified Vreedenberg correlation to 12.1% for this geometry.

Several interesting effects can be noted using the modified Vreedenberg correlation. Solving Leva's void relation (equation 76) for V and substituting directly into equation 80 yields:

$$\frac{h\, d_t/k_g}{Pr^{.3}} = 900(1-\varepsilon)\left[18\,\frac{\varepsilon^3}{1-\varepsilon}\,\frac{d_t}{d_p}\right]^{.326} \tag{83}$$

or, with rounding the power .326 to .33,

$$\frac{h\, d_t/k_g}{Pr^{.3}} = 2300(1-\varepsilon)^{.66}\;\varepsilon\;(d_t/d_p)^{.33} \tag{84}$$

Hence, the tube Nusselt number is only a function of void, particle and tube size, and Prandtl number. Fluid and particle properties are all hidden in the void relation. However, this relation is no more convenient than equation 80, as the prediction of void must be made using fluid and particle properties.

Further, the modified Vreedenberg equation allows a calculation of the optimum particle diameter for heat transfer. Substituting the linearization (equation 77) of Leva's void relation into equation 80 yields:

$$\frac{Nu_t}{Pr^{.3}} \simeq 730\left(\frac{V\, d_t\, \mu}{\rho_p\, d_p^{\,3}\, g}\right)^{.33} - 430\left(\frac{V^2\, \mu^2\, d_t}{18\, \rho_p^{\,2}\, g^2\, d_p^{\,5}}\right)^{.33} \tag{85}$$

where again the power .326 in equation 80 has been approximated by .33. Differentiating this with respect to d_p, equating to zero, and solving for d_p yields

$$d_{p\ \text{optimum}} = \left(\frac{V\, \mu}{18\, \rho_p\, g}\right)^{1/2} \tag{86}$$

which relates d_p to the fluid parameter which are used in the void determination. Substitution of $d_{p\ \text{optimum}}$ back into equation 77 gives

$$\varepsilon_{\text{optimum}} = .66 \tag{87}$$

or, optimum heat transfer occurs when void equals .66.

In other words, for a specific particle density and fluid velocity and viscosity, the optimum particle diameter is one which will result in a void fraction of .66. Stated simply, it is the void fraction, not the particle diameter, which is optimized. Void fractions of about .66 were

experimentally achieved.

From equation 84 it can be seen that at optimum void, the Nusselt number is only a function of particle and tube diameters, and the Prandtl number. The use of heavier particles does not increase the maximum achievable h. They do however, require more air pumping power to achieve optimum void, and allow a greater air mass flow rate. As discussed in Appendix 5, the heat rejected is proportional to the mass flow rate.

Using optimum void and equation 85, for d_p = .028", and sand and air parameters, $h_{optimum}$ = 37.3 BTU/hr ft^2 °F. Experimental values of about 33 BTU/hr ft^2 °F were achieved.

IV.5 Experimental Pressure Drops

Within the accuracy of the measurements, the pressure drop across the bed after correcting for the loss across the distributer was equal to the bed weight per unit of frontal area.

The pressure drop across any given distributer increased with velocity, and was between 20 and 80% of the total pressure drop across both the bed and the distributer. The lower percentage was achieved for some of the low velocity cases. For these cases, the bed was still stable, or actively fluidized over the entire test area. Presumably, a stable bed could be maintained at any velocity with only 20% of the total pressure drop occuring across the distributer. Experimentally, this could have been achieved by removing some or all of the cloth backings which were immediately upstream of the wire cloth distributer.

Some pressure drop across the distributer is necessary to maintain bed stability. With a distributer with no pressure drop, the bed pressure drop at any locale is equal to the weight of the particles supported. Also the local velocity, and hence the void, is inversely proportional to the local pressure drop. This leads to an instability. Any random local increase in the bed weight will decrease the local velocity and void while increasing (by continuity) the velocity and void at some other locale. Particles will be 'pumped' from the high velocity locale to the low velocity locale. The velocity at the low velocity locale eventually will be reduced to below minimum fluidization levels. Particles will continue to be deposited there until the high velocity locale is void of particles.

A distributer whose pressure drop increases with velocity establishes a maximum velocity for the high velocity locale. If this maximum velocity is low enough, the velocities at other locales will be high enough for fluidization. As long as the entire bed remains fluidized, any random local variation in the bed weight will be evened out.

IV.6 Economic Comparison of Fluidized Beds to Finned Tubes

Fluidized beds large enough to reject 5.4×10^9 BTU/hr, or about that rejected from a 1000 mw power plant, require an extremely large frontal area. The frontal area is in the range of 2×10^6 ft^2, or about 45 acres. Unlike finned tubes, fluidized beds cannot be vertically wrapped about a tower or chimney because the frontal area must lie normal to the gravitational field, or parallel to the ground. However, they can be tiered as in fig. 50. Conceivably, beds could be tiered as either cylindrical towers with a single central fan or as long shelves with multiple fans (fig. 51). The 'long shelf' concept is the more desirable, as it requires only the use of straight pipes. Headers would run the length of both sides of the trays, with tubes running across the trays through the fluidized beds. The heat exchanger would use the indirect system, where condensation does not occur in the fluidized bed tubes, but rather steam from the turbine outlet is mixed with cool water from the heat exchanger in a spray condenser. Some of the condensate flow is routed back to the boiler, while the rest of the water recycles through the heat exchanger. The indirect system requires a greater mass flow of water through the heat exchanger than does the direct system, where the steam is condensed in the exchanger, but because of the difference between the specific volumes of steam and water, ducting sizes and costs are smaller for the indirect system. For power plants larger than about 200 mw, the indirect system is the more economical [30].

An economic comparison between a power plant sized finned tube cooling tower and a fluidized bed cooling tower was made using an optimized design program described fully in ref. 1 & 31. The design program designs the most economically favorable heat exchanger by optimizing heat transfer and thermodynamic relations with economic trade-offs. The

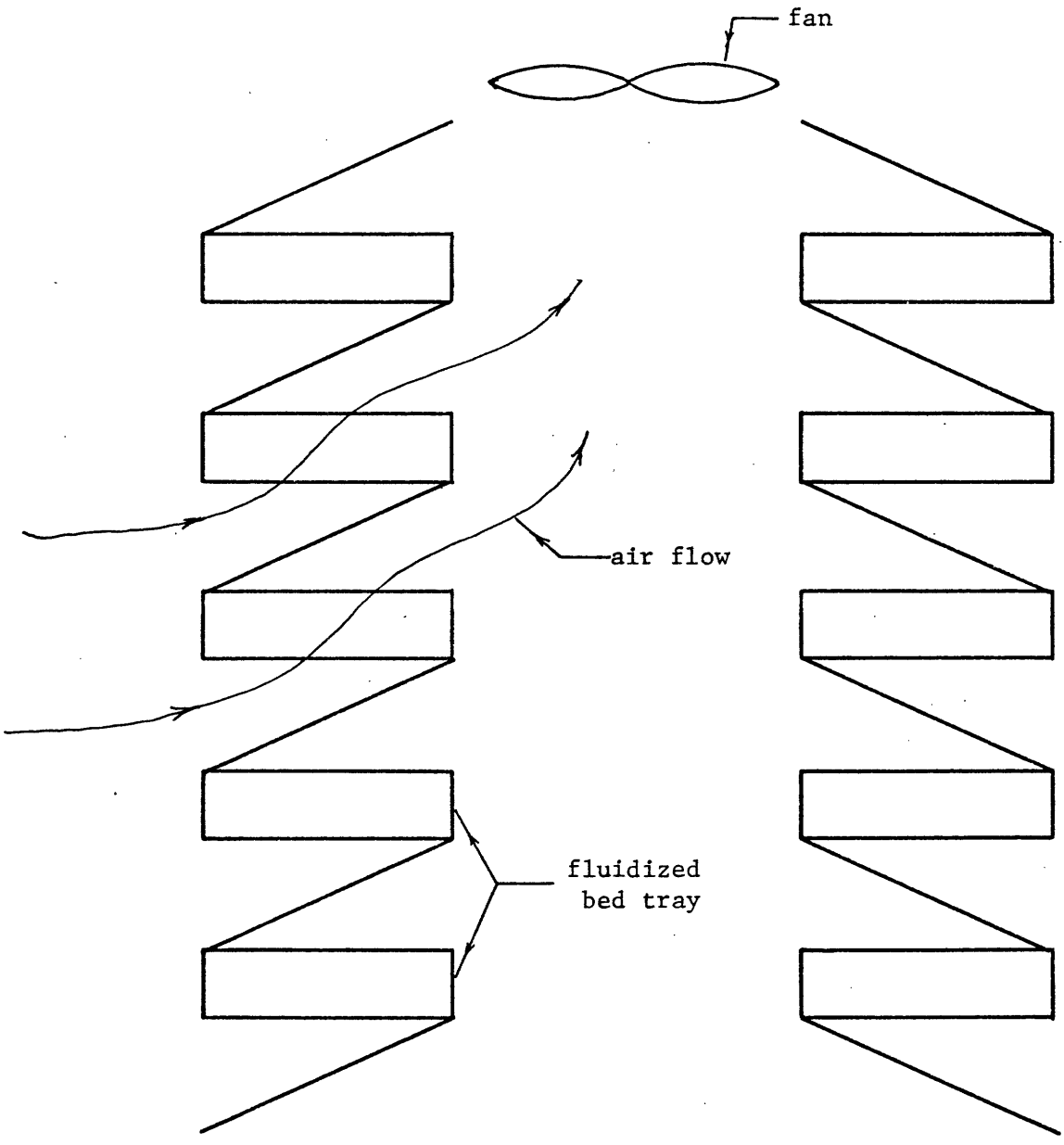

TIERED FLUIDIZED BEDS

-for cooling tower use-

Figure 50

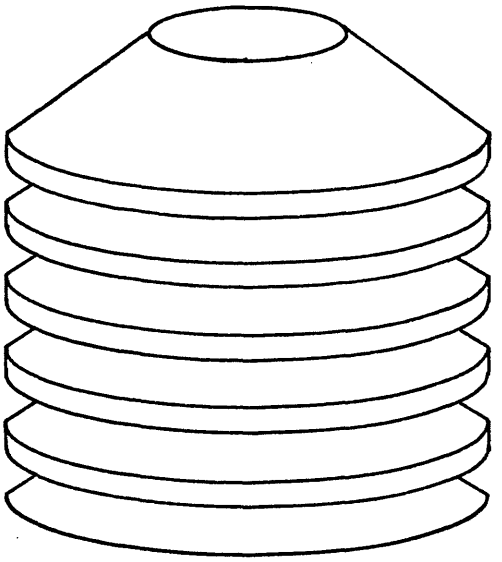

Cylindrical

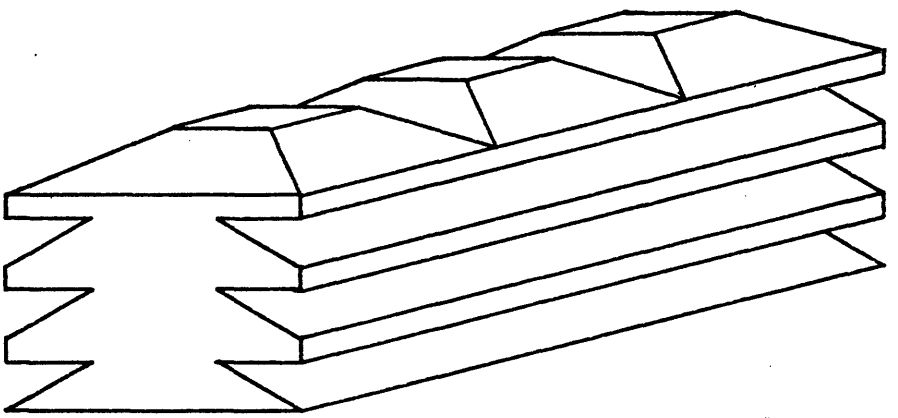

'Long Shelves'

CONCEPTUALIZATION OF FLUIDIZED BED COOLING TOWERS

Figure 51

routine, given the performance and characteristic dimensions of the heat transfer surface, efficiencies, cost factors, and the yearly atmospheric temperature profile, designs a heat exchanger. The program than minimizes the incremental increase in the average yearly cost of power generation (mills/kwh) resulting from the use of a dry cooling tower by systematically varying the design of the heat exchanger and the turbine back pressure. Included in this incremental cost are all costs associated with adding a dry cooling tower to the system and maintaining the same net generating power. As an example of additional costs incurred because of including a dry cooling tower, the Rankine efficiency of the system generally drops because of a higher heat sink temperature (ambient dry bulb temperature as opposed to the ambient water temperature for a once through system), which, to maintain the same net generated power, requires a larger boiler for the required larger steam throughput. The incremental cost yielded by the program is the cost increase over a power plant operating at 40% efficiency throughout the year with a negligible cost condenser. Accordingly, under these percepts, the cost of adding a conventional once through cooling system to a power plant is about 0.14 mills/kwh [1]. Hence the additional cost of installing a dry cooling tower, rather than a once through system, is the difference between the incremental cost and 0.14 mills/kwh. All costs mentioned in this section are referenced to a 1971 time frame, and are for comparitive purposes only. The present rapid increase of fuel, labor and parts costs are not included in the analysis. The incremental cost is figured from capital costs, maintenance and operating costs, increased plant size required to generate

power for fans and fluid pumping, increased fuel and boiler costs resulting from a decreased thermal efficiency, tower land costs, costs of piping between the turbine and the tower, and the cost of replacement power resulting from lost capacity at high ambient air temperatures. Lost capacity at high ambient air temperatures penalizes the operating cost at a fixed rate (mills/kwh).

Implicitly assumed in this dry cooling tower system optimization is the use of an indirect cooling system with an induced draft, single pass, cross flow heat exchanger. The nominal power plant output is 1000 Mw.

The program of reference 1 and 31 was modified to work with fluidized bed data and design parameters by two methods. In method number one, experimental data representative of the different experimental particle diameters was used. Experimentally measured h's for different particle diameters and different particle loads were expressed as a function of air velocity, with velocities limited to the experimentally measured region. Particle loads were chosen which had experimentally yielded the highest h for each particle size. By this method, the particle load per unit area remains constant throughout the optimization; and as the air side pressure drop through the bed is roughly equivalent to the particle load per unit area, the air side pressure drop remains constant. The second method used the modified Vreedenberg correlation (equation 80) to determine the h. Void was determined by using the linear approximation (equation 77) to Leva's expression of void (equation 76). Also assumed by this method is that the bed depth, regardless of the void fraction, is constant. This implies that as the air velocity increases, the particle fraction decreases, causing the particle load per unit area or the air side pressure drop to

decrease. In both cases, the pressure drop through the distributer is assumed to be 20% of the bed pressure drop.

In fig. 52 is plotted the optimized incremental cost versus design temperature for a finned surface [31] and four various fluidized bed configurations as determined from experimental data. Design temperature is defined as the maximum ambient air temperature for which 100% of the plant's rated power can be generated. It should be noted that each point along a given curve represents a differently designed heat exchanger, namely the optimum for that particular design temperature. The incremental cost is determined by prorating the heat exchanger performances over the temperature spectrum New York City experiences.

Figure 52 shows that the best fluidized bed cost is some 15% greater than finned tube costs. There figures are quite dependent upon the input cost used. This 15% discrepency is within the accuracy range of the input data. Figure 52 also indicates a strong dependency of fluidized bed incremental cost on particle size. A smaller sized particle would reduce the incremental cost to less than that for a finned tube. However, 40-50 mesh particles already have a sizable practical problem. They elutriate at velocities of about 2.5 - 3.0 ft/sec. The problem of maintaining this magnitude of velocities over vast areas of bed is a sizable air distribution problem. Smaller particles elutriate at even lower velocities, heightening the distribution problem.

Figure 53 plots the same type of data as figure 52, only determined by using the modified Vreedenberg correlation. Two different assumed fluidized bed depths were used (2" and 2.5"), and it is obvious that the

cost is a strong function of the bed depth. The pressure drop increases in direct proportion to the bed depth (assuming constant void), and the power consumed in fluidizing this additional depth is significant. In the optimized cases, with d_p = 0.014", the additional power consumed in supporting the extra half inch of bed was about 11 Mw, or a 24% increase over that of a 2" bed.

Being able to assume an even smaller bed depth will further decrease the incremental cost, thereby approaching the finned tube incremental costs. However, one must consider if one can control the height of a of a shallow bed that accurately. This uncertainty led to the use of a factor of 2 to 2.5 difference between the bed depth and tube diameter that were used in the optimization.

Pursuing the reduction of bed depth further, the optimization program and the modified Vreedenberg correlation were used to evaluate a fluidized bed heat exchanger with a bed depth of 1.5", assuming the tube diameters are 0.6", and have a pitch of 2. The results are graphed in fig. 54 for the different particle sizes. As expected, the incremental costs decreased and, for a particle size of .014", are rapidly approaching the finned tube costs.

Table 8 breaks down the cost of the minimum fluidized bed cases in figures 52, 53, and 54, and the finned tube case. Compare the finned tube to the optimum fluidized bed based on data. Because of the use of cheaper bare tubes (assumed price: 2.5 $/ft^2 of air side area), the fluidized bed results in a 13% savings in heat exchanger costs, but all other costs are higher. Because the optimal water temperature in the

the fluidized bed tubes is higher than that for finned tubes, the thermal efficiency is reduced, resulting in a 24% increase in additional boiler capacity over that which is needed by the finned tubes to maintain the required power generation. The increased frontal area of the fluidized bed increased the land area requirement by 67% and the piping cost by 53%.

But boiler, land and piping costs are small in magnitude, and after summing them with heat exchanger costs, fluidized beds still represent a 5% savings over finned tubes. The big difference lies in fluid pumping power. Power consumed in keeping the bed fluidized is 77% greater than power required by the finned tubes. Water pumping power is also increased by 62%. The program compensates for this consumed power by increasing the gross plant size such that after consuming power for fluid pumping the net power generated remains as 1000 Mw. The greatly increased fluid pumping power of the fluidized beds necessitated increasing the plant size by 75% over the increase required by finned tubes. According to this model, 41% of the cost of adapting a fluidized bed heat exchanger is the cost of keeping the bed fluidized. It is this cost of fluid pumping power which makes the incremental cost of fluidized beds 16% greater than that of finned tubes.

Similar effects are evident for the other tabulated values in Table 8.

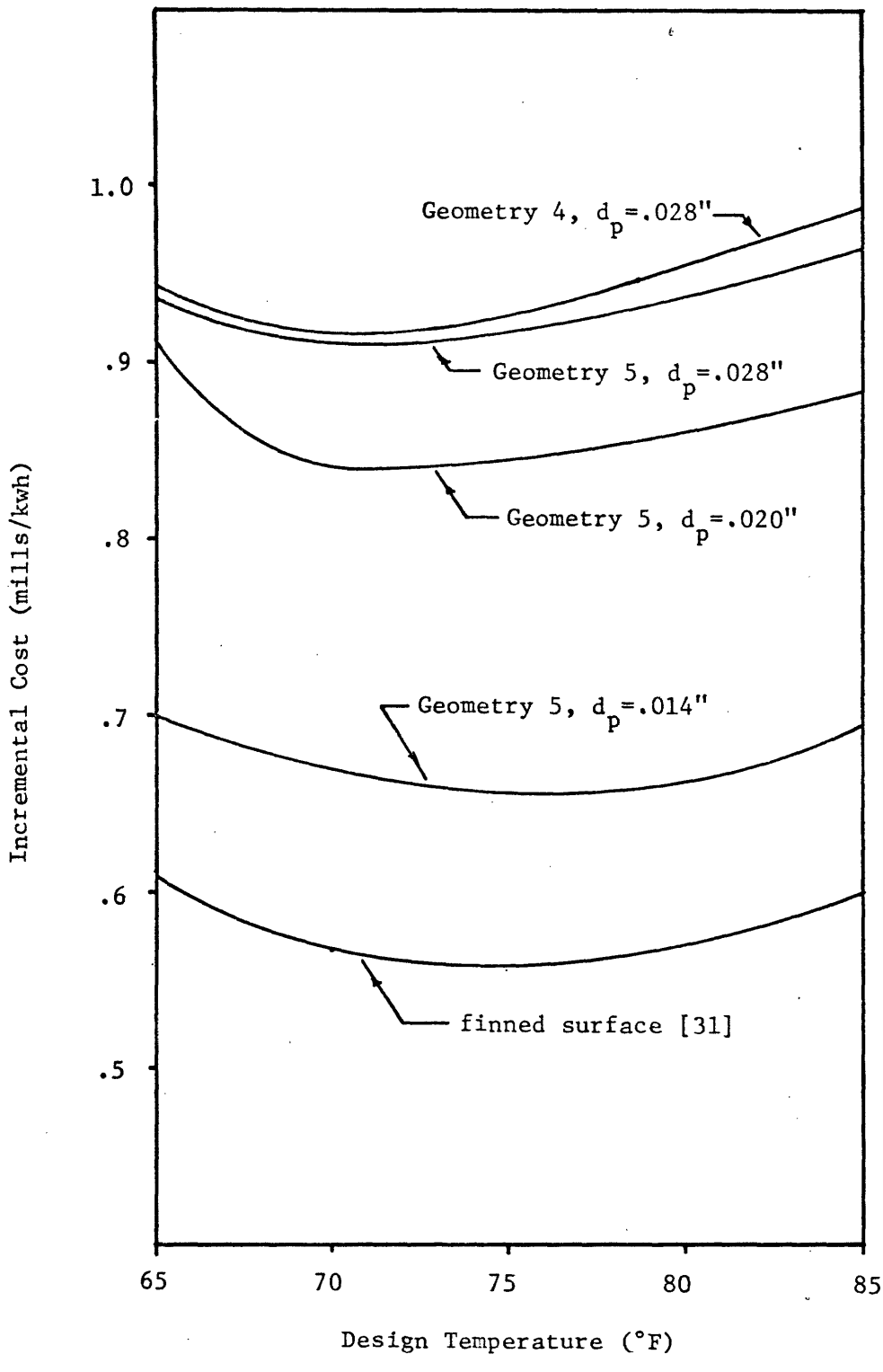

INCREMENTAL COST VS. DESIGN TEMPERATURE
for a fluidized bed cooling tower
using experimental data

Figure 52

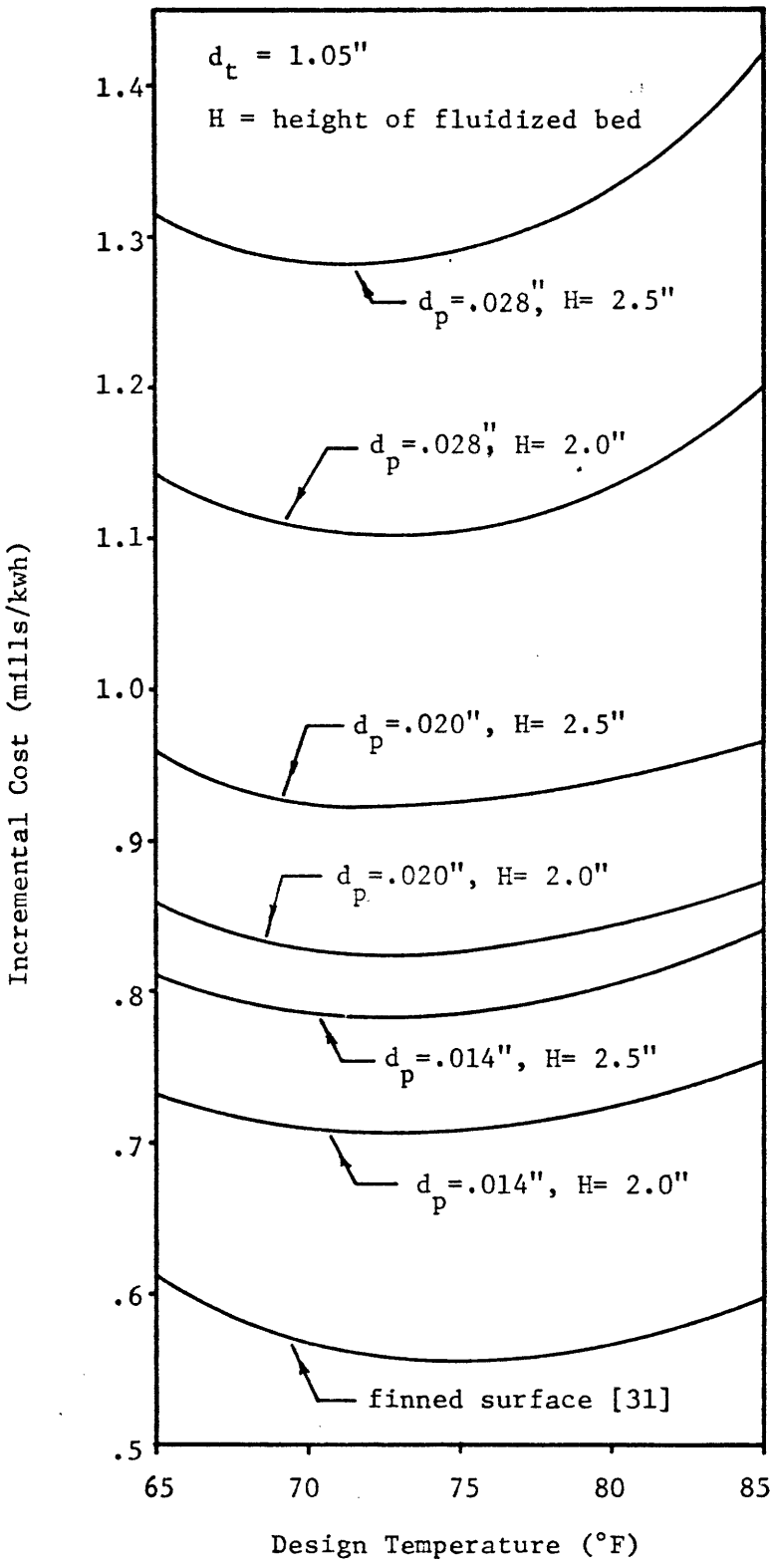

INCREMENTAL COST VS. DESIGN TEMPERATURE
for a fluidized bed cooling tower
using modified Vreedenberg correlation

Figure 53

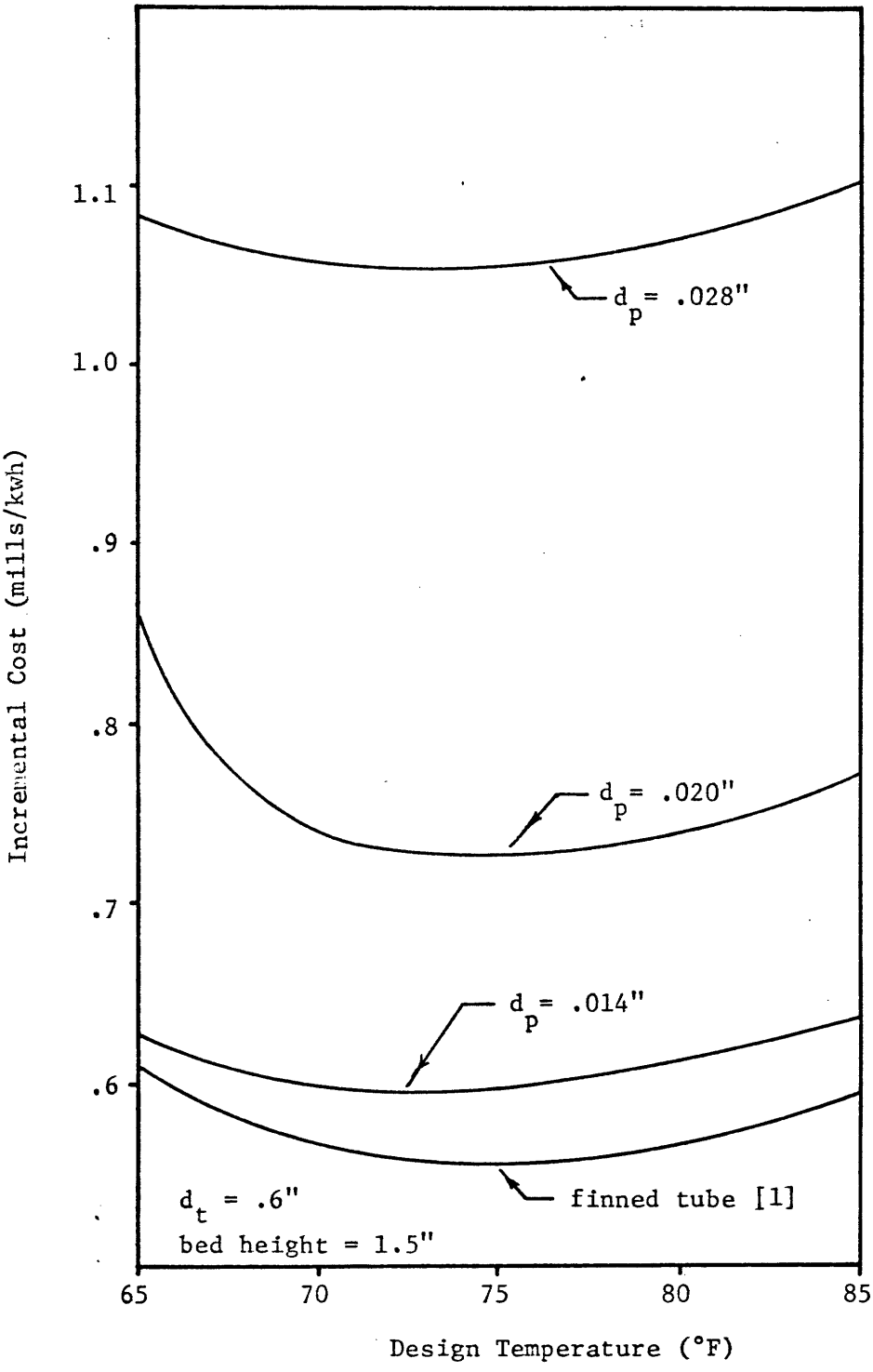

INCREMENTAL COST VS. DESIGN TEMPERATURE
for a fluidized bed cooling tower
using the modified Vreedenberg Correlation

figure 54

Table 8

ECONOMIC BREAKDOWN OF FLUIDIZED BED AND FINNED TUBE OPTIMIZATIONS

	finned tubes [31]	Fluidized beds			
		data	correlation		
Tube diameter (in)		1.05	1.05	1.05	0.6
Bed depth (in)	--		2.5	2.0	1.5
Total capital cost ($ x 10^{-6})	20.91	24.38	28.12	25.26	21.15
Cost of heat exchanger ($ x 10^{-6})	13.15	11.38	13.01	12.29	9.72
Cost of increased boiler size ($ x 10^{-6})	1.11	1.38	1.32	1.19	1.06
Cost of increased plant size ($ x 10^{-6})	5.7	10.0	12.1	9.8	8.4
Cost of land ($ x 10^{-6})	.09	.15	.164	.161	.221
Piping cost ($ x 10^{-6})	.94	1.44	1.54	1.82	1.78
Water pumping power (kw)	3100	5050	3600	3700	4900
Air side pumping power (kw)	25500	45100	56800	45200	36900
Incremental cost (mills/kwh)	.57	.66	.79	.71	.60

IV.7 Fluidized Beds with Water Injection

A certain amount of water may be injected into a fluidized bed without the particles sticking together or the particles aglomerating. Water injection has the advantage that heat would then be rejected not only by the sensible temperature rise of the air, but also by the latent heat of vaporization for water. With a given heat load and ambient air temperature, the added utilization of the latent heat of water allows for either a reduction of the condensate temperature for a given fluidized bed, or a reduction of the fluidized bed size for a given condensate temperature. Therefore water injection could be used as a topping system to maintain a lower condensate temperature (lower turbine back pressure) during the summer months, or could be used year-round and thereby reduce the overall size of the heat exchanger. In the year-round method, the turbine back pressure may be maintained roughly constant by increasing the water injection rate during the summer months.

Water injection transforms the dry tower into a wet tower. This poses the question as to the actual rate of water consumption in a wet fluidized bed. Topping the fluidized bed capacity by injecting water can be compared to the use of a conventional wet tower as a topping unit to a dry fluidized bed. This is done in Appendix 6 with the conclusion that, ignoring blowdown, the water consumed in a wet tower topping unit would be less than three fifths that consumed by water injection for a constant heat load. From a consumption viewpoint, then, year-round water injection is not desirable. However, there are other considerations to be made.

Blowdown and water treatment: Conventional wet towers with continual water evaporation require a blowdown of the remaining water to maintain mineral concentration below a specified level. Also, with plastic or wood fills, the water for conventional wet towers require specialized treatment to prevent biological growth. With fluidized beds with water injection, the injected water in no way chemically affects the cooled condensate water within the pipes; consequently no water blowdown is required, as no mineral concentrations occur. Minerals from the injected water are deposited upon the fluidized particles as the water evaporates. As the bed fluidization is a function of particle size, maintaining a constant sized particle necessitates the blowdown and continual replacement of fluidized particles. Due to the inertness of sand, and the high activity of a fluidized bed, it is doubtful that water treatment would be necessary.

Other economic costs: The addition of either a water injection system or a separate water tower topping unit will increase the capital cost of the system. The capital cost of the water injection system is dependent upon how uniformly the water need be dispersed. The inherent mixing of the bed may be sufficient so that water could be injected relatively crudely and inexpensively, without too much regard for uniformity. If a uniform spray is needed, it could require a water injection tube for each tube already in the fluidized bed. This would virtually double the capital expenditure. The presence of a direct water to air contact in the wet tower necessitates the separation of the boiler and wet tower water. This requires at least the use of a secondary loop, or a heat exchanger between the tower and condensate water, significantly

increasing the cost of adding a wet tower topping unit.

Because of the high rate of water consumption and the potentially high cost of a water distribution system, it is unlikely that water injected fluidized beds would be a viable alternative to other means of heat rejection. Water injection is most attractive as a means of overcoming the capacity losses a dry tower experiences during summer months, but only if the water injection need not be uniform. A non-uniform injection would be simple, and considerably less costly than a uniform injection system.

V. Conclusions and Recommendations

The order of magnitude analysis yielded the same general dependency of h on particle diameter, particle fraction and velocity as is exhibited by the three major correlations. Although velocity is not expressly included in the model of section II.2.6, it is hidden in the particle fraction term. The h in the model of section II.2.6 is dependent upon $(1 - \varepsilon)^{2/3}$, where as the correlations (with the exception of Vreedenberg's original correlation) have h dependent upon $(1 - \varepsilon)\ V^{a}$, where 'a' is between .24 and .34. This is essentially the same as the model, as particle fraction is roughly inversely proportional to velocity.

The model, derived from first principles, correlates the data within 10-20%. The success of this model gives strength to the belief that fluidized bed heat transfer results from two effects: (1) sensible heat being transferred from the wall to the bed core by the small temperature rise of numerous discrete particles, and (2) the mixing of hot and cold fluid at the tube surface because of the interaction of the fluidized particles with the boundary layer. Further, the order of magnitude analysis indicates that as the particles become smaller (with V and ε constant) the effective h from sensible heat transport grows faster than the effective h from boundary layer mixing.

The original Vreedenberg correlation did not include a dependency on particle fraction. The Vreedenberg relation modified to encorporate particle fraction $(1 - \varepsilon)$ correlates data better (both numerically and in shape) than other correlations. The reasoning for the use of the dimensionless parameters is questionable, especially when no fluidizing agent besides air was used, but it seems to utilize the variables d_t, d_p,

and V properly. The relation was derived for a single tube in a deep bed over a fairly wide range of these variables. Petrie found the original correlation adequate for tube bundles, and with the inclusion of $(1 - \varepsilon)$ the correlation (as shown in section IV.4.3) was even better. The present experiment shows the modified correlation accurate over a wide range of flow conditions for a shallow sand bed with one or two tube rows. As the modified Vreedenberg relation has only been shown to be accurate with beds fluidized by air, caution must be used in employing the relation generally until further testing has shown that the variables as the Prandtl number, viscosity, and gas density are used properly.

For power plant considerations, the economic benefits of using fluidized beds are, at best, moderate. Heat transfer coefficients are good, but large frontal areas required because of the low throughput velocities and the power required to keep the bed fluidized are severely penalizing fluidized beds with repect to finned tubes. Increasing the h by 30-50% by maintaining more of the tube area actively fluidized would greatly enhance the economic profile. In this respect, smaller flattened tubes should be further investigated. By the Vreedenberg relation, the smaller tube size should enhance the heat transfer coefficient, plus the flattened tube should reduce the fraction of tube area lost to active fluidization by stagnant particles on the downstream side, and should reduce anomalies between free stream air velocities and inter-tube velocities. The flattened tubes tested in this study were grossly out of proportion because of the heating and instrumentation system employed.

It has been shown that with the reduction of particle size and bed depth, fluidized beds can be competitive with finned tubes. For smaller

heat loads (sub power plant size) fluidized beds may be attractive. Reduced heat loads, and hence size, would also reduce the total frontal areas to possibly a manageable level. Fluidized beds have the advantage of being able to be run partially wet. Small amounts of water can be sprayed into the bed without the particles agglomerating, making use of the latent heat of vaporization to augment the heat rejection capacity. For such wet use, the purity of the water is of no consequence, and any water may be used.

As the single largest cost of adapting a fluidized bed cooling tower to a power plant is the cost of the heat exchanger (see Table 8), a reduction in the cost of fluidized tubes would enhance the fluidized bed's economic competitiveness. The cost savings could result from either a less expensive surface or novel fabrication techniques.

Even without a further reduction in tube costs, the main advantage of present fluidized beds lies in its low capital cost for the heat exchanger. It is conceivable that fluidized beds could be used intermittently as a heat exchanger topping unit - used only under high heat loads or when adverse conditions for conventional heat rejection exists.

A wholly untapped region for fluidized bed use would be in corrosive atmospheres (salt, etc.). Here fluidized beds present the possibility of using a cheap, non-corrosive fluidized medium which continually scours the tube surface of scale buildup.

References

1. Andeen, B.R., & Glicksman, L.R., "Dry Cooling Towers for Power Plants", report #DSR 73047-1 , Engineering Projects Laboratory, Department of Mechanical Engineering, Massachusetts Institute of Technology, Cambridge, Mass. February 1972.

2. Leva, M. Fluidization, McGraw-Hill Book Co, Inc., New York, 1959.

3. Mickley, H.S., & Trilling, C.A., "Heat Transfer Characteristics of Fluidized Beds", Industrial & Engineering Chemistry, Vol. 41, pp. 1135-1147, 1949.

4. Levenspiel, O., & Walton, J.S., Chemical Engineering Progress Symposium Series #50, pp. 1-16, 1954.

5. Mickley, H.S., & Fairbanks, D.F., "Mechanisms of Heat Transfer to Fluidized Beds", AIChE Journal, pp. 374-384, Sept 1955.

6. Fluidization, edited by Davidson, J.F. and Harrison, D., Academic Press, New York, 1971.

7. Kunii, D. & Levenspiel, O., Fluidization Engineering, John Wiley & Sons, Inc, New York, 1969.

8. Wicke, E. & Fetting, F., "Warmeubertragung in Gaswirbecschichten" Chenie-Ingenieur Technik, Vol 26, pp. 301, 1954.

9. Liu, B.Y.H. & Ilori, T.A., "On the Theory of Aerosol Deposition in Turbulent Pipe Flow", Particle Technology Laboratory Publication #210, Mechanical Engineering Department, University of Minnesota, Minneapolis, Minnesota, July 1973.

10. Davies, J.T., Turbulence Phenomena, Academic Press, New York, 1972.

11. Mickley, H.S., Trilling, C.A., & Hawthorn, R.D., "The Relation between the Transfer Coefficient and Thermal Fluctuations in Fluidized-Bed Heat Transfer", Chemical Engineering Progress Symposium Series #32, Vol 57, pp. 51-60, 1961.

12. Zabrodsky, S.S., Hydrodynamics and Heat Transfer in Fluidized Beds, M.I.T. Press, Cambridge, Mass. 1966.

13. Gardon, R. & Cobonpue, J., "Heat Transfer between a Flat Plate and Jets of Air Impinging on It", presented at 1961 International Heat Transfer Conference, Aug 28 - Sept 1, 1961, Boulder, Coloradl.

14. Mikic, B.B., & Rohsenow, W.M., "A New Correlation of Pool-Boiling Data Including the Effects of Heating Surface Characteristics", Journal of Heat Transfer, pp 245-250, May 1969.

15. Vreedenberg, H.A., "Heat Transfer between a Fluidized Bed and a Horizontal Tube", Chemical Engineering Science, Vol 9, pp 52-60, 1958.

16. Leva, M.,"Correlations of the Dense Phase Fluidized State and Their Applications", The Canadian Journal of Chemical Engineering, Vol 35, pp 71-76, August 1957.

17. Ainshtein, V.G., "An Investigation of Heat Transfer Process Between Fluidized Beds and Single Tubes Submerged in the Bed", in reference 12, pp 270-272.

18. Wender, L. & Cooper, G.T., "Heat Transfer between Fluidized-Solids Beds and Boundary Surfaces - Correlation of Data", AIChE Journal, Vol 4, p 15 1958.

19. Bright, A. & Smith, K.A., "Heat Transfer in Fluidized Beds", Final Report to National Air Polution Control Administration, Department of Chemical Engineering, Massichusetts Institute of Technology, Oct 1970.

20. Gel'perin, N.J., Ainshtein, V.G., & Aronovich, F.D., "The Effect of Screening on Heat Transfer in a Fluidized Bed", International Chemical Engineering, Vol 3, No 2, pp 185-190, April 1963.

21. Noack, R., "Lokaler Warmeubergang an horizontalen Rohren in Wirbelschichten", Chemie-Ingenieur Technik, Vol 42, pp 371, 1970.

22. Gelperin, N.I., Einstien, V.G., Korotjanskaja, L.A., & Perevozchkova, J.P., Teor, Osnovy, Khim. Tekhnol, Vol 2, p 430, in reference 6.

23. Petrie, J.C., Freeby, W.A., & Buckham, J.A., "In Bed Heat Exchangers", Chemical Engineering Progress, Vol 64, no. 7, pp. 45-51, July 1968.

24. Lese, H.K. & Kermode, R.I., "Heat Transfer from a Horizontal Tube to a Fluidized Bed in the Presence of Unheated Tubes", The Canadian Journal of Chemical Engineering, Vol 50, pp 44-48, Feb 1972.

25. Bowman, R., Masters Thesis, to be published, Massachusetts Institute of Technology.

26. Renean, L.R., Johnston, J.P., & Kline, S.J., "Performance and Design of Straight Two Dimensional Diffusers", Transactions of the ASME, March 1967.

27. Schlichting, H. Boundary Layer Theory, McGraw-Hill, New York, 1955.

28. Rohsenow, W.M. & Choi, H., Heat, Mass, and Momentum Transfer, Prentice-Hall, New Jersey, 1961.

29. Holman, J.P., Experimental Methods for Engineers, McGraw-Hill, New York, 1966.

30. Glicksman, L.R., "Thermal Discharge from Power Plants", ASME publication 72-WA/Ener-2.

31. Andeen. B.R., Glicksman, L.R., & Rohsenow, W.M. "Improvement of the Environmental and Economic Characteristics of Cooling Towers, Part I: Optimized Design Program, Fluidized Beds, and Non-Metalic Heat Exchangers", Engineering Projects Laboratory Report #DSR 80047-82, Department of Mechanical Engineering, Massachusetts Institute of Technology, Cambridge Mass, june 1973.

Appendix 1

Calculation of spacing between particles (x_n)

Assuming 1. Uniform void

2. Close pack formation (HCP or BCC)

3. Spacing equals minimum distance between particles.

Consider a unit volume:

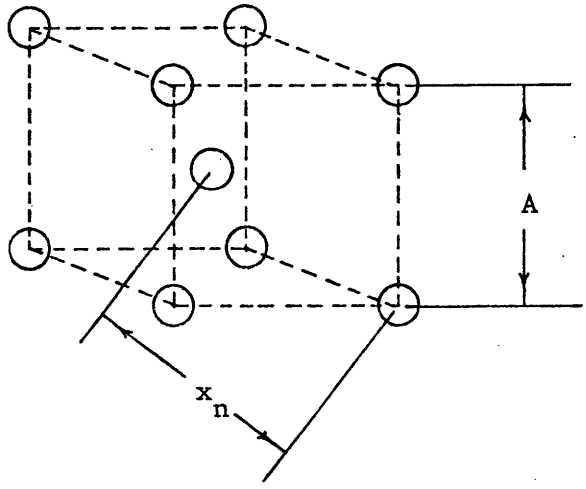

$$x_n = \frac{1}{2} \text{ diagonal of cube} = \frac{1}{2}\sqrt{3\,A^2} = \frac{A}{2}\sqrt{3} \qquad \text{(A1.1)}$$

$$\text{volume of cube} = A^3 \qquad \text{(A1.2)}$$

$$\text{particle volume in cube} = 2\left(\frac{\pi\, d_p^{\,3}}{6}\right) = \frac{\pi\, d_p^{\,3}}{3} \qquad \text{(A1.3)}$$

$$\text{particle fraction in cube} = 1 - \varepsilon = \frac{\pi\, d_p^{\,3}}{3\, A^3} \qquad \text{(A1.4)}$$

substituting equation (A1.1) into (A1.4) and solving for x_n:

$$x_n = d_p\left(\frac{\pi\sqrt{3}}{8\,(1-\varepsilon)}\right)$$

Appendix 2

Calculation of particle collisions per unit area (n)

Same assumptions as in appendix 1.

Plane view:

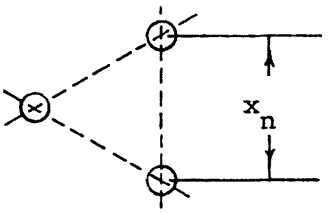

For the triangle in the plane view:

$$n = \frac{\#\ \text{particles}}{\text{area}} = \frac{1/2}{\frac{\sqrt{3}}{4}\ x_n^{\,2}} = \frac{2}{x_n^{\,2}\sqrt{3}}$$

using x_n from appendix 1,

$$n = \frac{8}{d_p^{\,2}\ \sqrt{3}} \left(\frac{1-\varepsilon}{\pi\ \sqrt{3}} \right)^{2/3}$$

Appendix 3

Resistance of metal spacer between heated tube sections

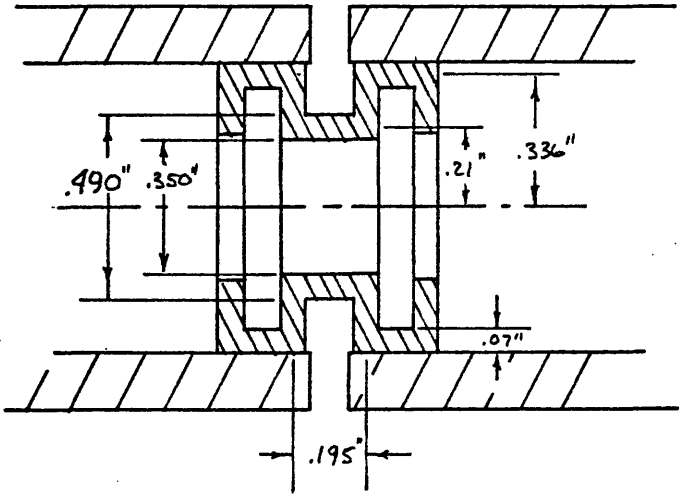

Assume can be modeled as two dimensional flow through two disks and a tube. From reference 28, for this case,

$$R_{disk} = \frac{\ln (r_2/r_1)}{2 \pi L_1 k}$$

where r_1 & r_2 are the inner and outer radii respectively, and L_1 is the disk thickness, and

$$R_{tube} = \frac{L_2}{k A}$$

where L_2 and A are the tube length and cross sectional area, respectively. Therefore,

$$R = \frac{\ln(r_2/r_1)}{2 \pi L_1 k} + \frac{L_2}{k A} + \frac{\ln(r_2/r_1)}{2 \pi L_1 k}$$

From the figure, $r_2 = .336"$, $r_1 = .210"$, $L_1 = .07"$, $L_2 = .195"$, and $A = .092\ in^2$. For steel, $k \simeq 25$ BTU/hr-ft^2-°F. Therefore,

$$R = 2\,\frac{\ln(.336/.210)}{2\quad(25)\ (.07/12)} + \frac{(.195/12)}{(25)(.092/144)} = 1.02\ \frac{\text{hr °F}}{\text{BTU}}$$

Appendix 4

Uncertainty of q_{rej} and $(T_W - T_b)$

From reference 29:

For the function

$$R = R\ (x_1, x_2, x_3, \ldots, x_n) \tag{A4.1}$$

the uncertaintly (w_r) of R is expressed as:

$$w_r = \left[\left(\frac{\partial R}{\partial x_1} w_1 \right)^2 + \left(\frac{\partial R}{\partial x_2} w_2 \right)^2 + \cdots + \left(\frac{\partial R}{\partial x_n} w_n \right)^2 \right]^{1/2} \tag{A4.2}$$

where $w_1, w_2, \ldots w_n$ are the uncertainties of $x_1, x_2, \ldots x_n$, respectively.

Uncerainty of q_{rej}

$$q_{rej} = (\text{amps x volts}) - \text{leaks}$$

by the use of equation (A4.2) above,

$$w_q = \left[(\text{amps} \cdot w_v)^2 + (\text{volts} \cdot w_a)^2 + w_1^2 \right]^{1/2}$$

or

$$\frac{w_q}{\text{amps} \quad \text{volts}} = \left[\left(\frac{w_v}{\text{volt}} \right)^2 + \left(\frac{w_a}{\text{amps}} \right)^2 + \left(\frac{w_1}{\text{amps} \cdot \text{volts}} \right)^2 \right]^{1/2} \tag{A4.3}$$

where the subscripts q, v, a, and 1 refer to q_{rej}, volts, amps, and losses, respectively, and where (w_q/amps·volts) etc, can be recognized as the percent error in each case.

Hence, using values of section III.5,

$$\%\ \text{error in}\ q_{rej} = (4^2 + 4^2 + 1^2)^{1/2} = 5.5\% \tag{A4.4}$$

Uncertainty of $(T_W - T_b)$:

$$(T_w - T_b)_{actual} = (T_w - T_b)_{measured} + \Delta T_b$$

where ΔT_b is a function of location, and $\Delta T_b = 2$ °F, or a variation of ± 1 °F. With a thermocouple uncertainty of 1 °F, and using equation (A.4.2),

$$\text{uncertainty } (T_w - T_b)_{actual} = (1^2 + 1^2 + 1^2)^{1/2} = 1.73 \text{ °F}$$

Assuming a $(T_w - T_b)$ of 50 °F, the uncertainty in percent is 3.46%

Note that from equation (A4.3) above, it follows that for

$$A = B \cdot C \cdot D$$

$$\% \text{ error in } A = \left[(\% \text{ error in } B)^2 + (\% \text{ error in } C)^2 + (\% \text{ error in } D)^2\right]^{1/2}$$

Appendix 5

The Effectiveness of a Fluidized Bed Heat Exchanger

The fact that a fluidized bed is nearly isothermal has unusual effects on the bed's effectiveness. An isothermal bed implies (1) the incoming air reaches bed temperatures almost immediately after entering the bed, and (2) the maximum temperature the air can leave the fluidized bed is at the bed temperature.

As air is the limiting fluid, the conventional expression for heat exchanger effectiveness is the ratio of the actual heat transfer rate in the exchanger to the thermodynamically limited maximum possible heat transfer rate. The actual heat transfer rate is proportional to the temperature rise of the air ($T_b - T_a$). Because of the isothermal properties, the thermodynamic maximum heat transfer rate is proportional to ($T_w - T_b$). With the air being the limiting fluid:

$$\varepsilon = \frac{T_b - T_a}{T_w - T_b} \qquad \text{(A5.1)}$$

The effectiveness has an upper limit of 1.0, and consequently, the maximum T_b can be is midway between T_w and T_a.

Note that to double the rate of heat rejection, T_b must be doubled. This more than doubles the heat exchanger effectiveness, for in equation (A5.1), the numerator is doubled and the denominator is decreased. Even in the linear region of a effectiveness vs. NTU plot, with the velocity and density of air being constant, this means to double the rate of heat rejection the tube area must be more than doubled.

To look at this from a slightly different prospective, consider

an air side energy balance:

$$q_{rej} = C_a \dot{m} (T_b - T_a) = h_t A_t (T_w - T_b) \qquad (A5.2)$$

where $\dot{m} = \rho_a V_a A_f$.

Rearranging this yields:

$$\frac{A_t}{A_f} = \frac{T_b - T_a}{T_w - T_b} \quad \frac{C_a \rho_a V_a}{h_t} \qquad (A5.3)$$

For a given particle size and a given air velocity, h_t is approximately a constant, and as noted before $(T_b - T_a)/(T_w - T_b)$ has an upper limit of 1.0. Therefore as a maximum,

$$\frac{A_t}{A_f} = (\text{constant}) \cdot C_a \rho_a \qquad (A5.4)$$

or, the amount of tube side area required per unit frontal area is upper limited by the specific heat and density of air.

Appendix 6

Comparison of Water Consumption Between a Fluidized Bed with Water Injection or With a Wet Tower Topping Unit

Assuming that air entering the bed achieves the bed temperature almost immediately, which is consistant with the assumption of an isothermal bed (see appendix 5), and that the mean temperature of the water being cooled by the bed is $\overline{T}_w$, the temperatures within the dry fluidized bed can be sketched as:

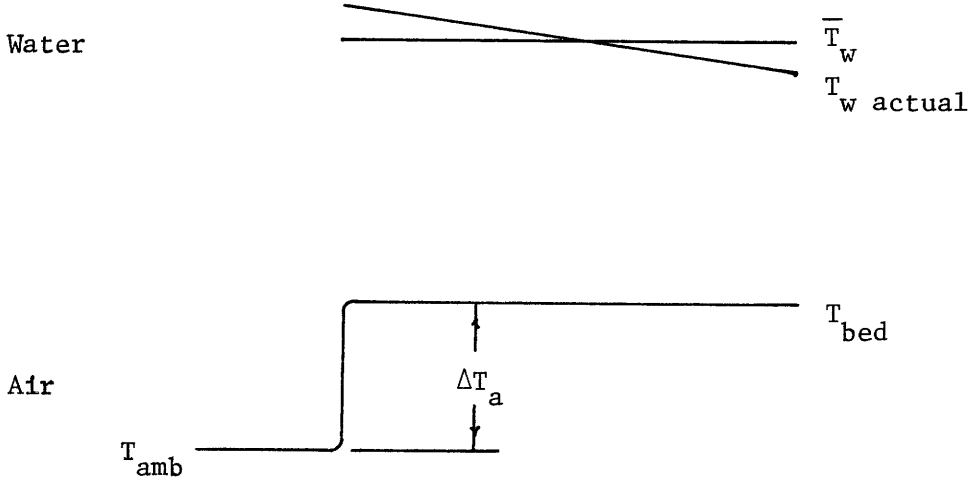

where ΔT_a is the temperature rise in the air upon entering the bed. Here,

$$q_{total} = h\ A\ (\overline{T}_w - T_{bed}) = h\ A\ (\overline{T}_w - T_{amb} - \Delta T_a) \qquad (A6.1)$$

by an energy balance:

$$q_{total} = \dot{m}_a\ C\ (\Delta T_a) \qquad (A6.2)$$

where $\dot{m}_a$ is the flow rate of air. These yield:

$$\frac{h\,A}{\dot{m}\,C} = \frac{\Delta T_a}{\overline{T}_w - T_{amb} - \Delta T_a} = \frac{1}{\left(\dfrac{\overline{T}_w - T_{amb}}{T_a}\right) - 1} \qquad \text{(A6.3)}$$

Therefore, in order to maintain the right hand side positive,

$$\frac{\overline{T}_w - T_{amb}}{\Delta T_a} > 1 \qquad \text{(A6.4)}$$

The larger this inequality, the smaller the required heat exchanger area (A) becomes. This, in turn, is reflected in the capital cost of the fluidized bed. For the economic optimization runs discussed in Section IV.6,

$$(hA/\dot{m}C) \simeq 1.5, \text{ or } \frac{\overline{T}_w - T_{amb}}{\Delta T_a} \simeq 1.66.$$

With the injection of water in the fluidized bed, some of the sensible heat of ΔT_a goes into the latent heat of vaporization of the injected water. This reduces the net difference between T_{bed} and T_{amb} by a quantity of δ. Pictorially, the case with water injection can be shown as:

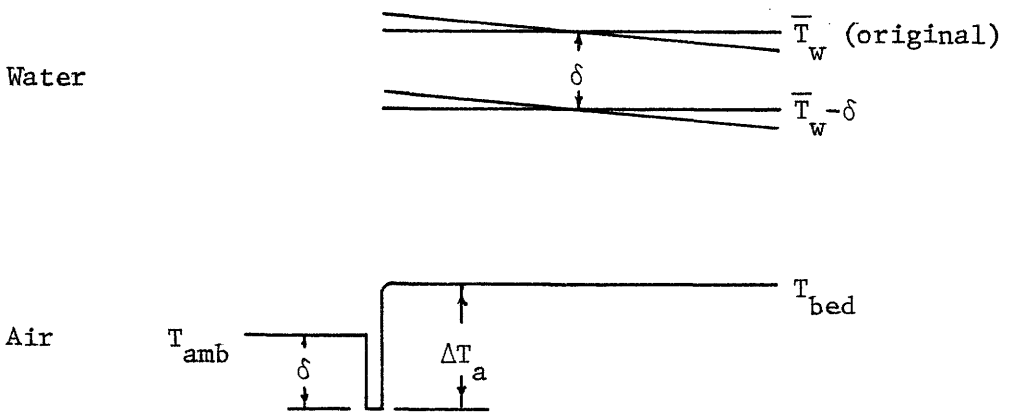

Rejecting the same quantity of heat as before requires the same 'driving force' in the temperature difference. Since the effective bed temperature is lower, the water temperature (T_w) can also be lowered by δ and still reject the original q_{total}.

As the effective lowering of sensible heat is due to the vaporization of injected water.

$$\dot{m}_i \, h_{fg} = \dot{m}_a \, C \, \delta \tag{A6.5}$$

where $\dot{m}_i$ is the flow rate of the injected water, and h_{fg} is the latent heat of vaporization. Rearranging eq. (A6.5) and substituting eq. (A6.2) yields:

$$\delta = \frac{\dot{m}_i \, h_{fg}}{\dot{m}_a \, C} = \frac{\dot{m}_i \, h_{fg} \, \Delta T_a}{q_{total}} \tag{A6.6}$$

or,

$$\delta = \frac{(q_{\text{latent heat}}) \, \Delta T_a}{q_{total}} \tag{A6.7}$$

Now compare the fluidized bed with water injection to a fluidized bed using a wet tower as a topping unit. For the comparison, it is assumed that both units have the same q_{total}, T_{amb}, and the temperature difference driving force in the fluidized bed. This assures the same thermal load on the wet topping unit and on the water injection.

For the case of a fluidized bed with a topping unit, the fluidized bed portion can be pictorially shown as:

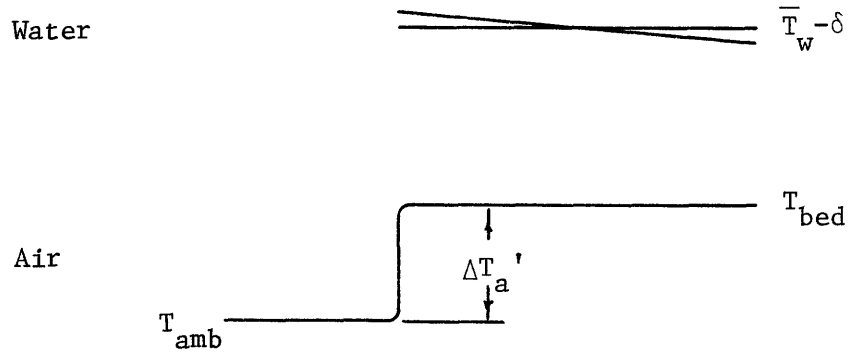

Now for this fluidized bed portion, in a fashion similar to eqs. (A6.1) and (A6.2),

$$q_{f.b.} = h\,A\,(\overline{T}_w - \delta - T_{amb} - \Delta T_a') \tag{A6.8}$$

$$q_{f.b.} = \dot{m}_a\,C\,\Delta T_a' \tag{A6.9}$$

Eliminating $\Delta T_a'$ from these two equations yields:

$$q_{f.b.} = \frac{h\,A\,\dot{m}_a\,C}{h\,A + \dot{m}_a\,C}\,(\overline{T}_w - T_{amb} - \delta) \tag{A6.10}$$

Substituting eq. (A6.6) for δ,

$$q_{f.b.} = \frac{h\,A\,\dot{m}_a\,C}{h\,A + \dot{m}_a\,C}\left(\overline{T}_w - T_{amb} - \Delta T_a \frac{\dot{m}_i\,h_{fg}}{q_{total}}\right)$$

and using eq. (A6.2),

$$\frac{q_{f.b.}}{q_{total}} = \frac{h\,A}{h\,A + \dot{m}_a\,C}\left(\frac{\overline{T}_w - T_{amb} - \Delta T_a\,\dot{m}_i\,h_{fg}/q_{total}}{\Delta T_a}\right)$$

$$= \frac{1}{1 + \frac{\dot{m}_a\,C}{h\,A}}\left(1 - \frac{\Delta T_a\,\dot{m}_i\,h_{fg}/q_{total}}{\overline{T}_w - T_{amb}}\right)\frac{\overline{T}_w - T_{amb}}{\Delta T_a} \tag{A6.11}$$

Using equation (A6.3),

$$1 + \frac{\dot{m}_a C}{h A} = \frac{\overline{T}_w - T_{amb} - \Delta T_a}{\Delta T_a} + 1 = \frac{\overline{T}_w - T_{amb}}{\Delta T_a} \tag{A6.12}$$

and substituting this into eq. (A6.11),

$$\frac{q_{f.b.}}{q_{total}} = 1 - \frac{\Delta T_a \dot{m}_i h_{fg}/q_{total}}{\overline{T}_w - T_{amb}} \tag{A6.13}$$

The heat not dissipated in the fluidized bed must be dissipated in the wet tower, Hence,

$$q_{c.t.} = q_{total} - q_{f.b.} \tag{A6.14}$$

This and eq. (A6.13) yield:

$$q_{c.t.} = \frac{\Delta T_a \dot{m}_i h_{fg}}{\overline{T}_w - T_{amb}} \tag{A6.15}$$

For a wet tower, about 80% of the heat is rejected by latent heat, therefore,

$$q_{c.t.} > \dot{m}_{c.t.} h_{fg} \tag{A6.16}$$

where $\dot{m}_{c.t.}$ is the flow rate of the water evaporated by the cooling tower. Using eqs. (A6.15) and (A6.16),

$$\dot{m}_{c.t.} < \frac{\Delta T_a}{\overline{T}_w - T_{amb}} \dot{m}_i \tag{A6.17}$$

Using equation (A6.4),

$$\dot{m}_{c.t.} < \dot{m}_i \tag{A6.18}$$

and using the value for the optimized economic runs,

$$\dot{m}_{c.t.} < \frac{\dot{m}_i}{1.66}$$

Therefore, water injection in fluidized beds will consume more than two-thirds again the quantity of water consumed by a fluidized bed using a wet tower as a topping unit.

Equation (A6.18) can also be arrived at by a different means. In a dry fluidized bed all the heat rejection is by sensible heat, or by the rise in air temperature while passing through the bed. Injecting water will not increase this air temperature rise, therefore the sole purpose of water injection is to achieve a latent heat load.

Hence

$$q_i = \dot{m}_i \, h_{fg} \qquad \text{(A6.19)}$$

where q_i is the rate of heat transfer due to water injection. Since the basis of comparison was

$$q_i = q_{c.t.}$$

equation (A6.16) and (A6.19) yield (A6.18).

Appendix 7

Data

	Geometry	d_p (in)	T_w (°F)	T_b (°F)	V_a (ft/sec)	pressure drop net (lbm/ft^2)	pressure drop distributer (% of net)	particle load (lbm/ft^2)	q_{rej} (watts)	h_t (BTU/hr-ft^2-°F)
1	1	.028	147.2	79.8	6.67	18.8	86	2.5	147.0	27.0
2	1	.028	141.7	80.7	5.83	18.2	79	3.8	147.0	29.8
3	1	.028	145.0	81.8	6.32	20.4	82	3.8	147.0	28.7
4	1	.028	138.1	80.2	5.14	17.5	71	5.0	147.0	31.4
5	1	.028	138.3	79.7	4.75	17.2	71	5.0	147.0	31.0
6	1	.028	139.4	80.0	5.43	18.8	73	5.0	147.0	31.1
7	1	.028	143.4	82.3	4.21	15.9	61	6.2	147.0	29.8
8	1	.028	140.8	82.3	5.14	18.8	67	6.2	147.0	31.1
9	1	.028	141.3	83.4	5.69	21.1	70	6.2	147.0	31.4
10	1	.028	144.1	83.3	2.89	15.6	52	7.5	147.0	29.9
11	1	.028	140.5	79.3	3.41	17.5	57	7.5	147.0	29.7
12	1	.028	143.3	84.2	2.50	18.8	47	10.0	147.0	30.7
13	1	.028	143.9	85.2	3.60	21.7	54	10.0	147.0	31.0
14	1	.028	144.3	85.7	4.82	26.3	62	10.0	147.0	31.0
15	2	.028	149.1	81.0	2.41	16.9	41	10.0	139.4	25.3

	Geometry	d_p (in)	T_w (°F)	T_b (°F)	V_a (ft/sec)	pressure drop net (lbm/ft^2)	pressure drop distributer (% of net)	particle load (lbm/ft^2)	q_{rej} (watts)	h_t (BTU/hr-ft^2-°F)
16	2	.028	142.6	81.4	1.30	14.0	28	10.0	121.6	24.6
17	2	.028	138.4	79.9	1.81	15.5	35	10.0	121.6	25.7
18	2	.028	137.3	80.4	2.12	16.6	40	10.0	121.6	26.4
19	2	.028	134.3	76.7	2.94	18.8	47	10.0	121.6	26.1
20	2	.028	135.7	78.5	4.98	23.4	57	10.0	121.6	26.3
21	2	.028	137.4	81.4	6.25	27.9	64	10.0	121.6	28.9
22	2	.028	143.6	83.9	2.31	16.9	41	10.0	121.6	25.2
23	2	.028	142.6	82.6	1.46	16.5	25	12.4	114.7	23.6
24	2	.028	138.7	83.5	1.83	18.2	32	12.4	114.7	25.7
25	2	.028	137.1	80.6	2.25	19.5	37	12.4	121.6	26.6
26	2	.028	136.9	81.1	2.59	21.4	42	12.4	121.6	27.0
27	2	.028	137.6	82.2	3.00	23.4	47	12.4	121.6	27.1
28	2	.028	137.4	82.8	4.00	26.3	53	12.4	121.6	27.5
29	2	.014	146.4	82.2	1.14	9.7	38	6.1	192.0	37.0
30	2	.014	148.4	81.3	1.41	10.7	43	6.1	192.0	35.4

	Geometry	d_p (in)	T_w (°F)	T_b (°F)	V_a (ft/sec)	pressure drop net (lbm/ft^2)	pressure drop distributer (% of net)	particle load (lbm/ft^2)	q_{rej} (watts)	h_t (BTU/hr-ft^2-°F)
31	2	.014	142.4	80.8	1.71	12.0	50	6.1	162.8	32.7
32	2	.014	137.8	82.0	0.93	9.4	36	6.1	164.7	36.5
33	2 1/2	{.014 .028	137.1	79.2	1.08	9.9	36	6.2	162.8	34.8
34	2 1/2	{.014 .028	136.2	78.7	1.33	10.4	40	6.2	162.8	35.0
35	2 1/2	{.014 .028	137.0	78.8	1.54	11.4	45	6.2	162.8	34.6
36	2 1/2	{.014 .028	140.3	80.9	1.97	13.0	52	6.2	162.8	33.9
37	3	.028	140.4	83.0	4.12	7.8	20	6.2	121.6	26.2
38	3	.028	147.6	81.1	4.88	9.1	31	6.2	121.6	22.6
39	3	.028	136.8	80.6	2.77	6.5	25	6.2	121.6	26.8
40	3	.028	148.0	80.6	2.41	5.8	23	6.2	121.6	22.3
41	3	.028	142.9	77.6	1.46	14.0	19	12.2	121.6	23.0
42	3	.028	140.4	77.1	1.73	15.6	22	12.2	121.6	23.7
43	3	.028	139.6	77.0	2.20	18.8	35	12.2	121.6	24.0
44	3	.028	135.7	77.5	2.77	21.7	44	12.2	121.6	25.8
45	3	.028	134.5	81.7	4.18	29.9	59	12.2	118.1	27.7

	Geometry	d_p (in)	T_w (°F)	T_b (°F)	V_a (ft/sec)	pressure drop net (lbm/ft^2)	pressure drop distributer (% of net)	particle load (lbm/ft^2)	q_{rej} (watts)	h_t (BTU/hr-ft^2-°F)
46	4	.028	140.7	79.4	2.53	11.7	66	2.5	86.4	17.4
47	4	.028	130.1	83.0	4.10	23.4	73	2.5	83.5	21.9
48	4	.028	128.3	69.9	1.74	15.3	20	12.2	118.1	25.0
49	4	.028	126.6	70.3	1.94	16.9	25	12.2	114.7	25.3
50	4	.028	123.7	70.6	2.41	20.8	34	12.2	118.1	27.5
51	4	.028	114.9	72.3	3.25	27.3	45	12.2	118.1	34.3
52	4	.028	116.7	75.3	5.05	39.6	56	12.2	134.0	40.1
53	4	.028	126.8	79.5	2.47	14.9	49	5.0	106.5	27.9
54	4	.028	118.6	81.6	4.18	27.9	63	5.0	105.0	35.0
55	4	.028	130.1	80.4	2.36	16.6	41	7.5	121.6	30.3
56	4	.028	125.3	83.4	3.69	28.6	52	7.5	121.6	36.0
57	4	.028	129.4	81.0	2.34	19.1	34	10.0	121.6	31.1
58	4	.028	128.5	79.8	2.30	16.9	38	7.5	113.4	28.8
59	5	.028	132.5	78.1	2.08	10.4	19	7.5	151.2	32.3
60	5	.028	133.4	78.0	3.32	12.3	39	7.5	151.2	33.7

	Geometry	d_p (in)	T_w (°F)	T_b (°F)	V_a (ft/sec)	pressure drop net (lbm/ft^2)	pressure drop distributer (% of net)	particle load (lbm/ft^2)	q_{rej} (watts)	h_t (BTU/hr-ft^2-°F)
61	5	.028	137.2	81.1	6.44	19.1	61	7.5	151.2	33.4
62	5	.028	142.0	78.4	2.39	14.3	19	10.6	151.2	29.3
63	5	.028	141.5	79.2	4.20	17.5	38	10.6	151.2	30.0
64	5	.028	138.6	79.6	5.73	11.7	83	2.5	76.5	16.0
65	5	.028	132.0	82.0	7.19	15.9	85	2.5	76.5	18.9
66	5	.028	134.0	79.0	2.25	8.4	29	5.0	88.0	19.4
67	5	.028	129.0	75.8	3.16	10.1	45	5.0	136.0	31.3
68	5	.028	129.7	76.0	5.23	14.0	63	5.0	136.0	31.3
69	5	.014	113.0	77.1	1.69	6.5	14	5.8	103.5	35.7
70	5	.014	111.1	78.2	1.94	8.1	19	5.8	103.5	38.9
71	5	.014	114.0	79.9	2.59	9.4	34	5.8	103.5	37.5
72	5	.014	137.4	77.5	1.46	5.2	6	5.8	103.5	21.3
73	5	.020	136.0	79.8	3.46	7.8	66	2.5	86.4	19.0
74	5	.020	121.8	83.1	4.66	10.4	73	2.5	86.4	27.7
75	5	.020	124.5	84.9	6.01	14.9	71	2.5	86.4	27.0

	Geometry	d_p (in)	T_w (°F)	T_b (°F)	V_a (ft/sec)	pressure drop net (lbm/ft^2)	pressure drop distributer (% of net)	particle load (lbm/ft^2)	q_{rej} (watts)	h_t (BTU/hr-ft^2-°F)
76	5	.020	128.3	79.9	1.65	6.5	12	5.0	89.6	22.9
77	5	.020	114.5	79.9	2.08	7.8	25	5.0	89.6	32.0
78	5	.020	114.0	80.7	2.97	9.7	42	5.0	88.0	32.7
79	5	.020	116.4	83.3	4.90	14.3	57	5.0	88.0	32.9
80	6,B=3/4	.028	130.9	82.5	2.10	13.6	38	7.5	102.0	26.1
81	6,B=3/4	.028	130.6	84.3	2.70	21.4	41	7.5	102.0	27.2
82	6,B=3/4	.028	144.4	85.7	3.16	27.3	42	7.5	102.0	21.5
83	6,B=1/2	.028	135.9	82.3	2.63	8.1	41	5.0	103.5	23.8
84	6,B=1/2	.028	137.3	82.7	3.88	10.1	59	5.0	106.8	24.1
85	6,B=1/2	.028	136.3	85.3	5.61	13.6	71	5.0	106.8	25.9
86	6,B=1/2	.028	128.5	83.8	2.79	10.7	34	7.5	106.8	29.5
87	6,B=1/2	.028	132.9	85.2	4.95	15.6	53	7.5	109.8	28.4
88	7,P=2	.028	125.2	78.9	2.36	13.0	21	7.5	148.0	18.2
89	7,P=2	.028	113.6	79.6	4.44	16.9	42	7.5	148.0	24.9
90	7,P=2	.028	114.4	80.6	7.01	21.7	60	7.5	150.0	25.4

B = distributer blockage
P = tube pitch

	Geometry	d_p (in)	T_w (°F)	T_b (°F)	V_a (ft/sec)	pressure drop net (lbm/ft^2)	pressure drop distributer (% of net)	particle load (lbm/ft^2)	q_{rej} (watts)	h_t (BTU/hr-ft^2-°F)
91	7,P=2	.028	117.8	80.3	1.94	17.5	9	11.2	189.0	28.8
92	7,P=2	.028	112.5	80.5	3.29	20.8	23	11.2	189.0	33.8
93	7,P=5	.028	128.5	77.6	1.98	14.0	12	11.2	148.0	16.6
94	7,P=5	.028	125.7	81.6	2.40	15.9	18	11.2	148.0	19.1
95	7,P=5	.028	118.0	83.7	3.58	18.8	29	11.2	144.2	24.0
96	7,P=5	.028	118.6	85.4	5.66	23.0	42	11.2	186.8	32.2
97	7,P=5	.028	114.6	83.1	1.60	21.4	3	18.8	184.5	33.5
98	7,P=5	.028	121.8	84.7	2.23	25.3	9	18.8	230.0	35.5
99	7,P=5	.028	123.3	86.7	3.56	29.2	18	18.8	230.0	35.9

P= tube pitch